MISCELLANEOUS PAPER CERC-88-14

**US Army Corps
of Engineers**

AD-A200 478

NEARSHORE WIND-STRESS MEASUREMENTS: BACKGROUND PRELIMINARY FIELD WORK AND EXPERIMENT DESIGN

by

Charles E. Long, Jon M. Hubertz

Coastal Engineering Research Center

DEPARTMENT OF THE ARMY
Waterways Experiment Station, Corps of Engineers
PO Box 631, Vicksburg, Mississippi 39181-0631

**DTIC
ELECTE
NOV 0 1 1988
H**

September 1988
Final Report

REPORT DOCUMENTATION PAGE

Form Approved
OMB No 0704-0188
Exp Date Jun 30 1986

1a REPORT SECURITY CLASSIFICATION	1b RESTRICTIVE MARKINGS
Unclassified	

2a SECURITY CLASSIFICATION AUTHORITY	3 DISTRIBUTION/AVAILABILITY OF REPORT
	Approved for public release; distribution unlimited.
2b DECLASSIFICATION/DOWNGRADING SCHEDULE	

4 PERFORMING ORGANIZATION REPORT NUMBER(S)	5 MONITORING ORGANIZATION REPORT NUMBER(S)
Miscellaneous Paper CERC-88-14	

6a. NAME OF PERFORMING ORGANIZATION	6b. OFFICE SYMBOL (If applicable)	7a NAME OF MONITORING ORGANIZATION
USAEWES, Coastal Engineering Research Center	CEWESCR	

6c. ADDRESS (City, State, and ZIP Code)	7b ADDRESS (City, State, and ZIP Code)
PO Box 631 Vicksburg, MS 39181-0631	

8a. NAME OF FUNDING/SPONSORING ORGANIZATION	8b OFFICE SYMBOL (If applicable)	9 PROCUREMENT INSTRUMENT IDENTIFICATION NUMBER
US Army Corps of Engineers		

8c. ADDRESS (City, State, and ZIP Code)	10 SOURCE OF FUNDING NUMBERS See reverse.			
Washington, DC 20314-1000	PROGRAM ELEMENT NO	PROJECT NO	TASK NO	WORK UNIT ACCESSION NO

11 TITLE (Include Security Classification)
Nearshore Wind-Stress Measurements: Background, Preliminary Field Work, and Experiment Design

12. PERSONAL AUTHOR(S)
Long, Charles E.; Hubertz, Jon M.

13a. TYPE OF REPORT	13b TIME COVERED	14 DATE OF REPORT (Year, Month, Day)	15 PAGE COUNT
Final report	FROM ___ TO ___	September 1988	123

16. SUPPLEMENTARY NOTATION
Available from National Technical Information Service, 5285 Port Royal Road, Springfield, VA 22161.

17 COSATI CODES			18 SUBJECT TERMS (Continue on reverse if necessary and identify by block number)
FIELD	GROUP	SUB-GROUP	Measurements
			Theory
			Wind stress

19 ABSTRACT (Continue on reverse if necessary and identify by block number)

Wind stress, as a forcing term in nearshore circulation and wave generation models, is commonly represented as a product of the square of representative mean wind speed times a closure (or drag) coefficient. Specification of a drag coefficient then becomes a problem of great concern because it contains implicitly all of the physics of air-sea interaction and atmospheric boundary layer flow. A review of recent observations indicates that drag coefficients can vary by a factor of ten or more. In the simple case of steady, uniform winds blowing over the open ocean, the drag coefficient is simply a function of sea surface roughness and total mass flux. However, in the more common cases of interest to the Corps of Engineers, water depths are frequently shallow (in the sense of wind-wave behavior) and conditions are often unsteady and nonuniform. From a survey of recent theoretical considerations and associated field experiments, it is evident that drag coefficients

(Continued)

20 DISTRIBUTION/AVAILABILITY OF ABSTRACT	21 ABSTRACT SECURITY CLASSIFICATION
☒ UNCLASSIFIED/UNLIMITED ☐ SAME AS RPT ☐ DTIC USERS	Unclassified

22a NAME OF RESPONSIBLE INDIVIDUAL	22b TELEPHONE (Include Area Code)	22c OFFICE SYMBOL

DD FORM 1473, 84 MAR

83 APR edition may be used until exhausted
All other editions are obsolete

10. SOURCE OF FUNDING NUMBERS (Continued).

Civil Works Research Work Unit 31672

19. ABSTRACT (Continued).

-in shallow and nearshore waters depend on a broader suite of parameters than in the open ocean case. Among these are more detailed characterizations of sea state, water surface currents, wind direction, water depth, and distance from shore as well as buoyancy parameters.

To help clarify this dependency, a two-part experiment has been conducted wherein all of the hypothetically relevant parameters have been measured. The experiments were conducted at the Coastal Engineering Research Center's Field Research Facility (FRF) on the coast of the Atlantic Ocean near Duck, North Carolina, where advantage could be taken of low land relief, reasonably uniform alongshore topography and bathymetry, and a pier, 600 m in length, which could act as a stable, over-water instrument platform.

The first experiment was conducted in fall 1985 during a larger scale experiment known as DUCK85. Its purpose was to provide an exploratory survey of the horizontal vari- ability of winds at the site and to investigate adequacy of various platforms for detailed wind-stress measurements. Data from that experiment (which includes passage of Hurricane Gloria) indicate that wind differences from the landward end of the pier to the seaward end are finite, varying by up to 40 percent in speed, but highly systematic. Anemometers on the roof of the FRF building and near the pier deck at the seaward end of the pier indi- cated substantial flow distortion due to the proximity of wind-blocking structures. From this, it is concluded that extreme caution is necessary when mounting anemometers to avoid platform distortion effects and that careful interpretation is necessary when using beach- based anemometers to characterize winds over water.

The second experiment was conducted in fall 1986 during a very large-scale experi- ment known as SUPERDUCK. Its purpose was to provide detailed wind-stress measurements. Coupled with measurements made by other investigators during SUPERDUCK of other relevant parameters, data from this experiment can be used to develop and test various models of drag-coefficient variability. Experiment rationale and design are described here. Experi- ment results and analysis will be given in a subsequent report.

PREFACE

This report provides a description of background physics and a survey of recent research observations and hypotheses concerning the nature of wind-stress drag-coefficient closures for shallow and nearshore waters. Further, it describes a series of experiments designed to augment understanding and refine formulation for these closures. Such work is necessary to enable accurate modeling of wind-driven nearshore waves and currents.

CONTENTS

NEARSHORE WIND-STRESS MEASUREMENTS: BACKGROUND,

PRELIMINARY FIELD WORK, AND EXPERIMENT DESIGN

PART I: INTRODUCTION

1. Wind plays a very important role in the dynamics of the upper ocean
and shallow-water bodies. Momentum imparted by the wind to the water surface
gives rise to waves and currents, and through turbulence, a much increased
diffusive capability over pure molecular processes. In the deep ocean, the
effects of wind are readily detectable to depths on the order of 100 m. In
waters shallower than this, such as coastal regions, harbors, entrance chan-
nels, and lakes, wind can affect the dynamics of the whole water column. The
interaction of the water with solid or semisolid boundaries is of particular
importance to those who dwell near water. Wind-generated waves radiate energy
shoreward to beaches, coastal dwellings, and shore protection structures. In
high winds, the wind-generated water levels can surge over land and cause
flooding. Wind-induced turbulence can add to wave- and current-induced tur-
bulence and thereby enhance the diffusive character of the flow which, in
turn, has a direct impact on coastal erosion, alongshore sediment transport,
and redistribution of biological nutrients and waterborne contaminants.

2. Wind forcing is not the only source of energy at a given shallow-
water site. Tides, planetary scale waves, lateral processes from large-scale
currents driven by distant winds (such as the Gulf Stream), waves in the wind-
wave frequency band radiating in from distant storms (swell), and, in enclosed
bodies, seiching can all contribute to nearshore dynamics. In addition, local
areas where water runoff from land occurs, as in estuaries and near river out-
falls, are influenced strongly by currents and turbulence from this source.
At any given time, forcing by any of these processes may be present. However,
high-energy water motions, i.e., those which can do work (or damage) at the
highest rate, are associated with high wind conditions. In a carefully de-
signed and highly instrumented study of coastal dynamics in Lake Erie,
Schwab et al. (1984) found from an analysis of four storms that wind forcing
was a dominant source of energy throughout the nearshore zone. This is impor-
tant because it means that wind has a strong influence not only in deep and
transitional water, where active wave generation is classically thought to

3

occur, but also in shallow water where waves shoal and break and where wave-induced currents are often considered dominant. Schwab et al. (1984) and Hubertz (1986) found wind-driven currents to be comparable with wave-induced currents. Hence, a complete dynamic description of nearshore processes must include a characterization of wind input.

3. To do this accurately and directly is not a straightforward task. The simplest estimator of the intensity of wind forcing is a measurement of the average wind speed just above or near the water surface being forced. It is intuitive that as the mean wind speed increases the force imparted to the water increases. All observations indicate that, for all other system variables held constant, this is approximately (but only approximately) true. This type of reasoning prompted Taylor (1916) to propose that the mean wind stress τ with units of force per area, the air density ρ with units of mass per volume, and the mean wind speed U with units of length per time (and aligned with the stress, both being taken here to be in the x-direction) form a closed system.* Dimensional analysis then requires $\tau/\rho U^2$ = constant $= C_D$, where C_D is called the drag coefficient. This result is called the quadratic drag law or the bulk parameterization of wind stress and is usually written in the form

$$\tau = \rho C_D U^2 \tag{1}$$

4. If Equation 1 is true, then C_D is constant and measurements would provide its value. Table 1 shows ranges of C_D given by several authors from measurements made over water. Some of the references cite the authors own observations. Others are compendia of several experiments. For example, Garratt (1977) cites 23 references and Huang et al. (1986) cite 21 with very little redundancy in citation. Amorocho and DeVries (1980) cite virtually the same data as these last two, but their paper is included for completeness. Clearly there is doubt about the constancy of C_D. The ratio of maximum to minimum value for the table as a whole is about 32. The average from individual authors is about 6.

5. This is less than satisfactory for accurate modeling. If wind

---

* For convenience, symbols and abbreviations are listed in the Notation (Appendix A).

4

Table 1

Ranges of Drag Coefficient Over Water Measured or

Cited by Various Authors

Source	Minimum	Maximum
Hsu (1972)	1.1	6.4
SethuRaman and Raynor (1975)	0.5	3.0
Garratt (1977)	0.6	4.2
SethuRaman (1979)	0.3	2.1
Amorocho and DeVries (1980)	0.2	4.5
Wu (1980)	0.8	2.3
Large and Pond (1981)	0.5	2.3
Geernaert and Katsaros (1986)	1.3	2.5
Geernaert, Katsaros, and Richter (1986)	0.7	3.2
Huang et al. (1986)	0.2	4.2

stress is as important as other effects in nearshore processes and its magnitude is not known to within a factor of 6, then it can be expected that model results will vary similarly. Relying on such a model for design of coastal protection could result in exhorbitantly expensive overkill or woefully inadequate protection depending on how the model is used or interpreted.

6. The range of values in Table 1 suggests and, in fact, most of the authors cited there propose, that if a model represented by Equation 1 is to be used, then C_D must implicitly contain all of the physics not explicit in Equation 1. The necessary physics are contained in the fields of boundary-layer turbulence and air-sea interaction. A number of investigations in recent years have led to improved characterization of C_D in terms of other measurable wind-field and sea-state parameters. Some are well founded in turbulence theory; others are more conjectural but physically reasonable. Part II of this report contains a brief summary of this latest work. It also

5

describes the shortcomings of our present understanding and gives justification for ongoing field experiments to refine and test parametric relationships.

7. It is not proposed that bulk parameterization (i.e., drag and exchange coefficients) be abandoned. They are the most reasonable of practical tools available since they rely on a finite number of specifically defined mean environmental parameters of a quality which can be measured at remote coastal sites, instrumented buoys, and vessels of opportunity. Many of the models used at the Coastal Engineering Research Center (CERC) rely on bulk parameterization for wind effects in coastal flooding models (e.g., Sheng and Butler 1982) and nearshore wave and current models (e.g., Hubertz 1987). Alternatives are either to deploy wind-stress measuring devices on ships, buoys, and coastal sites or to employ a large-scale numerical model to represent the balance of forces present in coastal meteorology. Neither of these is as practical for large-scale, long-term studies as the bulk method although both are attractive conceptually.

8. Direct measurements of wind stress require highly accurate, three-dimensional anemometers with good frequency response to about 5 Hz. Indirect methods (other than the bulk method) require either arrays of low-frequency-response temperature, humidity, and horizontal wind-speed sensors or single high-frequency (20 Hz to 1 kHz, depending on method) sensors for the same variables. Though impractical for remote, long-term, unattended deployment, such instrumentation and methods are necessary to quantify the interrelationships among parameters used in the models which form the basis of the bulk method. Part IV of this report gives a brief description of currently used methods, instruments, and platform requirements and limitations for making wind-stress measurements. Part V of this report describes an experiment which tests various platforms at CERC's Field Research Facility for adequacy in making wind-stress measurements by various methods.

9. Meteorological models such as the one described by Resio, Vincent, and Corson (1982) for the open ocean would be attractive, if applicable, for use in coastal regions. However, as described by Hsu (1970, 1979) in studies near the coast of Texas, and Resio and Vincent (1977) in analysis of winds over the Great Lakes, conditions are frequently highly nonuniform in both cross-shore and vertical directions. Highly variable surface roughness from water to land (and possibly over the water itself, see Part II) and sharp

contrast in surface heat, moisture, and momentum fluxes give rise to baroclinic circulations (among them the sea breeze) and the formation of internal boundary layers (Stunder and SethuRaman 1985), the effects of which are noticeable for kilometres to tens of kilometres landward and seaward of the coast. Furthermore, such models require characterization of the surface fluxes of mass and momentum. Conventionally, this is done in the same way that the surface bulk coefficient models are derived. Any limitation in our ability to characterize the bulk coefficients will certainly be reflected as inadequacies in a large-scale meteorological model.

10. Hence, it seems most productive to confine attention to the lowest few tens of metres of the atmosphere, where mean wind speed, temperature, and humidity measurements are most often made, and to deduce the laws that relate these quantities to their respective fluxes. In consideration of observations and hypotheses given in Parts II and III of this report, and measurement methods described in Part IV, an experiment design is described in Part V which should add significantly to our ability to formulate these laws.

PART II: RECENT WORK IN BULK COEFFICIENT FORMULATION

11.   To account for the broad range of drag coefficients shown in
Table 1, it is assumed either that there is substantial instrument and experi-
ment error or that the drag coefficient depends on other parameters. While
early methods of wind-stress measurement were often inaccurate, modern methods
and instrumentation are substantially better. The broad range of investiga-
tions represented by Table 1, some of which are quite recent, suggests that a
parametric dependency of drag coefficients is legitimate.

12.   Several investigators have compiled data from other sources to ex-
amine behavior of drag coefficients. One of the most frequently cited papers
is that by Garratt (1977). In that paper, a large number of investigations,
selected for reasonable accuracy and lack of atmospheric stability effects, is
analyzed for a dependence of the drag coefficient on the wind speed at a 10-m
elevation above the sea surface. Though the scatter of results is high, there
is a clear correlation. Furthermore, Garratt (1977) was able to show the
major trend of the data with a simple atmospheric-surface-layer model, a major
step in accounting for some of the variability of the drag coefficient.

13.   The model described by Garratt (1977) and modifications to it will
be described below. In the paragraphs that follow some of the equations and
scaling laws of turbulence theory will be used, often without pretext or cita-
tion. Substantial background material on the governing equations and common
scaling arguments can be found in such classic texts as those by Hinze (1959),
Phillips (1969), Kraus (1972), and Tennekes and Lumley (1972). Equations will
only be used as needed for clarity. It is noted that because of its complex-
ity, turbulence is a highly empirical field with many of its hypotheses based
on scaling arguments (dimensional analysis) and experiments. Some of these
are well founded, others less so. An attempt will be made here to distinguish
among them.

Basic Concepts

14.   The environment for which the drag coefficient formulae are de-
signed is considered to be horizontally homogeneous, turbulent air flow over
water with deviations from horizontal homogeneity assumed negligible. The
wind stress to be defined is not the true Newtonian viscous stress but a

8

vertical advection of fluctuating horizontal momentum known as a Reynolds stress. In a coordinate system with the x-axis aligned with the mean wind and the vertical axis positive upward from the sea surface, the total velocity in the x-direction u can be thought of as having mean U and fluctuating u' parts where

$$U = \frac{1}{T_a} \int_0^{T_a} u \, dt \tag{2}$$

T_a is an appropriate averaging time (see Part III) and integration is with respect to time. The total vertical velocity w has no mean value in this idealized flow, but only a fluctuating part w' .

15. The total momentum per unit volume in the x-direction is $\rho u = \rho$ $(U + u')$ where ρ is the air density (mass per unit volume). The mean vertical advection of this by the fluctuating (turbulent) vertical velocity is the correlation between ρu and w' . This is usually found to be negative so the negative correlation is considered a positive stress τ as

$$\tau = -\frac{1}{T_a} \int_0^{T_a} \rho u w' \, dt = -\rho \, \overline{u'w'} \tag{3}$$

where the overbar represents the time average, U does not contribute because it is constant for this period by Equation 2, and fluctuating parts of the density field are assumed negligible through the Boussinesq approximation. Equation 3 is considered a stress because it is a flux of momentum, albeit advective instead of molecular. It is positive because, on the average, when $\rho u'$ is positive, w' is negative. This represents a downward momentum flux which tends to accelerate fluid layers below, including the water surface. When $\rho u'$ is negative, w' tends to be positive. This tends to decelerate fluid layers above (including the mean air flow).

16. The mean flow U is a strong function of z in the vicinity of the water surface. At the water surface, the air molecules are coupled to water molecules by molecular viscosity such that the mean air velocity equals the mean water velocity. Well above the water surface the air is forced by

9

very large-scale pressure and gravitational forces and often moves much faster than the water. In between, the mean flow is sheared, i.e., varies with respect to the vertical coordinate z. Fluctuations in vertical velocity tend to carry faster air down and slower air up, which suggests a coupling between the mean shear $\partial U/\partial z$ and the stress given by Equation 3. Since u' and w' are correlated, organized rotary motions, or eddies, are suggested. The eddies cannot penetrate the water surface, so a maximum size for eddies in the vicinity of the water surface is likely to be the distance z to the water surface. If τ, ρ, and z form a closed set, then by dimensional analysis

$$\frac{z}{u_*} - \frac{\partial U}{\partial z} = \text{constant} = \frac{1}{\kappa} \tag{4}$$

where

$u_* = (\tau/\rho)^{1/2}$ friction velocity

κ = von Karman constant

17. The model given by Equation 4 will not work for air flow in the troughs between wave crests because the flow is not horizontally homogeneous and becomes extremely complex. This is shown theoretically by Chalikov (1986) and Jacobs (1987) and in laboratory work by Papadimitrakis, Hsu, and Street (1984) and Papadimitrakis, Hsu, and Wu (1986). In analogy with flow over solid roughness elements (Schlichting 1979), it is usually assumed that flow distortion and stress redistribution by wave surfaces decays by about three wave heights above the surface. Equation 4 should hold for some distance above that, i.e., the air acts as if it is flowing over a horizontally uniform surface. This provides one constraint on the region of applicability of Equation 4, i.e., $z \gtrsim 3H_s$, where H_s is a characteristic wave height.

18. Equation 4 provides a very powerful tool for air-sea interaction studies since it allows a relation between the wind stress ρu_*^2 and the mean velocity U at some distance above the water surface. The point of this discussion is that by the continuum hypothesis the flux is continuous through the level z at which measurements are made. If the flow is horizontally homogeneous, then the only way momentum can get to the water surface from the air is vertically through elevation z. Sufficient knowledge of this and the water response is all that is needed to form a closed model. Detailed

10

knowledge of the air flow in and near the wave troughs is then unnecessary which is an enormous simplification of the problem.

19. The bulk of recent work focuses on two main topics. One is the specification of the constants of integration in the solution of Equation 4. The other is accounting for atmospheric stability, i.e., variations of air density due to fluxes of heat and water vapor, which is known to modify Equation 4 from studies of steady, horizontally uniform flow over land. These are discussed in turn and are followed by considerations of unsteadiness and horizontal nonuniformity.

20. If the wind stress is constant or a weak function of distance from the sea surface, then Equation 4 can be integrated simply between two levels of flow. Long (1981) in a similarity solution of an idealized, neutrally stable planetary boundary layer model given by Businger and Arya (1974) showed that the stress is approximately linear in the lowest part of the boundary layer with a slope $\partial\tau/\partial z$ on the order of $-6\rho u_* f_c$, where f_c is the Coriolis parameter ($= 2\Omega \sin \Lambda$, where Ω is the radian rotation rate of Earth and Λ is latitude). The height at which τ is still 90 percent of its boundary value is then on the order of $u_*/60f_c$. For a standard anemometer height of 10 m, this imposes a constraint that $u_* > 60f_c \times 10$ m $= 0.06$ m/sec or $U(10$ m$) \gtrsim 1$ m/sec based on the drag coefficient curve of Garratt (1977). The corresponding constraint for an anemometer height of 20 m is, at most, $U(20$ m$) \gtrsim 2$ m/sec. Since wind speeds of interest are usually much greater than this, i.e., 5 m/sec and higher, it is reasonable to treat τ as approximately constant in the lower few tens of metres of the atmosphere. As a result, this region is often called the "constant stress" or "constant flux" layer of the atmosphere with the understanding that some caution is to be exercised at very low wind speeds.

21. Equation 4 is then expected to apply for $z \geq 3H_s$, as noted previously, and for $z \lesssim u_*/60f_c$. An observation height of 10 m should be adequate for wave heights less than about 3 m. For seas to 6 m, an elevation of about 20 m is necessary. Violations of these constraints, e.g., 10-m observations during hurricanes where seas exceed 3 m, could be expected to yield suspicious results.

Logarithmic Profiles and Limits of Applicability

22. With τ , and therefore u_* , assumed constant in the atmospheric

11

surface layer, Equation 4 can be integrated between two arbitrary levels of
the flow such that

$$U(z) - U_o = \frac{u_*}{\kappa} \ln \frac{z}{z_o} \tag{5}$$

where U_o and z_o are, mathematically, constants of integration. For gen-
eral application, they must be specified as constants, functions of other flow
parameters, or specific velocity and level within the region where Equation 5
applies. From Equations 1, 3, and 5, along with the definition of u_* fol-
lowing Equation 4, a drag coefficient expression can be written as

$$C_D(z) = \frac{u_*^2}{[U(z) - U_o]^2} = \frac{\kappa^2}{\left[\ln\left(\frac{z}{z_o}\right)\right]^2} \tag{6}$$

where, as discussed below, the inclusion of U_o modifies the form given in
Equation 1.

23. From Equation 6 it is seen that a drag coefficient is a function of
z in general. Setting a standard anemometer height of, say, $z = z_r = 10$ m
compensates for this dependency. Equation 6 is often used to correct for data
collected at heights other than $z = 10$ m to standardize comparisons.

24. In standard form, C_D depends on κ, U_o, and z_o. The value
of κ is usually taken to be 0.41. Frenzen and Hart (1983) give a list of
recent estimates based on atmospheric studies. Nowell and Long (1983) in a
detailed and comprehensive analysis of pipe-flow data, find $\kappa = 0.408 \pm 0.004$
at 95-percent confidence. However, in a very well executed atmospheric exper-
iment over land (Haugen, Kaimal, and Bradley 1971), the data analysis by
Businger et al. (1971) found $\kappa = 0.35$. This value is given some weight be-
cause of the high quality of the experiment. On the other hand, a reanalysis
of the same data by Wierenga (1980), who took flow blockage effects into ac-
count (see Part IV), found $\kappa = 0.41$. The difference is important since κ
is squared in Equation 6. A 17-percent difference in κ yields about a
34-percent difference in C_D and any stress computed using C_D. Note that
data scatter reported by an investigator who uses a single value of κ to

12

estimate C_D is not affected by this, but the application of a model of C_D to estimate stress is affected. The concensus of investigations shown by Frenzen and Hart (1983) supports the higher value of κ . While the debate continues (see Högström (1985) and a reply by Telford and Businger (1986), for example) it is assumed here that $\kappa = 0.41$.

25. In studies of fluid flow over solid, impermeable boundaries, Equation 6 is generally applied with $U_o = 0$ and z_o , called the surface roughness scale, is the level at which an extrapolation of the logarithmic profile toward the boundary gives $U(z_o) = 0$. As discussed above concerning the complex flow in the region very near a water-wave surface, extrapolation of a logarithmic profile to a region very near a solid surface does not provide legitimate velocity estimates in this so-called sublayer region. Hence, z_o is an artifice both of integration of Equation 4 and of application of the no-slip boundary condition. By the continuum hypothesis, however, the mean velocity must be continuous into the sublayer such that z_o can be considered a measure of the elevation at which the mean velocity in the sublayer matches the velocity in the overlying logarithmic layer. Since the matching height is the lowest region of applicability of the logarithmic region, the turbulent stress, i.e., Reynolds momentum flux, must also be continuous at this height.

26. Within the sublayer, the flow can be quite complicated depending on the physical geometry of the solid boundary. If the boundary is smooth enough, then momentum transfer at the boundary is purely by Newtonian viscous shear stress. In this case $\tau = \mu \partial U/\partial z$, where μ is the dynamic viscosity, or in equivalent form, $u_*^2 = \nu \partial U/\partial z$, where $\nu = \mu/\rho$ is the kinematic viscosity (with dimensions of length squared per time). The velocity scale of this flow is u_* and the length scale is ν/u_* . The mean flow itself is $U(z) = u_*^2 z/\nu$. This profile has been found empirically (Schlichting 1979) to match an overlying logarithmic profile at $z \simeq 10 \nu/u_*$, such that, from this, $z_o \simeq \nu/9u_*$. This flow is called "dynamically smooth," and occurs if the solid boundary has no deformations or protuberances with length scales larger than about $5 \nu/u_*$. Note that the total vertical flux of momentum is considered constant through the sublayer. The turbulent advection of momentum, which scales with z , decreases toward the boundary, but is compensated by viscous stress which increases to ρu_*^2 at the boundary.

27. If the physical boundary contains roughness elements of length scale $k_R \gg \nu/u_*$, then momentum is transferred through the sublayer to the

boundary not only by viscous shearing stress (skin friction) but also by the net dynamic pressure (normal or form drag) forces induced by the fluid as it is diverted around and over roughness elements. In this case, known as "dynamically rough," the mean flow is very complex and, in general, has no simple solution. The length scale of this flow is dominated by the size of the roughness elements k_R such that for boundaries with roughness of a single scale it can be expected that z_o and the sublayer matching height both scale with k_R. This was verified empirically (Schlichting 1979) for flow over close-packed sand grains of diameter k_R. It was found that $z_o = k_R/30$ and the sublayer matching height was about $3 k_R$. While this scale for z_o is often assumed for dynamically rough flows in general, it is important to note that over surfaces with multiple length scales the roughness height alone is not sufficient. For instance, Schlichting (1979) finds $k_R/200 \leq z_o \leq k_R/10$ for flow over elements of height k_R but of different separation and pattern scales. That is, length scales of surface geometry appear to dominate the definition of z_o, but, for surfaces of multiple scales, in complex combination. The total momentum flux into the sublayer at the matching height is $\tau = \rho u_*^2$ as noted above. Within the sublayer, the division of this flow into form drag and skin friction is a complicated function of local surface geometry, local flow scales, and viscosity. For total force on a rigid surface (like the inside of a pipe) it is not necessary to know the detailed flow in the sublayer to relate the stress to the velocity above the sublayer, if the net mean roughness scale z_o is known.

28. The discussion above is necessary as background because the success of the reasoning used for flow over solid boundaries suggests that similar reasoning can be used for flow over a water surface. Such reasoning is bound to be incomplete, however, because a water surface differs from a rigid surface in that it deforms under the action of wind stress. In geophysical flows, this deformation is characterized by a broad range of length scales. In dynamic conditions, vertical length scales vary from millimetres (for the amplitudes of capillary waves) to 10 m in storm conditions at sea, shoaling of long waves, or standing tidal motions. Horizontal length scales vary from centimetres for capillary waves to hundreds of kilometres for tidal and planatary scale waves. In calm conditions, length scales are very small, displacements being on the order of molecular mean free paths as governed by surface tension and thermodynamic constraints on intermolecular forces.

14

29. Relating water surface displacement and motion to the mean and fluctuating parts of the driving wind is, of course, the very heart of air-sea interaction. A primary objective in this field is to determine which scale or combination of scales of the sea surface characterizes the surface roughness scale z_o in Equation 5 so that C_D from Equation 6 can be determined.

30. Remember that Equation 5 is assumed legitimate in steady, horizontally uniform, neutrally stratified flow. As for flow over solid surfaces, the sea surface is considered uniform if statistics of surface displacements and motions do not vary substantially in any horizontal direction. Furthermore, if the sea is considered to consist of wind-driven waves only, and these waves are assumed linear (i.e., all motions are purely cyclic), then there is no mean motion at the air-sea interface. In this case $U_o = 0$ in Equations 5 and 6 and C_D depends entirely on z_o for a fixed reference elevation z_r and reference wind speed $U_r = U(z_r)$.

31. Equation 6 can be solved for z_o which results in

$$z_o = z_r e^{-\kappa/\sqrt{C_D}} = z_r e^{-\kappa U_r/u_*} \tag{7}$$

From a collection of observations of wind stress and wind speed made prior to 1970, Kitaigorodskii (1973) noted that, apparently, z_o varies by over seven orders of magnitude from about 10^{-7} m to about 10^{-1} m for virtually the same value of wind stress. He suggested that much of the scatter was due to uncertainty in investigative method and cited the need for proper parameterization of z_o .

32. A simple parameterization of surface roughness was proposed by Charnock (1955). His argument was, in essence, that gravity waves (i.e., motions whose restoring force is gravity, characterized by gravitational acceleration g) being driven by wind stress (with principal varying part being u_* since ρ is more nearly constant) might be expected to have a surface roughness dictated by the two parameters u_* and g . The only possible dimensionally correct form is

15

$$z_o = \alpha \frac{u_*^2}{g} \tag{8}$$

where α = a universal constant. From his own observations in a 16-m-deep reservoir with lateral dimensions on the order of 1 km, Charnock (1955) estimated $\alpha = 0.0067$.

33. Following a slightly different reasoning but arriving at the form given by Equation 8, Kitaigorodskii (1973) treated his collection of scattered (pre-1970) data as samples from a random process. By averaging z_o estimates within bands of u_* , he deduced a mean $\alpha = 0.035$ with 80-percent confidence intervals spanning about three orders of magnitude in z_o . This α differs substantially from that given by Charnock (1955).

34. A third estimate of α is given by Garratt (1977), mentioned previously. Citing experiments from the late 1960's to the mid-1970's (and, hence, largely independent of data cited by Kitaigorodskii (1973)), he found $\alpha = 0.0144$. This differs substantially from both of the estimates given above. His data are grouped by reference wind speed U_r before averaging. His estimate of confidence is the standard deviation of resulting C_D estimates. Use of the two α estimates given above yields C_D estimates within Garratt's error bars for wind speeds below about 20 m/sec. Above 20 m/sec, they lie outside his error bars. However, his data are sparse at speeds above 20 m/sec so the alternate curves might not exceed a 90-percent confidence interval (which is not given), and so may not be significantly different.

35. At $U_r = 40$ m/sec, C_D varies by a factor of about 2 for α varying from 0.0067 to 0.035. Hence, the difference is important in high winds. Note that though α varies by a factor of about 5 in this comparison, the difference in C_D is less. This is because it is the logarithm of z_o , and, hence, α , that enters Equation 5 so that C_D is less sensitive to large variations in estimates of α . At $U_r = 10$ m/sec, C_D varies by about 50 percent for the two α's cited. Garratt's (1977) results lie between these cases.

36. A fourth work, Wu (1980), discusses values of α which cover the middle part of the range given above. Citing his own research entirely, Wu (1980) states that he has found $\alpha = 0.012$ from laboratory work alone, $\alpha = 0.0156$ as a mean value joining laboratory and field data, $\alpha = 0.0185$ for data excluding reference winds less than about 5 m/sec (for which z_o may

16

be affected by viscosity or surface tension), and $\alpha = 0.027$ based on scaling arguments for wind flow separation over the crests of oceanic waves of low phase speed. He concludes that a general expression for z_o should include parameters other than u_* and g, and notes the need for further research. He suggests $\alpha = 0.0185$ for the z_o regime he believes is most nearly governed by u_* and g. This differs by about 25 percent from the $\alpha = 0.0144$ found by Garratt (1977).

37. Both Kitaigorodskii (1973) and Garratt (1977) averaged results from many experiments to obtain statistically meaningful estimates of α from data with much scatter. To test the hypothesis of a constant α, Amorocho and DeVries (1980) conducted wind-stress measurements in a wind tunnel and over an aquaduct. They report a broad range of α from about 0.001 to 1.0 in their wind tunnel and from about 0.0001 to 1.0 for the aquaduct. For a given wind speed, the scatter in the data is large, being about one order of magnitude in their lab work and about two orders of magnitude in their field work. Amorocho and DeVries (1980) use these results to argue in favor of a simple three-range drag law wherein C_D is constant within each of two ranges of U_r, and a transition range joins them. However, the scatter of C_D measurements remains high. One interpretation of their results is that Charnock's model does not include all of the parameters necessary to define z_o in general.

38. A more straightforward approach to the definition of z_o was described by Kitaigorodskii (1973). He tested the hypothesis that wave displacements act solely as roughness elements. In any sea of interest, a typical wave height is $>> \nu/u_*$ so the sea surface is everywhere dynamically rough in this scheme. The roughness parameter z_o should then be proportional to some measure of surface displacement. Kitaigorodskii (1973) chose sea-surface variance σ_η as such a measure. However, he found no general indications of correlation between z_o measured from wind profile data and σ_η.

39. This is a reasonable result since, as Munk (1955) pointed out, basing z_o on simple displacement would suggest that a 1-m wind-driven sea would have the same roughness as a 1-m tide. Kitaigorodskii (1973) next made the hypothesis that surface slope is important since it is a measure of the extent to which a wavy surface presents a bluff obstruction to wind flow. He estimated a mean slope as σ_η/λ_o, where λ_o is the mean wavelength deduced from mean wave period T_o by the deepwater dispersion relation $\lambda_o = gT_o^2/2\pi$.

17

With z_o , τ_- , and σ_r/λ_o as variables in a set (assumed closed), he sought a correlation between z_o/σ_η and σ_η/λ_o but found none.

40. Results of these two tests do not necessarily mean that surface displacement, with or without surface slope, is not important. They indicate that these variables are incomplete descriptors of z_o , possibly because of the smoothing effect of using mean wave properties in their definitions or because such definitions treat the sea surface as static, whereas, in nature, it is dynamic.

41. Following the logic of this statement, Kitaigorodskii (1973) reasoned that if roughness elements are mobile, then it is wind speed relative to speed of roughness elements that is important in their interaction. For roughness elements as waves with phase speed C (and still assuming no mean velocity at the water surface) the logarithmic profile of Equation 5 can be expressed relative to C as

$$U(z) = C + \frac{u_*}{\kappa} \ln \frac{z}{z_a} \tag{9}$$

where z_a is the elevation at which $U(z_a) = C$. Manipulation of Equation 9 enables transformation from a coordinate system moving at speed C to one that is fixed. The result is

$$U(z) = \frac{u_*}{\kappa} \ln \frac{z}{z_a e^{-\kappa C/u_*}} \tag{10}$$

Comparison with Equation 5 shows $z_o = z_a \exp(-\kappa C/u_*)$. On the asymptote of $C/u_* \to 0$ (i.e., static roughness) the expression $z_o = z_a$ is recovered.

42. For finite C/u_* , Kitaigorodskii (1973) made the somewhat tenuous assumption that z_a for a monochromatic wave is proportional to the wave amplitude. If a spectrum of waves is present, then $(1/2)z_a^2$ is the variance of the sea surface in a narrow band of frequencies $\Delta\omega$ centered at frequency ω (in radians per second), i.e.,

$$\frac{1}{2} z_a(\omega)^2 = S(\omega)\Delta\omega \tag{11}$$

18

where $S(\omega)$ = spectral density. Since phase speed is uniquely related to frequency for a given water depth d (at least in linear wave theory where $C = (g/\omega) \tanh (\omega d/\lambda)$), then the expression for z_o , above, is frequency dependent. Kitaigorodskii (1973) makes the further assumption that the roughness associated with each spectral band is a linear contributor to the total roughness k_R such that

$$\Delta k_R^2 = 2S(\omega) \; e^{-2\kappa \; C(\omega)/u_*} \; \Delta\omega \qquad (12)$$

For a continuous spectrum in deep water (where $C = g/\omega$), integration over all frequencies and solution for k_R yields

$$k_R = \left[2 \int_0^\infty S(\omega) \; \exp \; (-2\kappa g/\omega u_*) \; d\omega \right]^{1/2} \qquad (13)$$

Total roughness is thus a weighted sum of all spectral components. It is emphasized that Equation 13 is derived for deep water and tacitly assumes all waves are propagating in the direction of the wind. For $k_R \gg \nu/u_*$ it is assumed, in this model, that z_o is proportional to k_R .

43. The estimate of roughness given by Equation 13 depends strongly on the definition of $S(\omega)$ used in evaluation and on the size of the exponent in the weighting function. For very low frequencies, $\omega \rightarrow 0$, the weighting function prevents much contribution from the spectrum. The most emphasis is given to high-frequency waves. To evaluate Equation 13 in a simple way, Kitaigorodskii utilized Phillips' (1969) equilibrium spectral model for high-frequency wind waves. This takes the form

$$S(\omega) = \begin{cases} \beta g^2/\omega^5 & \omega \geq \omega_o \\ & \text{for} \\ 0 & \omega < \omega_o \end{cases} \qquad (14)$$

where

ω_o = spectral peak frequency

β = constant (according to Phillips (1969))

This spectrum represents a state of saturation of a wave field wherein energy added from wind is transferred to turbulence through wave breaking or to low-frequency waves through nonlinear interaction. This last mechanism tends to lower ω_o in Equation 14 during a condition where a wind-driven sea is building.

44. Kitaigorodskii (1973) identified three general regimes dependent on the variables involved when Equation 14 is substituted in Equation 13. First is the case wherein a high wind acts on a relatively undeveloped sea. In this case, u_* is much greater than the phase speeds of any spectral components (g/ω), such that the exponential weighting function in Equation 13 is essentially unity for all frequencies. Roughness elements thus act as if they are rigid and $k_R^2 = (1/2)\beta g^2/\omega_o^4$, which is simply the variance of a sea surface with a spectrum given by Equation 14.

45. If the wind continues to act, then the spectrum broadens, ω_o is reduced and the phase speed at the spectral peak $(C_o = g/\omega_o)$ becomes more comparable to u_* . In this second regime, Kitaigorodskii treats the exponential weighting function in Equation 13 as a slowly varying function (relative to ω^{-5}) characterized by $\omega = \omega_o$. In this case, the surface roughness length squared is the spectral variance attenuated by the exponential function evaluated at $\omega = \omega_o$. Thus, $k_R^2 = (1/2)\beta g^2 \omega_o^{-4} \exp(-2\kappa g/u_* \omega_o)$
$= (1/2)\beta g^2 \omega_o^{-4} \exp(-2\kappa C_o/u_*)$. This is an important theoretical result since it is one of the first to show that sea-surface dynamics (i.e., moving roughness elements) have a direct influence on the structure of flow in the overlying atmosphere. Furthermore, it shows a reduction in surface roughness for the dynamic case as compared with the static roughness case. This corresponds, at least qualitatively, with observations.

46. The third regime represents the somewhat idealized case where the sea has developed to the point where $\omega_o \to 0$. Equation 13, using the spectrum of Equation 14, can then be evaluated directly. The result is $k_R = \sqrt{3\beta}/2\kappa^2 u_*^2/g$. Comparison of this result with Equation 8 shows that this has the same parametric dependency as Charnock's (1955) z_o . If, in analogy with flow over uniform sand grains, $z_o \approx k_R/30$, then $z_o = \sqrt{3\beta}/60\kappa^2 u_*^2/g$, and Charnock's coefficient is $\alpha = \sqrt{3\beta}/60\kappa^2$. SethuRaman (1979) evaluated

this expression using $\kappa = 0.35$ (from Businger et al. 1971) and $\beta = 0.0117$ (as suggested by Phillips (1969)). He found $\alpha = 0.026$. This is between the values $\alpha = 0.0144$ (given by Garratt (1977)) and $\alpha = 0.035$ (deduced by Kitaigorodskii (1973)). Remember that the two latter values were found by averaging large amounts of data without discriminating regimes. Variation in α is quite possible due to variations in Phillips' coefficient β . Geernaert, Katsaros, and Richter (1986) note that typical measured values of β range from 0.008 to 0.020, and found values spanning this range from wave measurements in 16-m water depth in the North Sea. With the more frequently cited $\kappa = 0.41$ and still assuming $z_0 \simeq k_R/30$, this yields Charnock's coefficient in the range $0.015 < \alpha < 0.024$. This is consistent with the range cited above and suggests that parameters which affect β such as fetch, water depth, or degree of saturation (Geernaert et al. 1986) will have a direct effect on α . The same effects can also violate the assumptions leading to this regime as is discussed below.

47. In the first two regimes, Kitaigorodskii (1973) found a reasonable correlation between his model and observations in cases where waves were only of local wind-driven type. Estimates of z_0 scattered about the theoretical curves by about one order of magnitude. Compared with the seven orders of magnitude discussed above, this is a major improvement. He classified his regimes by ratio of u_* to spectral peak phase speed $C_0 = g/\omega_0$ such that for $u_*/C_0 \gg 1$ (regime of initial wave growth) and $u_*/C_0 \simeq 1$ (intermediate wave growth regime) his hypotheses were justified.

48. However, for the last stages of wave growth ($u_*/C_0 \ll 1$), i.e., the regime for which Charnock's relation was derived, Kitaigorodskii did not find a clear correlation between his model and his observations in the Central Pacific Ocean. Specifically, for $u_*/C_0 \leq 0.05$, he found z_0 to be highly variable, generally larger than the exponentially weighted sea-surface standard deviation, and inconsistent with a constant coefficient in Charnock's expression. Part of the reason for this lies in the way Kitaigorodskii's model is derived. Equation 9 relates wind speed and wave-phase speed. Noting from Table 1 that drag coefficients at standard elevation ($z_r = 10$ m) are typically in the range $C_D = u_*^2/U_r^2 \simeq 0.5 \times 10^{-3}$ to 3×10^{-3} , it is seen that $u_*/U_r \simeq 0.02$ to 0.05 . Comparing this with $u_*/C_0 \simeq 0.05$ indicates that the point of inconsistency in Kitaigorodskii's theory occurs when $C_0 \simeq U_r$. Arguments leading to Equation 9 essentially treat the sea surface as rigid and

moving at phase speed C . If $C = U$, then there would be not mean shear and, hence, no stress. Finite stresses were reported by Kitaigorodskii (1973) under these conditions so that additional physical mechanisms apparently become dominant when seas become more fully developed. His results suggest that his model is valid for initial and intermediate stages of growth as identified by the parameter u_*/C_o . The inverse of this, C_o/u_* , called the saturation parameter by Geernaert and Katsaros (1986), is considered significant for rejection of Kitaigorodskii's model when it is on the order of 20 or larger.

49. In the discussion of the work of Charnock and Kitaigorodskii, the surface roughness parameter z_o has been discussed in terms of six integral parameters associated with waves. They are: u_* , g , ν , C_o , σ_n , and λ_o . Along with z_o this forms a set of seven variables in which length and time are the only dimensions. From dimensional analysis a set of five dimensionless groups can be formed from these variables. Combinations formed from discussions above are $z_o g/u_*^2$ (Charnock's equation, if constant), $z_o u_*/\nu$ (dynamically smooth flow, if constant), C_o/u_* (saturation parameter), z_o/σ_n (Kitaigorodskii's initial wave growth formula, if constant), and σ_n/λ_o (wave steepness). This is a complicated set with different parameters or combinations of parameters important in different regimes, only a few of which have been discussed above. Other combinations of parameters have been proposed by other investigators.

50. For example, Hsu (1972) made wind-stress measurements over water of depth less than 5 m on the Florida coast of the Gulf of Mexico and found rather large drag coefficients (see Table 1). In consideration of water shallowness and its effect on wave steepness, he proposed (Hsu 1974, 1976) that Charnock's relationship be modified by the steepness of the dominant waves in the form

$$z_o \propto \frac{4\sigma_n}{\lambda_o} \frac{u_*^2}{g} \tag{15}$$

where $4\sigma_n$ is significant wave height assuming a Rayleigh distribution of wave heights. He did not test this expression in shallow water, but noted that for linear deepwater waves, $\lambda_o g = 2 \pi C_o^2$ such that Equation 15 becomes

22

$$z_o \propto \frac{4\sigma_n}{\lambda_o} \frac{u_*^2}{g} \qquad (16)$$

in deep water. Hsu (1974) evaluated this expression citing 19 sources, but only 34 data points, all from deepwater observations. Data were grouped in five ranges of values of the right side of Equation 16 and averaged geometrically. He found the mean values to correlate very well with Equation 16 using a coefficient of 1.0. Maximum deviation by mean values was about 20 percent. Standard deviations of the geometric averages of z_o were about half an order of magnitude, similar to what Kitaigorodskii (1973) reported for his intermediate stage roughness.

51. In a second test, Hsu (1976) found similar results from four additional sources. It is of interest to note that for most of the data cited in this test the saturation parameter was in the range $20 < C_o/u_* < 90$, i.e., a region where Kitaigorodskii's (1973) model was found to be inadequate. A major difference between the two models is that Kitaigorodskii's model becomes independent of C_o for $C_o/u_* \gg 1$, whereas, Hsu's model does not. This suggests that Hsu's model (or at least a continued dependence on C_o/u_*) may be more appropriate in the latter stages of sea development.

52. SethuRaman (1978) reports a dependence of drag coefficient on C_o/u_* from measurements in water depths of 33 m at a location 5 km from the south shore of Long Island. For C_o/u_* varying from about 15 to about 60, the drag coefficient (reference elevation $z_r = 8$ m) dropped from about 2×10^{-3} to about 0.5×10^{-3}. In accordance with Equation 7, a drop in C_D corresponds to a reduction in z_o . SethuRaman did not include σ_n in his analysis, so Hsu's model was not tested. There is sufficient scatter in the data to support the hypothesis of $C_d =$ constant for $C_o/u_* > 35$, i.e., C_D independent of C_o/u_* . Hence, these data support the ideas of general dependence of C_D on C_o/u_* , but cannot be used to distinguish validity for either Hsu's or Kitaigorodskii's model.

53. A theoretical and experimental treatment of these models was reported recently by Huang et al. (1986). In this work, they used Kitaigorodskii's definition of physical roughness, given here as Equation 13, coupled with a wave spectral definition for the band of frequencies for which waves are fully developed--known as the simplified Wallops spectrum

23

(Huang et al. 1981). This spectrum has the form

$$S(\omega) = \begin{cases} \dfrac{\hat{\varepsilon}g^2}{\omega_o^5(\omega/\omega_o)^m} & \omega \geq \omega_o \\[4mm] & \text{for} \\[4mm] 0 & \omega < \omega_o \end{cases} \tag{17}$$

where m is a function in the simplified Wallops spectrum

$$m = \left| \frac{\left[\log\left(2^{1/2} - \sigma_\eta/\lambda_o\right)\right]^2}{\log 2} \right|$$

$$\beta = (m - 1)(2\pi\sigma_\eta/\lambda_o)^2$$

and ω_o is the spectral peak frequency (in radians per second). The spectral shape is fixed when ω_o and σ_η/λ_o are specified. Again, by using the deep-water dispersion relation in the exponent of Equation 13, substituting Equation 17 in Equation 13 and integrating yields the general result

$$k_R = G\left(\frac{C_o}{u_*} , \frac{\sigma_\eta}{\lambda_o}\right) \cdot \frac{\sigma_\eta}{\lambda_o} \cdot \frac{u_*^2}{g} \tag{18}$$

where G , a function in the simplified Wallops spectrum, is defined as follows:

$$G = \left[\frac{\pi^2(m - 1)}{4\kappa^4} \left(\frac{2\kappa C_o}{u_*}\right)^{-m+5} \gamma\left(m - 1 , \frac{2\kappa C_o}{u_*}\right) \right]^{1/2}$$

where γ is the incomplete gamma function (Abramowitz and Stegun 1970).

54. Huang et al. (1986) note that although Equation 18 is a somewhat complicated function, the result relates two models through a third under the assumption $z_o \propto k_R$. To within a coefficient (assumed constant) the function $G\sigma_\eta/\lambda_o$ corresponds to Charnock's (1955) coefficient α in Equation 8. Also

24

to within a coefficient, the function G corresponds to a generalized coefficient for Hsu's (1972) model, given here as Equation 15. Both are found from Kitaigorodskii's (1973) integral.

55. The importance of the work of Huang et al. (1986) is that their spectral model, derived from other considerations, suggests one possible set of relationships among the dimensionless parameters $z_o g/u_*^2$ and σ_η/λ_o when incorporated in Kitaigorodskii's integral. It shows that generalized forms of both Charnock's and Hsu's models can evolve from this. On the other hand, it illustrates the sensitivity of Kitaigorodskii's roughness definition to the spectral form employed (compare Equation 18 with the result obtained above when Phillips' spectrum, Equation 14, is used). It is also restricted, as discussed above for Kitaigorodskii's results, to developing seas, i.e., $C_o/u_* \leq 20$, and to deepwater conditions.

56. The experiment program of Huang et al. (1986) had some curious features. They required a coefficient of proportionality between z_o and k_R , the latter represented here as Equation 18. To find this, they used data from a wind-wave tank. In one set of experiments, the relation k_R/z_o was found for waves generated by wind alone. In six other sets, paddle-generated waves of varying amplitude and spectral content were established in the water during wind-stress observations. Seven mean values, one for each set of runs, of k_R/z_o were found to lie in the range $11 \lesssim k_R/z_o \lesssim 30$ with a net mean $k_R/z_o \simeq 20$. This is close to $k_R/z_o \simeq 30$ for rough flow over uniform sand grains and well within the range $10 \lesssim k_R/z_o \lesssim 200$ described by Schlichting (1979) for less regular roughness. It is also close to the value $k_R/z_o \simeq 17$, found by Kitaigorodskii (1973).

57. However, for each of the seven sets of runs the standard deviation was large, varying from 41 to 123 percent of the mean, with a net standard deviation of 87 percent. Furthermore, there was a rough indication of a decrease in k_R/z_o for increasing background wave amplitude, though the scatter was so large that no statistical significance could be assigned to this. Huang et al. (1986) were careful to examine data having $C_o/u_* \lesssim 10$ which would correspond to initial wave growth regions in both their model and that of Kitaigorodskii (1973). In this regime z_o should vary with σ_η directly. The large scatter suggests either that the model is overly simple or that secondary effects in the experiment regime (horizontal nonuniformity, secondary flow in either air or water, unnatural side or end boundary conditions)

25

modified their results. The indicated variation with background wave conditions suggests that when wind and waves are not in equilibrium the effective surface roughness is modified.

58. The data of Huang et al. (1986), in combination with laboratory and field observations from eight other campaigns and when plotted in the form z_0/σ_η versus $(C_0/u_*)^{-1}$, show a distinct decrease with increasing C_0/u_* as was found by Kitaigorodskii (1973) and Hsu (1976). The scatter in z_0/σ_η is about one order of magnitude as has been noted also in results of these latter two investigations. The model results of Huang et al. (1986) pass through these data and so are viable. It is noted, however, that the data source for the largest C_0/u_* used by Huang et al. (1986) is the same as was used by Hsu (1976) so that within the variability of the data the two models are indistinguishable.

Model Comparisons, Observations, and Additional Parameters

59. In an effort to compare several models for drag coefficients, Geernaert, Katsaros, and Richter (1986) conducted wind stress and wave measurements from a fixed mast in water of 16-m depth located 28 km offshore of West Germany in the North Sea. In this study they noted that tides, waves, and wind all induce mean currents such that the water surface mean flow boundary condition is not $U_0 = 0$ in Equations 5 and 6 as has been assumed in all investigations discussed above. They estimated U_0 from tidal theory, local tide records, and estimates of sea-surface slope. The drag coefficient was then estimated from mean wind speed, the component of U_0 in the direction of the wind and measured wind stress using Equation 6, first equality. Data they used were constrained to speeds above 6 m/sec from a direction of infinite fetch and were also corrected for atmospheric stability as discussed below. Six models of z_0 were then tested by incorporation in Equation 6, second equality, and comparison with measured values of C_D . Comparison was done in several ways, and in each case the models of Charnock (1955) (Equation 8), Kitaigorodskii (1973) (Equation 13), and Hsu (1974) (Equation 15) performed best based on mean square deviation from measurements. Measured rather than idealized wave spectra were incorporated in Kitaigorodskii's model.

60. In the first comparison, the single free coefficient required for each model was determined from the author's own work or from published best

26

estimates from other investigators. For example, Charnock's α of 0.0144 from Garratt (1977) and 0.0185 from Wu (1980) were both compared. In this test, Charnock's model with $\alpha = 0.0185$ and Hsu's model had the lowest root mean square (RMS) differences of about 10 percent of the mean measured drag coefficient given by Geernaert, Katsaros, and Richter (1986) (this was $C_D \approx 1.6 \times 10^{-3}$). Charnock's model with $\alpha = 0.0144$ was off by about 12 percent and Kitaigorodskii's model was off by about 27 percent. In this test the measured C_D adjusted for the estimated drift current (but not the tidal current, for an unexplained reason) to be nearer the zero-drift surface velocity assumed by the modelers.

61. In the second test, the coefficients were allowed to vary to minimize differences between models and observations. Again, zero-drift surface velocity was assumed. Charnock's coefficient was found to be 0.0192, Hsu's coefficient went from 1.00 to 0.83, and Kitaigorodskii's $z_o = k_R/30$ became $z_o = k_R/106$. With these adjustments all three models had about 10 percent RMS differences from observations.

62. In the third test, surface drift velocity was included, and best fit coefficients were computed again. In this test, the models still had about 10-percent RMS differences from observations, but the coefficients changed. Charnock's α became 0.0288, Hsu's coefficient became 1.76, and Kitaigorodskii's z_o became $k_R/71$.

63. Evidently, the presence of surface currents has an effect on model results. This may account for some of the scatter in results discussed above where surface currents were not considered. This also suggests that, in regions where surface currents are strong, as occurs frequently nearshore, such effects need to be incorporated in both observations and models.

64. Geernaert, Katsaros, and Richter (1986) conclude that Kitaigorodskii's formulation performed best, to within a coefficient, but that results are too close to make a strong distinction among the various models. As they note, their data are from one site, are limited in number (53 points were used), and are limited in range of wind speed (6 m/sec $\lesssim U_r \lesssim$ 20 m/sec). Additional, careful field observations are required to discern the best of existing models.

65. However, Geernaert, Katsaros, and Richter (1986) point out two additional characteristics of their observations that may be of great importance in coastal and other shallow-water environments. The first of these is

27

temporal variability of the drag coefficient and the second is an apparent tendency for drag coefficients to increase in shallow water.

66. As regards the first effect, Geernaert, Katsaros, and Richter (1986) made additional measurements after their primary experiment at a time when their wave-measuring devices had been removed. Detailed observations were made at ti surrounding the passage of a storm front wherein wind changed direction by roughly 60 deg and speed dropped from about 20 m/sec to about 12 m/sec in the course of about 2 hr. Since they lacked sea state information, they predicted a drag coefficient based on a regression of measured drag coefficients on wind speed difference (10-m wind speed minus water surface speed) from their primary experiment. These data had about 10-percent scatter about the regression line. However, when they compared predicted C_D during the frontal passage, they found variations of ± 20 percent, which is significant.

67. Other observers have reported similar findings. SethuRaman (1978) reported a 100-percent change in drag coefficient in the course of 2 hr when wind changed direction by about 80 deg. His observations included some wave information. He noted that when the sea was in the process of adjusting to the new wind direction, the saturation parameter (C_o/u_*) rose from about 13 immediately following the wind shift (when C_D doubled) to about 25 an hour later when C_D dropped again. This behavior is qualitatively consistent with models discussed above (all of them, in fact, excepting Charnock's model) wherein C_D depends strongly on C_o/u_* .

68. A third observation is described by Boyle, Davidson, and Spiel (1987) based on an experiment in deep water in the Gulf of Alaska. They also estimated C_D from a purely wind-speed-dependent model (Large and Pond 1982), corrected for atmospheric stability, and used this to estimate wind stress. Measured wind stresses were then compared with estimates. They found very good correlation between the two during steady wind conditions. However, immediately preceding passages of large-scale weather systems (fronts, pressure troughs, and pressure ridges) they observed that measured stresses exceeded predicted stresses by a factor of two to three. They conclude that adjustments of sea state (of which they had no quantitative observations) are extremely important in unsteady conditions.

69. The importance of these observations to modelers of waves and currents is twofold. It is common practice in modeling to employ a wind drag

28

coefficient based on wind speed alone (see, e.g., Sheng and Butler (1982) or Hubertz (1987)). Many investigations have proposed formulae for such dependence. A few of these have been referenced in this report: Hsu (1972), Garratt (1977), Wu (1980), Amorocho and DeVries (1980), and Large and Pond (1982). However, if wind stress depends on other parameters, such as those associated with sea state, then the more elementary models will be incorrect at least part of the time. The times at which such models are likely to be remiss are those of most importance in coastal dynamics, i.e., during storms, where observations noted above indicate large variations in C_D . Clearly, further research is needed to relate C_D to sea state and wind speed, either to verify existing models or to identify parametric dependencies not yet proposed.

70. The other important consequence of temporal variation is a little more heuristic but, nonetheless, plausible. The changes in C_D observed during rapid changes in wind conditions suggest that C_D will vary whenever wind and waves are not in equilibrium. The models described above were almost entirely in consideration of unobstructed, steady winds acting in the initial and intermediate stages of wave growth in deep water and with wind primarily in the direction of wave propagation. If the wind changes direction alone then there will be a tendency for a modification of the existing sea and initiation of a sea in the new wind direction.

71. A simplified application of this idea can be used in conjunction with Kitaigorodskii's (1973) model as represented by Equation 9. If the wind speed is, say, twice the phase speed such that $U = 2C$ and $U - C = C$, then a simple 180-deg reversal of wind causes $U - C = -2C - C = -3C$ since the wave phase speed vector is now opposite the wind vector. The ratio of magnitudes of relative winds is a factor of 3. The square of this is roughly the ratio of stresses, which is 9, with the larger stress acting until the sea adjusts to the new wind direction. While this is an oversimplification of the problem, the qualitative concept is clear.

72. A similar effect would be expected for wind waves entering or being generated in shoaling waters such as coastal regions. Water of finite and spatially varying depth is known to modify waves independently of the wind and so can change the equilibrium conditions described above for wind acting in deep water. First, wavelengths decrease so that even if wave heights are constant, the wave steepness increases. This means that if Hsu's (1974) model,

29

Equation 15, is correct, then surface roughness and therefore the drag coefficient increases. Second, phase speeds (at least of some waves) are modified by finite depth. In the limit of shallow water, all phase speeds are $C = (gd)^{1/2}$ where d is water depth. In Kitaigorodskii's (1973) model, Equation 12, C is then no longer a function of ω so the weighting function can be removed from Equation 13. The solution of Equation 13 is then

$$k_R = 2\sigma_\eta \, e^{-\kappa(gd)^{1/2}/u_*} \tag{19}$$

Since shallow-water phase speeds are always less than deepwater phase speeds at the same frequency, then k_R (and C_D) will tend to increase in shallow water (for the same σ_η) by this model.

73. A third effect occurs if the wind is not parallel to the gradient of the bottom. In this case, at least some waves will propagate by refraction in a direction different from the wind. It is difficult to make a hypothesis about how this affects wind stress. In the case of nearly shore-parallel winds, the dominant wave crests can be nearly parallel to the wind such that the component of dominant wave-phase speed vector in the direction of wind is negligible. This suggests that C_o/u_* may drop out of the problem such that both directional and spectral characteristics of high-frequency waves are important. There are no direct, quantitative observations of these effects. This lack of knowledge emphasizes the need for a field program specifically designed to examine wind stress in shallow water under a variety of measured wind and sea conditions.

74. A fourth effect is that wind- and wave-induced currents, which can reach to a depth on the order of 30 m in deep water (Long 1981), as well as tidal and other currents all extend through the whole water column in shallow water and so are affected by the bottom. Bottom friction tends to retard the flow. Wave radiation stresses tend to drive alongshore flows of cross-shore varying intensity. All of these effects are different from deepwater behavior and so will affect U_o in Equations 5 and 6 with a consonant effect on C_D. Note that the retarding effect of bottom friction on purely wind-driven mean flow will reduce U_o in shallow water and, by Equation 6, increase C_D.

75. A fifth effect is a constraint on σ_η in shallow water. There is a tendency for waves to break when wave height and depth are of the same

order. Surface roughness estimates based on sea surface variance, Equation 19 for example, would then be reduced. Hence, C_D would be expected to be smaller in the breaker zone than in deep water due to   is effect.

76. There is little direct evidence of a quantitative relationship between C_D and water depth though there is some indirect evidence that water depth is important. The large C_D found by Hsu (1972) (see Table 1) in very shallow water may be due to shoaling effects. Storm surge models sometimes require larger wind stress coefficients to correspond with observations.* Geernaert, Katsaros, and Richter (1986) noted that their regression of C_D on wind speed had larger values at high wind speeds than curves derived from observations by Garratt (1977) and Large and Pond (1981). These latter two investigations were in the open ocean whereas Geernaert, Katsaros, and Richter (1986) made their observations in 16-m water depth. Their observations compared favorably with several other investigations in shallow water of similar depths. They conclude that C_o/u_* is an important parameter in coastal regions because C_o depends implicitly on depth and also on fetch which is often considered an important parameter of wind stress (Wu 1980).

77. While there is some merit in the above conclusion, the complete coastal problem may be more complex in light of possible misalignment of winds and dominant waves due to shoaling, as mentioned above. In this case, wind stress may depend not only on the variance in the wave frequency band most strongly coupled to the wind but also on the way in which these waves are modified by (if they are not identical to) other waves, particularly low-frequency waves, in the spectrum. If low-frequency waves are important to wind stresses, then their effect will be more dramatic in shoaling water because they are affected by the sea bottom in deeper water than are higher frequency waves.

78. There are two scaling arguments which suggest that dominant wind input to waves occurs at frequencies equal to or higher than the spectral peak frequency. The first of these is based on Kitaigorodskii's integral, Equation 13, using Phillips' spectrum, Equation 14. As discussed by Geernaert, Katsaros, and Richter (1986), the frequency of maximum contribution to surface roughness can be found by differentiating the integral of Equation 13 with

---

* Personal Communication. H. Lee Butler, 1987, Chief, Research Division, Coastal Engineering Research Center, US Army Engineer Waterways Experiment Station, Vicksburg, MS.

31

respect to . setting the result equal to zero, and solving for ω , the
result here being called ω_{max} . Using Equation 14, this yields ω_{max}
$= 0.4 \kappa g / u_*$. In deep water, the spectral peak phase speed C_o is related to
peak frequency ω_o by $C_o = g / \omega_o$. From this, $\omega_o = g / C_o$. The ratio of
these frequencies is $\omega_{max} / \omega_o = 0.4 \kappa C_o / u_*$. Since Equation 14 allows no vari-
ance for $\omega < \omega_o$, then $\omega_{max} = \omega_o$ for $0.4 \kappa C_o / u_* < 1$ or $C_o / u_* \lesssim 6$ (for
$\kappa \simeq 0.4$). This corresponds roughly to the initial stages of wave growth as
identified by Kitaigorodskii (1973) (wherein $z_o \propto \sigma_\eta$) and the region identi-
fied by Huang et al. (1986) using the simplified Wallops spectrum $(1 < C_o / u_*$
$< 10)$, where, likewise, $z_o \propto \sigma_\eta$. In the latter stages of wave growth, where
$C_o / u_* \simeq 20$, the ratio of frequencies becomes $\omega_{max} / \omega_o \simeq 3$. This result sug-
gests that for much of wind wave growth in deep water $\omega_{max} > \omega_o$ and the pri-
mary contribution from wind occurs at frequencies higher than the spectral
peak.

79. The second argument arises from the model of Charnock (1955) and is
discussed by Wu (1980). If $z_o = \alpha u_*^2 / g$, with α in the range $0.01 \leq \alpha$
≤ 0.03 , and if $z_o \propto k_R$ (i.e., dynamically rough flow) with the ratio z_o / k_R
broadly in the range $1/10 \leq z_o / k_R \leq 1/200$, as discussed previously, then k_R
will be in the range $0.1 \, u_*^2 / g \lesssim k_R \lesssim 6 \, u_*^2 / g$. Furthermore, if k_R is
representative of the heights of waves at saturation, i.e., at a limiting
steepness of $k_R / \lambda \simeq 1/7$ (Kinsman 1984), then the wavelength λ is in the
range $0.7 \, u_*^2 / g \lesssim \lambda \lesssim 42 \, u_*^2 / g$. In deep water, λ can be expressed in terms
of phase speed C as $\lambda = 2 \pi C^2 / g$. If this is inserted in the previous
expression, the ratio C_{max} / u_* , where C_{max} is the C of maximum interac-
tion, is found to be in the range $0.3 \lesssim C_{max} / u_* < 2.6$. That is, under the
assumptions given, the waves which contribute to Charnock's roughness scale
all have phase speeds C_{max} of order u_* . Since C_o / u_* based on spectral-
peak phase speed can be equal to or larger than this (values to at least
$C_o / u_* \simeq 20$), then $C_o / C_{max} \gtrsim 1$. From this, $(g / \omega_o) / (g / \omega_{max}) = \omega_{max} / \omega_o \gtrsim 1$
such that contributing frequencies can be equal to or up to 20 times the spec-
tral peak frequency.

80. This last scaling argument, with the result that $C_{max} \simeq u_*$, has a
consequence which could possibly introduce another parameter into the problem.
According to linear wave theory, if surface tension is included with gravity
as a restoring force, then there occurs a minimum in wave phase speed which is
on the order of 0.2 m/sec (Kinsman 1984). This corresponds to a wavelength of

about 1.7 cm for typical air-water interfacial surface tension. Phase speeds increase rapidly for shorter wavelengths (pure capillary waves) and increase more gradually for longer wavelengths (pure gravity waves). For C_{max}/u_* $\simeq 1$, then u_* must be about 0.2 m/sec before momentum exchange occurs with roughness characterized by Charnock's model (subject, of course, to limitations in the above scaling arguments). At lower u_* surface roughness may be characterized by the dynamically smooth regime ($z_o \propto \nu/u_*$) or possibly by a combination of this with scales associated with pure capillary waves.

81. A value of $u_* = 0.2$ m/sec corresponds to 10-m wind speeds of 5.6 m/sec $< U_r < 6.2$ m/sec using Charnock's z_o with α in the range $0.01 < \alpha < 0.03$. For wind speeds lower than this, one might expect a variation in characterization in surface roughness which would have an effect on drag coefficient estimates. At higher wind speeds, which are generally the wind speeds of interest, u_* increases. If $C \propto u_*$, then wave phase speeds of interest are more nearly those of pure gravity waves.

82. Munk (1955), Phillips (1969), Wu (1980), Kinsman (1984), and others have discussed the importance of capillary waves (in which surface tension is important) in wave growth. Munk (1955) and Geernaert, Katsaros, and Richter (1986) cite experiments in which a reduction in surface tension (by addition of detergent or by biological activity) serves to reduce C_D in general. By the above scaling a reduction in surface tension reduces the minimum phase speed which corresponds to a smaller u_* (for $u_* \propto C$). This leads to a smaller z_o by Charnock's model and, by Equation 6, to a smaller C_D . This should affect primarily C_D for winds with u_* near this minimum phase speed. If it affects C_D for a wider range of wind speeds, then this suggests that the presence of capillary-gravity waves is more generally important in air-sea interaction. As Wu (1980) points out, this has not been fully resolved yet. It is less important if surface tension (and therefore the minimum wave phase speed) is constant. However, in coastal waters subject to seasonal planktonic blooms and riverborne surfactants (biological or otherwise) surface tension may vary significantly. It should then be considered a potentially important parameter in nearshore drag coefficient estimation.

83. Whether of capillary nature or not, the waves interacting most strongly with wind are generally at higher frequencies than the spectral peak frequency by the above scaling arguments. The models of Kitaigorodskii (1973) and Hsu (1974), both justified with experimental evidence, predict a decrease

33

in the ratio z_0/σ_η for increasing C_0/u_* . Since σ_η is the total variance of sea-surface displacement, this result simply means that low-frequency waves, especially those moving at near the mean wind speed, contribute less effectively to total surface roughness. This argument applies in deep water where wind and waves of all frequencies are moving in roughly the same direction. In shallow water, where low-frequency wave phase speeds are retarded and their directions are altered by refraction, it is possible that more or less of the total sea-surface variance will contribute to the effective roughness. If long waves are slowed and are in the wind direction, it is expected that z_0 and therefore C_D will increase relative to the deepwater case. If long waves have refracted so their direction of propagation is normal to the wind direction, it is possible that they make no contribution to surface roughness (if long crested, so no bluff surface is presented to the wind) or that they make maximum contribution to surface roughness (if short crested, so that larger surface displacements are effectively unmoving in the wind direction).

84. Clearly, the net effect depends critically on the wind direction and the detailed frequency distribution of wave propagation directions and variances, i.e., the directional wave spectrum. The arguments leading to this dependence are based on extensions of arguments applied to deep water and are therefore, hypothetical. Verification of these hypotheses requires observations. To date, no experiment testing the dependence of C_D on the directional spectrum in shallow or coastal waters has been found to be reported in the literature. This is one of the primary reasons for conducting the research program described in this report.

85. In summary, this section describes some of the previous work leading to formulations of the dependence of the drag coefficient on various observable parameters related to dynamics of both air and water for steady, uniform conditions in the deep ocean. All the models discussed showed C_D to depend solely on a characterization of the surface roughness parameter z_0 . The models suggest z_0 depends variously on the parameters ν , g , σ_η , C_0 , u_* , and, possibly, surface tension. Observed variations of these models for shallow water, changes in sea state, and variation of surface currents suggest that additional parameters are necessary. Extensions of arguments leading to and derived from the deepwater models indicate the nature of the added parameters. They are direction of reference wind θ_r , water

34

surface velocity U_o and its direction θ_o , water depth d , and replacement of σ_n and C_o with variances and phase speeds in frequency and directional bands, i.e., $\sigma_n(\omega,\theta)$ and $C(\omega,\theta)$, respectively. Dependence of C_D on these added parameters is to be determined empirically through detailed observations. Simplified formulae for purposes of application can then be derived from the empirical correlations.

PART III: PROCESSES WHICH MODIFY THE LOGARITHMIC PROFILE

86. The models described in Part II all depend critically on the existence of the logarithmic wind profile, Equation 5, as derived from the dimensional arguments leading to Equation 4. For Equation 5 to be valid, the flow and boundary conditions must be horizontally uniform and steady. Further, the air density must be constant. Violations of these conditions impart added variables to the flow dynamics and can modify the wind profile shape. In this case different wind stresses can occur for the same reference wind speed so that errors occur when a drag coefficient is used with wind speed to estimate stress. It is important, therefore, to account for processes which modify the wind profile. Improved accuracy is obtained where this can be done quantitatively. Where this cannot be done, qualitative uncertainty or limits of applicability of the model can be assigned.

87. The three general conditions listed above, density variations, unsteadiness, and nonuniformity, are discussed in this section. Reasonably good estimates can be made of the effects of density variation, and these are described first. Qualitative arguments on the effects of the remaining two conditions are then presented.

Stratification

88. Air density can vary in both space and time. For steady, uniform flow the primary effect of density variations in the surface layer of the atmospheric boundary layer is due to changes of density in the vertical direction. If density changes in the vertical direction, two effects occur. First, turbulence processes are altered due to buoyancy effects and, second, a flux of mass tends to occur. Buoyancy inhibits vertical turbulent motions under stable conditions (density decreasing upward) since fluid elements displaced upward tend to be more dense than the surrounding fluid such that gravity acts to retard their upward motion. Fluid elements displaced downward tend to be less dense than the surrounding fluid such that buoyancy retards their downward movement. Under unstable conditions (density increasing upward) buoyancy forces tend to enhance vertical motions. Mass flux occurs because there is a gradient in density which tends to cause diffusion. The mass fluxes of interest here are turbulent fluxes. Purely molecular fluxes are

generally much smaller. Relationships are thus sought which show the effect of stratification on the mean velocity profile and the fluxes in terms of measurable mean state variables.

89. One of the more successful theories leading to such relationships is the Monin-Obukhov similarity theory (Tennekes and Lumley 1972). Guidance for modification of the mean velocity profile by stratification is provided by the turbulent kinetic energy equation, derived from the total fluid kinetic energy equation by Reynolds averaging. For steady, homogeneous flow in the x-direction, this equation is

$$\overline{u'w'} \frac{\partial U}{\partial z} = -\varepsilon - \frac{g}{\rho} \overline{\rho'w'} - D \tag{20}$$

where

ε = viscous dissipation rate of turbulent kinetic energy

ρ' = fluctuating density

D = turbulent kinetic energy gradient diffusion term

The left side of Equation 20 represents production of turbulent kinetic energy. The first term on the right of Equation 20 is a symbol that stands for viscous dissipation of turbulent kinetic energy. Its formal expression is

$$\varepsilon = \nu \sum_{i=1}^{3} \sum_{j=1}^{3} \overline{\frac{\partial u'_i}{\partial x_j} \frac{\partial u'_i}{\partial x_j}} \tag{21}$$

where

u'_i = u' , v' , or w' , respectively, for $i = 1$, 2 , or 3

x_j = x , y , or z , respectively, for $j = 1$, 2 , or 3

It represents the conversion of turbulence to heat by the small-scale, high-frequency mean-square strain rate at which molecular viscosity is effective. The second term on the right of Equation 20 embodies the direct effect of buoyancy in the turbulent energy balance. It acts as a source or a sink term depending on the sign of $\overline{\rho'w'}$. The last term on the right of Equation 20 is called the diffusion term and is given by

$$D = \frac{1}{\rho} \frac{\partial}{\partial z} \overline{w'p'} + \frac{\partial}{\partial z} \overline{w'e'^2} \qquad (22)$$

where

p' = fluctuating pressure

$e'^2 = 1/2(u'^2 + v'^2 + w'^2)$, the instantaneous turbulent kinetic energy per unit mass

It is called the diffusion term since it contains gradients of turbulent properties. It is very difficult to quantify because fluctuating pressure and triple velocity correlations are difficult to measure. It is generally considered negligible in unstratified flow and more dominant in stratified flow (Long 1981, Frenzen 1983).

90. Equation 20 can be converted to usable form by rewriting its components in terms of measurable quantities. For the buoyancy term, the densities can be converted to measurable quantities through an equation of state for air. This is

$$p = \rho R_a T_v \qquad (23)$$

where

p = total atmospheric pressure

R_a = modified ideal gas constant

T_v = virtual temperature

Virtual temperature is an atmospheric state variable which includes the effects of both sensible (thermometric) temperature and humidity. In terms of measured temperature and humidity, the virtual temperature is

$$T_v = T(1 + 0.61q) \qquad (24)$$

where

T = air temperature, $^\circ K$

q = specific humidity, kg of water/kg of air

A summary of temperature, humidity, and pressure relationships is given by Blanc (1985). Expanding Equations 23 and 24 in terms of mean and fluctuating parts, averaging, subtracting the averaged equations from the expanded

38

equations, dividing by the averaged equations, and retaining the dominant terms yields, to within about 1 percent,

$$\frac{\rho'}{\overline{\rho}} \simeq - \frac{T'_v}{\overline{T}_v} \tag{25}$$

where

$T'_v \simeq T' + 0.61\overline{T}q'$

= fluctuating virtual temperature to within about 1 percent

T' = fluctuating (sensible) air temperature

$\overline{T}$ = mean (sensible) air temperature

q' = fluctuating specific humidity

$\overline{T}_v \simeq \overline{T}(1 + 0.61\overline{q})$

= mean virtual temperature to within about 1 percent

$\overline{q}$ = mean specific humidity

91. The buoyancy term in Equation 20 can be written using Equation 25 to yield

$$-\frac{g}{\overline{\rho}} \overline{\rho'w'} = \frac{g}{\overline{T}_v} \overline{w'T'_v} \tag{26a}$$

$$= \frac{g}{\overline{T}_v} (\overline{w'T'} + 0.61 \, \overline{T} \, \overline{w'q'}) \tag{26b}$$

Equation 26a shows the buoyancy term as a function of the flux of virtual temperature. Equation 26b shows it in terms of the actual fluxes of temperature and water vapor.

92. In Monin-Obukhov theory (Tennekes and Lumley 1972), turbulent fluxes of mass and momentum are all considered to vary weakly with z from the top of the sublayer through the surface layer in the same way that the model for neutral flow was derived. Thus, $u_*^2 = - \overline{u'w'}$ as before. When this is used with Equation 26a in Equation 20 and the result is normalized with the expression $\kappa z/u_*^3$, then a result similar to Equation 4 is obtained. This has the form

39

$$\frac{\kappa z}{u_*}\frac{\partial U}{\partial z} = \frac{\kappa z \varepsilon}{u_*^3} - \frac{\kappa g z \,\overline{w'T'_v}}{\overline{T}_v u_*^3} + \frac{\kappa z D}{u_*^3} \tag{27}$$

where the terms are in the same order as in Equation 20. The term on the left of Equation 27 is a dimensionless shear. In unstratified flow there is no mass flux and the diffusion term is considered negligible. In this case the term on the left is equal to unity by Equation 4. The only remaining term in Equation 27 is the dissipation term (first term on the right) which must also be unity by identity. Thus,

$$\varepsilon = \frac{u_*^3}{\kappa z} \tag{28}$$

is a reasonable estimate of dissipation in neutral flow.

93. When the flow is stratified, the second term on the right of Equation 27 becomes important. It can be written as $-z/L$ where $L = -u_*^3 \,\overline{T}_v / \kappa g \,\overline{w'T'_v}$ is called the Monin-Obukhov length scale. Stratification is important when L is of the same order as z in the surface layer. Note that $L \to \infty$ $(z/L \to 0)$ when there is no mass flux, i.e., in neutral conditions. The effect of stratification on dissipation and diffusion is not generally understood so Equation 27 cannot be used directly to resolve the effect on $\partial U/\partial z$. However, it suggests that the dimensionless shear is a function of z/L in the form

$$\frac{\kappa z}{u_*}\frac{\partial U}{\partial z} = \phi_m\left(\frac{z}{L}\right) \tag{29}$$

with $\phi_m(0) = 1$ to correspond to Equation 4. The form of ϕ_m must be determined empirically. Note that the assumption of dependence of z/L above is the simplest assumption that can be made based on Equation 27. If verified experimentally, the assumption can be said to be justified.

94. In the same sense that the turbulent kinetic energy equation is an equation for the rate of change of variance of the total velocity field, equations for the variances of temperature and humidity can be derived by Reynolds

averaging the mass conservation equations. Relationships between fluxes and gradients of temperature and humidity similar to that for momentum (Equation 27) are then found. The assumption of z/L dependence of the fluxes then requires formulae for temperature and humidity similar to Equation 29. They take the forms

$$- \frac{u_* z}{\overline{w'T'}} \frac{\partial \overline{T}}{\partial z} = \phi_T\left(\frac{z}{L}\right)$$

(30)

and

$$- \frac{u_* z}{\overline{w'q'}} \frac{\partial \overline{q}}{\partial z} = \phi_q\left(\frac{z}{L}\right)$$

(31)

where

ϕ_T = dimensionless mean temperature gradient

ϕ_q = dimensionless mean humidity gradient

95. Empirical expressions for ϕ_m , ϕ_T , and ϕ_q have been proposed by numerous investigators from observations over land. There is no reason to believe that the fundamental physics is different over water, so reliable land-based models should be applicable at sea. One set of expressions which has found broad support in independent experiments and which is used widely has the general form for stable conditions (z/L > 0)

$$\phi_m = 1 + a_1 \frac{z}{L}$$

(32)

$$\phi_T = \phi_q = a_2 + a_3 \frac{z}{L}$$

where a_1 , a_2 , and a_3 are dimensionless similarity model constants and for unstable conditions (z/L < 0)

41

$$\phi_m = \left(1 - b_1 \frac{z}{L}\right)^{-1/4}$$

(33)

$$\phi_T = \phi_q = b_2\left(1 - b_3 \frac{z}{L}\right)^{-1/2}$$

where b_1 , b_2 , and b_3 are dimensionless similarity model constants. There is agreement among several investigators on the functional forms given by Equations 32 and 33 but some disagreement on the values of the constants a_1 , a_2 , a_3 , b_1 , b_2 , and b_3 . Table 2 lists constants recommended by individual investigators. Note that von Karman's number κ is important as well by virtue of Equation 29.

Table 2

Constants Proposed by Various Investigators for the

Similarity Functions Given by Equations 32 and 33

Source	κ	Stable			Unstable		
		a_1	a_2	a_3	b_1	b_2	b_3
Dyer and Hicks (1970)*	0.41	--	--	--	16	1.00	16
Businger et al. (1971)*	0.35	4.7	0.74	4.7	15	0.74	9
Dyer (1974)	--	5	1.00	5	16	1.00	16
Lo and McBean (1978)*,**	0.40	--	--	--	--	--	--
Wierenga (1980)*	0.41	6.9	1.00	9.2	22	1.00	13
Dyer and Bradley (1982)	0.40	--	--	--	28	1.00	14

* Experiment considered only heat flux in stratification effects.
** With $\kappa = 0.40$ found results of Dyer et al. (1970) and Businger et al. (1971) to be statistically equivalent.

96. As noted by Dyer (1974), a basic difference between the results of Dyer and Hicks (1970) and Businger et al. (1971) is in the value of κ . A comparison of these two models for unstable stratification by Lo and McBean (1978) using the same data base as used by Businger et al. (1971) indicated consistency of results if $\kappa = 0.40$. A complete reanalysis of these data by Wierenga (1980) indicated a different set of constants if allowance is made for wind-flow distortion by the instrument platform. More recently, results of an independent experiment were reported by Dyer and Bradley (1982). They found constants which were very similar to those found by Wierenga (1980).

97. Uncertainty in the values of the constants represents either an

inadequacy of z/L as a similarity parameter or difficulties in making accurate measurements. Lo and McBean (1978) note that flux differences of 20 to 40 percent occur in comparing the models of Dyer and Hicks (1970) and Businger et al. (1971) with much of the difference due to differences in κ. They also note that similar differences can be incurred with a systematic 5-percent error in mean wind speed alone with no adjustment of temperature or flux measurements. This does not resolve the problem. It is usually assumed that the theory is adequate and that resolution of the constants awaits more refined experiments. Recent applied works use either Dyer's (1974) recommendations with $\kappa = 0.40$ (Large and Pond 1981, Geernaert and Katsaros 1986) or the recommended $\kappa = 0.40$ of Lo and McBean (1978) with the constants of Businger et al. (1971) (Blanc 1985, Wu 1986). Both approaches give similar results.

98. The advantage of these relationships is that they can be integrated to render relationships between fluxes and mean air and wind properties. Modification of the drag coefficient can then be estimated or, conversely, possible errors in results using an uncorrected drag coefficient can be estimated. The parameters added to the problem are minimal in number. They are mean air temperature $\bar{T}$ at reference elevation $z = z_r$, mean air temperature $\bar{T}_o$ at the air-sea interface $(z = z_o)$, mean humidity $\bar{q}$ at the reference elevation, and mean humidity $\bar{q}_o$ at the air-sea interface $(z = z_o)$. The latter quantity is often assumed to be the specific humidity corresponding to saturated air, i.e., 100-percent relative humidity.

99. Noting in Table 2 that all investigations yield $a_2 = b_2$ and assuming z_o is the same for all variables, Equations 29, 30, and 31 can be integrated using Equations 32 and 33 to yield

$$\bar{T}_o - \bar{T} = a_2 \frac{\overline{w'T'}}{u_*} \left[\ln \frac{z}{z_o} - \psi_T\left(\frac{z}{L}\right) \right] \tag{34}$$

$$\bar{q}_o - \bar{q} = a_2 \frac{\overline{w'q'}}{u_*} \left[\ln \frac{z}{z_o} - \psi_q\left(\frac{z}{L}\right) \right] \tag{35}$$

43

and

$$U - U_o = \frac{u_*}{\kappa} \left[\ln \frac{z}{z_o} - \psi_m \left(\frac{z}{L} \right) \right] \qquad (36)$$

where, in stable stratification $(z/L > 0)$,

$$\psi_m \left(\frac{z}{L} \right) = - a_1 \frac{z}{L} \qquad (37)$$

$$\psi_T \left(\frac{z}{L} \right) = \psi_q \left(\frac{z}{L} \right) = \frac{a_3}{a_2} \frac{z}{L} \qquad (38)$$

and, in unstable stratification $(z/L < 0)$,

$$\psi_m \left(\frac{z}{L} \right) = 2 \ln \left[\frac{1 + \left(1 - b_1 \frac{z}{L} \right)^{1/4}}{2} \right] + \ln \left[\frac{1 + \left(1 - b_1 \frac{z}{L} \right)^{1/2}}{2} \right]$$

$$- 2 \tan^{-1} \left[\left(1 - b_1 \frac{z}{L} \right)^{1/4} \right] + \frac{\pi}{2} \qquad (39)$$

$$\psi_T \left(\frac{z}{L} \right) = \psi_q \left(\frac{z}{L} \right) = 2 \ln \left[\frac{1 + \left(1 - b_3 \frac{z}{L} \right)^{1/2}}{2} \right] \qquad (40)$$

where

ψ_T = dimensionless integral of ϕ_T

$\overline{q}_o$ = mean specific humidity at the air-sea interface

ψ_q = dimensionless integral of ϕ_q

ψ_m = dimensionless integral of ϕ_m

The forms of Equations 39 and 40 were given by Paulson (1970). Equations 34 to 40 are all coupled through the variable z/L . In terms of measured properties (reference height, wind speed, water speed, temperatures, and humidities) and modeled surface roughness z_o , this variable is

44

$$\frac{z}{L} = - \frac{gz}{a_2\kappa} \frac{\left[\ln\frac{z}{z_o} - \psi_m\!\left(\frac{z}{L}\right)\right]^2}{\left[\ln\frac{z}{z_o} - \psi_T\!\left(\frac{z}{L}\right)\right]} \frac{\left[(\overline{T}_o - \overline{T}) + 0.61\overline{T}(\overline{q}_o - \overline{q})\right]}{\overline{T}(1 + 0.61\overline{Tq})(U - U_o)^2} \tag{41}$$

where ψ_T is used in the denominator to represent Equations 38 and 40. Equation 41 is transcendental in z/L and so must be solved by iterative approximation or through graphs or tables. Algorithms can be written readily to perform these calculations on a computer.

100. From Equation 36 a drag coefficient can be found as

$$C_D = \frac{u_*^2}{\left(U - U_o\right)^2} = \frac{\kappa^2}{\left[\ln\frac{z}{z_o} - \psi_m\!\left(\frac{z}{L}\right)\right]^2} \tag{42}$$

Comparison with Equation 6 shows the effect of stratification, for this model, to be due to the function $\psi_m(z/L)$ in the denominator of Equation 42. Note that transfer coefficients for temperature and humidity can be found from Equations 34, 35, and 42. They are not considered here because the primary concern is with momentum transfer.

101. To illustrate the importance of stratification in wind-stress estimates some computations were made using the equations given above. In this problem, wind stress (i.e., u_*) was held constant and air-sea temperature difference was varied from $-10°$ C to $10°$ C . No variation in humidity was considered. Estimates of 10-m elevation wind-speed difference and drag coefficient were then made. The constants used in the problem were those proposed by Wierenga (1980) as given in Table 2. Surface roughness was estimated by Charnock's model, Equation 8, with $\alpha = 0.02$, after Wu (1980).

102. Results are shown in Table 3 for two values of u_* . A low u_* (0.20 m/sec, corresponding to the minimum surface wave phase speed as discussed in Part II) and a somewhat higher u_* (0.90 m/sec) are indicated in Table 3. Results are somewhat dramatic in the low u_* case. For the temperature range shown the wind speed varies from 4.9 to 8.2 m/sec for the same stress (ρu_*^2). The corresponding drag coefficient varies by almost a factor of 3 from 0.6×10^{-3} to 1.7×10^{-3} . Conversely, this means that if

45

Table 3

Some Effects of Stratification on the Relation Between Wind Stress,
Wind Speed, and Drag Coefficient

$T_{air} - T_{water}$ °C	$u_* = 0.20$ m/sec		$u_* = 0.90$ m/sec	
	$U_r - U_o$ m/sec	$C_D \times 10^3$	$U_r - U_o$ m/sec	$C_D \times 10^3$
10	8.2	0.6	20.2	2.0
5	7.2	0.8	19.6	2.1
0	5.6	1.3	19.1	2.2
-5	5.1	1.5	18.7	2.3
-10	4.9	1.7	18.3	2.4

stratification effects are ignored, then wind stress estimates can vary by as much as 100 percent from true wind stresses at these wind speeds.

103. Less dramatic effects are seen for the higher u_* . In this case, the wind-speed difference varies by about 10 percent and the drag coefficient by about 20 percent over the temperature range shown. The reason for this can be seen in the basic definition of L following Equation 28. For about the same heat flux an increase in u_* gives a larger magnitude of L and so a smaller z/L at a fixed reference height. By Equations 32 and 33 a smaller z/L results in less effect by stratification. Wind speeds shown for the higher u_* are on the order of 20 m/sec and so are intermediate between low wind speeds and hurricane winds. At much higher wind speeds, effects of moderate temperature differences between sea and air are negligible according to this model.

104. These results suggest that stratification is important only part of the time over the full suite of conditions of interest in coastal dynamics. They should not be ignored, however, for at least two reasons. First, wind speeds less than 20 m/sec (for which stratification is important) are present for a far greater proportion of time than are higher wind speeds. Proper modeling of day-to-day wind-driven waves and currents along with processes which depend on these phenomena, such as mean sediment transport rates and long-term morphologic change, cannot be considered accurate if the primary forcing (i.e., wind stress) is unknown to within a factor of 3. Second, even in the evolution of large storm systems the wind during the initial stages of wave growth and wind fields at some distance from the region of maximum storm

winds are less than 20 m/sec. If the areal extent of these lesser winds is large relative to the area of intense winds, then the far field winds may do significant amounts of work on storm-driven waves and currents. The rate of doing work depends on the intensity of the wind stress. An uncertainty, by a factor of 3, will then have a significant effect on total storm response.

105. These arguments indicate that vertical variations in air density can have a significant effect on relationships between wind stress and wind profiles upon which drag coefficient formulae depend. The assumptions made for the flux-profile relationships presented here are among the simplest that can be made so the corrections to C_D must be considered of first order only. Verification of these effects by observations over land indicates that it is possible to reduce the uncertainity in C_D from about 300 percent to about 30 percent at low to medium wind speeds. This is a significant reduction. The remaining uncertainity must be considered to be the limit (due to physical arguments or observation techniques) of current understanding of this process. It is suggested that a complete model for wind-driven waves and currents must include consideration of stratification effects of the type presented here.

106. There are two other processes of air-sea mass exchange which are important dynamically at least part of the time. Their effects are beyond the scope of this report, but their existence is noted here for completeness. The first is precipitation. Particulate water condensed at some elevation above the sea surface and falling through the atmosphere accumulates vertical momentum from gravity and horizontal momentum from the air through which it falls. On striking the sea surface, some of this momentum is imparted to the sea surface either as a direct input to mean sea surface velocity or indirectly through the formation of splash waves, which would increase surface roughness. The addition of fresh water with a temperature different from sea temperature would also affect heat and humidity fluxes in the surface layer of the atmosphere. The second process relates to sea spray, of which significant amounts are exchanged with the atmosphere in very high winds. Its concentration should decrease with elevation above the sea surface so it would have a stabilizing effect (reduced C_D) based on gradients of total atmospheric density. A countering effect (increased C_D) occurs by accumulation of momentum in the spray from the wind and subsequent impact by the spray on the sea surface. The net effect of particulate water (rain and spray) in air-sea momentum exchange is not known. It may be important and so should be considered in future research.

47

Time Dependence

107. The relationship between the wind stress and the velocity profile, given in Equation 4, can be modified if the forcing of the system is strongly time dependent. This is important because momentum transfer to the sea surface is governed by flow dynamics (i.e., turbulence). If the turbulence cannot keep pace with changes in wind speed, then the velocity profile will be modified. Integration of the true velocity profile will then give velocities at a given reference elevation which are different from the integration of Equation 4. Use of observed wind speeds with drag coefficients based on the integration of Equation 4 will then be incorrect.

108. In steady, uniform conditions, the primary force balance in the atmospheric boundary layer is among Coriolis, pressure gradient, and fraction (stress divergence) forces. In natural systems, the pressure gradient is seldom steady. Fronts, centers of high and low pressure, and storm systems all migrate in time such that the boundary layer is almost constantly adjusting to new conditions. Such systems also vary in space, which means natural systems are not completely horizontally homogeneous. A complete treatment of natural systems requires modeling (or measuring) all terms in the governing equations, which is beyond the scope of this work. However, a simple scaling argument can provide at least an estimate of conditions where wind stress estimates from simple drag coefficient models can be considered reliable.

109. In typical numerical modeling of sea state evolution it is convenient to treat wind input at each time-step as if it were in an equilibrium steady-state force balance, even though the mean wind changes from one time-step to the next. That is, there can be a local flow acceleration $\partial U / \partial t$ due to an imbalance of the other forcing terms. Of importance is the magnitude of the acceleration necessary to cast doubt on the reliability of the velocity profile given by Equation 4.

110. One way to do this is to estimate the time scale of adjustment of the atmospheric boundary layer to a rapid change of forcing between two steady conditions. While the velocity scale u_* in steady flow is identified with the stress, it can also serve as a rough estimation of turbulent propagation rate. That is, a change of conditions at a point in the boundary layer can be considered to diffuse vertically away from that point at a velocity of about u_*. If the boundary layer has a thickness δ, then the time scale T_r for

48

a property to migrate from the boundary through the whole boundary layer thickness is $T_r \simeq \ell/u_*$. A typical boundary layer thickness is on the order of 1,000 m. For a reasonably small $u_* \simeq 0.2$ m/sec, the time scale is $T_r \simeq 5,000$ sec, which is slightly more than 1 hr.

111. For the shear $(\partial U/\partial z)$ in Equation 4 to be unchanged to, say, 10 percent, u_* must vary by less than 10 percent. If the drag coefficient stays about the same, then the wind speed must also change by less than 10 percent. If the acceleration is approximated as $\partial U/\partial t \simeq \Delta U/\Delta t$ with wind speed change $\Delta U \simeq 0.1 \, U_r$ and time scale $\Delta t \simeq T_r$ to represent the tolerable wind speed change in the time it takes for the boundary layer to readjust, then $\partial U/\partial t \simeq 0.1 \, U_r/T_r$. That is, if mean reference wind changes are on the order of 10 percent per hour or less, then time dependence can be neglected if allowance is made for a 20-percent uncertainty level in drag coefficient estimates.

112. Note that over the sea surface, a change in wind stress results in a change in sea state. This changes the surface roughness and, by Equation 5, the velocity. This effect is much less, however, than the change in u_* itself. This can be seen by using Charnock's model for z_o $(= \alpha u_*^2/g)$. A 10-percent change in u_* changes z_o by about 20 percent. Using Equation 5, the ratio of $(u_*/\kappa) \ln(z/z_o)$ to $(u_*/\kappa) \ln(z/1.2 \, z_o)$ is, with some manipulation of these expressions, about $1 + \ln(1.2)/\ln(z/z_o)$. This differs from 1 by approximately 1 percent for $z = 10$ m and $z_o = 0.01$ m. The difference is less for smaller z_o . Thus, the primary effect of a change in U of 10 percent is a change in u_* by about 10 percent with an additional change of about 1 percent or less due to change in roughness. This argument is subject to limitations on the applicability of Charnock's z_o and the assumption that sea state keeps pace with changes in wind stress. If sea state lags a change in wind speed (as it does because wind stress must work on the sea surface over a finite time to build or modify a sea), then change in roughness will be more gradual for moderate changes in wind speed. Dependence of z_o on C_o/u_* , as suggested in the models of Hsu (1974) and Kitaigorodskii (1973), is also affected slightly. A 10-percent change in u_* gives about 10-percent change in C_o/u_* . According to the work of Huang et al. (1986), which incorporates effects of both these models, a 10-percent change in C_o/u_* gives at most about an equivalent change of 10 percent in z_o/σ_η . By the logarithmic scaling above, the difference is still on the order of 1 percent or less in wind speed.

113. The boundary layer must also adjust if the wind changes direction. The magnitude of acceptable wind direction change can be estimated by assuming the wind speed constant and a change in direction such that the wind component in the original direction varies by less than 10 percent. This corresponds to an angle with a cosine of 0.9 or about 25 deg. If wind-stress direction follows wind direction, then surface roughness effects are of the same magnitude as given above.

114. Through these rough scaling arguments it appears that wind-stress estimates of about 20-percent accuracy can be attained for hour-to-hour wind speed changes of less than 10 percent and wind direction changes of less than 25 deg. If the mean wind changes by more than this, then larger errors will occur. The gross trend of the error can be anticipated, but its magnitude must rely on observations in the absence of a complete turbulence theory.

115. The argument concerning the error trend is based on the relative rates of growth and decay of the turbulence which couples wind shear and stress. In conventional turbulence theory (Tennekes and Lumley 1972) fluctuating flow properties exist over a broad range of frequencies and wave numbers. Turbulence is produced at large scales (i.e., sizes proportional to distance from the boundary) and dissipated at small scales where the fluctuating strain rate is high enough for molecular viscosity to convert turbulent energy to heat. The sizes of these small-scale motions can be estimated from Kolmogorov's scaling argument (Tennekes and Lumley 1972), which asserts that the length scale is based on the dissipation rate ε and kinematic viscosity ν. It takes the form $(\nu^3/\varepsilon)^{1/4}$. In steady, neutral flow it is often assumed that the rate of production of turbulence equals the rate of dissipation. This argument was noted above and resulted in Equation 28 wherein $\varepsilon = u_*^3/\kappa z$. Using this with typical values of atmospheric variables yields a dissipation length scale on the order of 1 mm at an elevation of $z = 10$ m. This is much less than the production length scale which is on the same order as z, i.e., 10 m.

116. Turbulence length scales intermediate between production and dissipation scales are assumed to relate to fluid motions interacting, through inertial processes, with motions at nearby scales. In this case, large-scale motions (or eddies) decay to small-scale motions at a rate governed by the magnitude of the dissipation term, but not by direct viscous processes. The variances at wave numbers associated with these length scales are said to be

in the inertial subrange of the turbulence spectrum. Because of the separation in scales of production and dissipation, there is a finite time required for large eddies to decay to heat. Production, on the other hand, is governed by the mean shear and the stress in accordance with the left side of Equation 20. If the mean shear changes, then the rate of production changes immediately even if the stress does not change. Once produced, the turbulent eddies reside at intermediate scales as they decay to scales small enough to be dissipated by viscous processes. Since this takes a finite time, there will tend to be residual turbulence even if the production term goes to zero.

117. The effect in the surface layer of the time-dependent boundary layer is to adjust rapidly to flow acceleration, but more slowly to flow deceleration. If the pressure gradient forcing the flow increases, the flow tends to accelerate. Because the flow at the boundary must move at the boundary velocity it does not accelerate as rapidly. This increases the shear at the boundary, which increases turbulent production of eddies. These act to exchange momentum with the boundary. Hence, the stress increases at the boundary. This retards the flow just above the boundary, increases the shear there, and thereby enhances momentum exchange. This readjustment moves outward from the boundary at a rate which can be estimated roughly by u_* and reaches reference elevation z_r in time z_r/u_*. For $z_r = 10$ m and $u_* \simeq 0.2$ m/sec, this is about 50 sec which is rapid relative to the readjustment time T_r of the whole boundary layer as discussed above. An anemometer at 10-m elevation would sense a high velocity relative to the new boundary stress for about a minute, and would then come into adjustment. If averaged for a time much longer than a minute, the anemometer output would be only slightly high for the new equilibrium boundary stress, based on a steady drag coefficient model.

118. On the other hand, if the pressure gradient forcing the flow decreases, then the flow decelerates and the shear at the boundary decreases. Though local shear production drops, the residual turbulence from the previous higher velocity flow continues to act to transfer momentum to the boundary. Until the residual eddies equilibrate to the new flow condition, the boundary stress will be higher than that deduced from the instantaneous velocity. Since eddies of the size of reference elevation from the boundary are distributed through the upper boundary layer flow, the time scale of readjustment is likely to be as long as T_r deduced above for readjustment of the whole boundary layer. Evidence of this behavior was provided in the extreme case of

oscillating boundary layer flow by Long (1981) in an analysis of water tunnel data reported by Jonsson and Carlsen (1976). In this case, the boundary stress behaved as if it were the product of one u_* based on the ensemble averaged instantaneous mean shear (i.e., from Equation 4) and another u_* based on the maximum mean shear. At times when the instantaneous mean shear was 20 percent of the maximum shear, the stress estimated from the velocity profile (i.e., Equation 5) was low by a factor of 5. This means that the scaling which led to Equation 4 is incorrect for this case and results deduced from it yield significant errors.

119. While natural atmospheric conditions are seldom this extreme, the results of the arguments presented here suggest that some caution should be exercised in application of drag coefficients to rapidly changing flow conditions. Data from experiments designed to obtain sequences of wind stress and mean velocity should be examined for biases in drag coefficient estimates during accelerating and decelerating flow. This can be done with data from an experiment like that described in Part V of this report.

Horizontal Nonuniformity

120. A flow is horizontally nonuniform if the forcing or boundary conditions vary in any horizontal direction. In such a flow, properties such as momentum or mass can accumulate or be depleted in a control volume by horizontal divergences of these properties. In this case the flux of momentum is not purely in the vertical direction, and so violates the assumptions leading to Equation 4.

121. In the case of air flow over coastal regions, conditions are never completely uniform. The primary cause of nonuniformity in such a system is the differences between wind flowing over land and wind flowing over water. Land has surface roughness elements which are generally fixed, of a broad variety of scales, and usually different from those of water. Land can have isolated, large-scale features which distort air flow in their vicinity and thereby cause local inhomogeneities. Sources of moisture and heat are different over land from those over water. This means that stratification effects which distort velocity profiles can cause horizontal variations in mean velocity. It also means that differential acceleration of air due to varying density (thermal wind) may be important. These features are in addition to normal

52

horizontal variability of large-scale weather systems which drive the wind.

122. Another effect which may affect horizontal uniformity over water is the change in roughness of the sea surface due to shoaling effects. That is, if shoaling-induced wave direction and steepness change induce strong horizontal gradients in z_o , then there will be a tendency for the mean wind to vary significantly.

123. It is important to obtain an idea of the areal extent of variations in flow properties which can lead to significant errors in drag coefficient estimates of wind stress. It is also useful to anticipate the nature of deviations so that such effects can be accounted for in observations.

124. Terms in the governing equations which become important in non-uniform flow are the advective terms of momentum, mass, and turbulence properties along with any added pressures necessary to divert flow around obstacles. A prominant advective term in the mean wind direction is $U\,\partial U/\partial x$ which represents the apparent acceleration due to advection of a wind field that varies in the x-direction. To estimate the size this term acquires before significant deviations of Equation 5 are incurred, a rough estimate is made of the horizontal distance required for the boundary layer to adapt to a change in conditions at the surface.

125. In the section on time dependence, a time scale $T_r = \delta/u_*$ was introduced as an estimate for temporal readjustment to a uniform change of surface condition. If a change occurs in space, then the new conditions will migrate outward from the boundary, as before, but will also be advected downwind. If U_r is a scale for wind speed, then the boundary layer adjusts in a distance of $\Delta x \simeq U_r T_r = U_r \delta/u_* = \delta/\sqrt{C_D}$. For δ on the order of 1 km and C_D in the range 1×10^{-3} to 4×10^{-3} , then Δx is on the order of 15 to 30 km. If it is required that wind speed varies by less than 10 percent over this distance such that $\Delta U \lesssim 0.1\,U_r$, then $U\,\partial U/\partial x \simeq U_r \Delta U/\Delta x \lesssim 0.1\,U_r/T_r$. Note that this is the same relationship as was found for time dependence. For a reference wind of 10 m/sec, this means that the wind must vary by less than 1 m/sec in 15 to 30 km.

126. While variations less than 1 m/sec may occur over the open ocean, this is a rather extreme requirement for coastal regions. A distance of 15 to 30 km encompasses the width of the coastal region in many locations. Resio and Vincent (1977), in a study of winds over the Great Lakes, noted that wind speeds over water were often 20 percent greater than wind speeds over land.

53

From this, it would appear that coastal regions are frequently subject to excessive nonuniformity. While this is true locally, the effect may not be as extensive as this gross scaling would suggest. For instance, if an onshore wind is uniform up to the beach such that boundary layer adjustments occur only inland, then the observations of Resio and Vincent (1977) would be supported and the air flow over the sea would be uniform. This is, in fact, suggested by the Shore Protection Manual (SPM) (1984) which recommends that wind measurements immediately adjacent to a water body are the same as winds over water for onshore flow. However, if sea state varies as the beach is approached or if the boundary layer begins to adjust upwind of the beach, then this hypothesis may be overly simple.

127. Several investigators have made valuable theoretical and empirical investigations into the relations between winds measured over land and winds that exist over water. Among these are Resio and Vincent (1977) and Hsu (1981, 1986). However, knowledge of the wind speed and direction over water is not sufficient to estimate accurately the wind stress over water, if the drag coefficient is not known or is applied in a region where it is invalid. The intent here is to identify regimes wherein the drag coefficient deduced from Equation 4 (or, as corrected for stratification, from Equation 29) is approximately valid. In these cases, reasonable wind-stress estimates can be expected from knowledge of wind speed, wind direction, sea state, and mean vertical density change, as discussed above. In cases where the simple model does not apply, wind stress will be related to a larger set of parameters.

128. In analogy with arguments given above for time-dependent flow, it is possible to assume that the atmospheric surface layer adjusts more rapidly to varying conditions than the whole boundary layer because of the close proximity of the boundary. In this case, the time scale for altered conditions at the surface to reach an elevation $z = z_r$ is z_r/u_* . The advective length scale for reference mean velocity U_r is $U_r z_r/u_* = z_r/\sqrt{C_D}$. For a 10-m reference elevation and C_D in the range 1×10^{-3} to 4×10^{-3} , this distance is on the order of 150 to 300 m (or 300 to 600 m for a reference elevation of 20 m). The constraint of less than 10-percent variation in velocity over distance of this order requires variation of less than 10 percent in u_* or z_r/L (for the stable case, i.e., the most sensitive) and roughly less than a factor of 2 in z_o for cases wherein only one of these variables is changing.

129. These constraints are much less stringent than those associated with readjustment of the whole boundary layer. It seems true intuitively that the constraints are met at least part of the time in open coastal waters. Exceptions would occur for very rapid spatial variation in forcing cr rapid change in bottom topography which leads to strong shoaling effects (wave steepening, refraction) over distances short compared with the advective length scale. As with time-dependent flow, differences would be expected in transitions over decreasingly rough surfaces compared with increasingly rough surfaces. If roughness increases in space, the turbulence is expected to keep pace (i.e., be locally in balance) since production rates are increasing. In cases of decreasing roughness, relict turbulence from upwind is expected to couple the wind more strongly to the sea surface so that the actual stress is higher than that deduced from a wind-speed-dependent drag coefficient.

130. Nearer to the coast, within several advective length scales of the beach, the flow may become more complicated. The surface roughness parameter z_c can increase by orders of magnitude over land as compared with over water. If roughness elements on land are not themselves on the order of the reference elevation z_r, then the problem is simplified somewhat. A primary variable in this case is the direction of the wind relative to the beach. Extreme cases are winds onshore and offshore. For onshore winds, the air flow is retarded as it progresses inland. While some effect is expected upwind of the beach, it is not expected to extend very far seaward. The reason for this is that the roughness over land (in this case) is not drastically different from that over water. If shoaling effects are not too abrupt, it can be expected that onshore winds can be considered uniform up to the beach.

131. If the wind is offshore (i.e., air moving seaward), then some variation in wind stress over water will occur. This is because turbulence from upwind is advected over water. This will be complicated by sea state. If there are no waves, then the air will tend to accelerate over the water. If a swell is running and z_o depends on wave amplitude and phase speed, then it is possible for the sea to be more rough than land. In this case, an offshore wind will decelerate over water. Such flows can still be considered uniform if the change in roughness does not incur a change in u_* or the characteristic fluctuating air density by more than 10 percent.

132. If these criteria are not met, then conditions can be considered nonuniform. Wind stress and velocity profiles will not scale together.

Accurate estimates of wind stress must then rely on more elaborate turbulence theory along with empirical correlations among measured field variables.

133. If the primary interest is in generation by wind of nearshore waves and currents, then nonuniformity of wind blowing offshore may not be important. Fetch and water-depth limitations result in much smaller wave and current generation close to a beach by winds blowing offshore than by winds blowing onshore. If offshore blowing winds are neglected in the interest of high-energy, wind-induced nearshore dynamics, then the problem is simplified somewhat. This is done here.

134. For onshore blowing winds, there are two additional conditions which can affect the assumption of uniformity near a beach. The first is the condition wherein physical roughness elements on land have a height scale much larger than nearshore waves. Sand dunes, buildings, trees, and mountainous cliffs are elements of this type. A wind encountering such elements from a smoother environment is diverted over or around them by pressure (form drag) forces on their upwind faces. The modification of mean streamlines is affected some distance upwind due to the incompressible nature of air at low Mach numbers. In analogy with flow around an isolated solid (Batchelor 1970), the streamline diversion can be assumed to exist at least three roughness heights upwind. Blanc (1983) cites work showing roughly 25 percent deviation of mean horizontal wind speed at least one roughness elevation upwind of the toe of an idealized beach with a 1:4 slope. Streamlines diverted upward will advect momentum out of the surface layer and thus reduce shear-induced momentum transfer to the sea surface.

135. The seaward effect of land roughness on horizontal uniformity over water depends on land roughness height (by this argument). Land of 5-m relief will not block the wind very far seaward. A stand of 30-m trees will have a direct influence roughly 100 m offshore. Low mountains of 500-m relief will affect the flow more than 1 km offshore. From this it can be seen that consideration of nearshore land relief can be of importance in estimating nearshore wind stress during times of onshore winds.

136. The second condition wherein nonuniformity may be important is related to the density field. If the vertical air density distribution over water is different from that over land, then a pressure gradient is induced across the intervening space due to the unequal weights of the two air columns. This baroclinic condition occurs frequently near the shore because the

boundary conditions for temperature and humidity can be very different for land as compared with the sea. A common cause of this is a differential response of land and sea surfaces to solar radiation. In this case, wind arising due to differential pressure is called sea breeze (or land breeze, depending on direction). It is usually transient, acting over less time than is required for geostrophic equilibrium, so winds tend to be directed down the pressure gradient, i.e., cross shore. If the phenomenon lasts for more than a few hours, then Coriolis effects will become important, and wind direction will vary.

137. If density differences result in forcing that is uniform with depth, then the effect is no different than a barotropic pressure field in the surface layer. As long as horizontal variations in barotropic pressure gradient are less than 20 percent in about 300 m (as discussed above), then the flow can be considered uniform. However, horizontal variations in density generally cause vertical variations in pressure gradient. The differential forcing in the vertical can cause shear ($\partial U/\partial z$) in the wind independent of any boundary layer effect. If this happens in the atmospheric surface layer, then reference wind speed can be altered without changing surface stress. If the change is significant, then reference wind coupled with a drag coefficient given by Equation 42 will give an incorrect estimate of stress.

138. The magnitude of this effect can be estimated from a simple force balance wherein flow acceleration is caused by a pressure gradient in the absence of friction. In this case,

$$\frac{\partial U}{\partial t} = -\frac{1}{\rho}\frac{\partial p}{\partial x} \tag{43}$$

If the pressure p is hydrostatic then $p = p_o - \rho g z$ where p_o is surface pressure (i.e., at $z = 0$). The horizontal gradient of this has two parts, one due to variation in surface pressure and the second due to horizontal variation in density. The magnitude of the second part is of interest here. This part causes Equation 43 to take the form

$$\frac{\partial U}{\partial t} = \frac{gz}{\rho}\frac{\partial \rho}{\partial x} = -\frac{gz}{T}\frac{\partial T}{\partial x} \tag{44}$$

where density variations are assumed to arise principally from temperature variations.

139. Equation 44 is z-dependent, indicating that in time increment Δt the velocity change ΔU at elevation z depends on gravity, a reference (absolute) temperature and the horizontal temperature gradient. Normal mean horizontal temperature gradients over land and over the open ocean are small enough to be neglected. Near a coast, however, they may become large enough to be significant. For example, Hsu (1970), in studies of the Texas coast of the Gulf of Mexico, found horizontal temperature gradients on the order of 1° K/km to persist for up to 6 hr. For $T = 300°$ K , $z = z_r = 10$ m and $\Delta t = 3$ hr, Equation 44 indicates $\Delta U = 3$ m/sec. That is, at $z = 10$ m, the wind speed is 3 m/sec different from the wind speed at the surface in the absence of any other forcing.

140. The change is significant. For a normal wind speed of 10 m/sec and a stress unaffected by baroclinity, the wind speed could vary from 7 to 13 m/sec (depending on direction of the temperature gradient). Estimated stress based on this range of wind speeds would vary by the ratio of the squares of these speeds, i.e., a factor of more than 3. Relative to the actual stress, the range of error is from about 50 percent low to about 60 percent high.

141. This effect is expected to occur only during times of low wind speeds and high land-sea temperature differences. At higher wind speeds, the percentage of difference is less. Furthermore, increased turbulence would tend to equilibrate land temperature more rapidly.

142. Several mechanisms have been proposed here which can violate strongly the assumption of horizontal uniformity necessary for the stability-corrected logarithmic velocity profile to relate directly to surface stress. From rough scaling arguments it appears that, if fluxes and surface roughness do not change significantly over distances of a few hundred metres, then the assumption of horizontal uniformity is justified. Variations from this are possible for offshore winds over distances of several tens of kilometres, onshore winds in regions of high relief, rapidly changing bottom bathymetry, or irregular coastlines at scales on the order of 1 km. Variations can also occur for winds of low to moderate speed in regions where large horizontal air density changes exist. These effects are in addition to errors due to large horizontal gradients in forcing which can occur in intense storms.

143. The arguments given here are physically meaningful but largely speculative. If, as indicated in the introduction, wind stress is an important forcing term in nearshore wave and current generation, then it seems imperative that over-water wind-stress measurements be made within a few hundred metres of a beach. Drag coefficients computed from such observations can then be correlated with wind direction, land-sea-air density difference, land relief, and nearshore bathymetry to deduce the viability of various drag coefficient formulations. An experiment of the type described in Part V of this report can, at least partially, address this matter.

PART IV: METHODS OF ESTIMATING WIND STRESS FROM MEASUREMENTS

144. In the course of making calculations of wind-generated waves and
currents it is generally inefficient, if not impossible, to resolve the wind
field at all space and time scales necessary to model directly the fluctuating
velocities which constitute turbulent stresses. This step can be bypassed if
wind stress is found to be a unique function of other integral parameters
which can be measured or modeled more directly. For instance, if wind stress
were directly proportional to square of mean wind speed (at some reference
elevation), then Taylor's (1916) model would be valid. A single experiment of
high quality wherein wind speed and wind stress are measured simultaneously
would then determine the universal constant coefficient of proportionality
(C_D), and the problem would be solved.

145. However, the references cited heretofore in this report suggest
that C_D is not constant for all wind speeds and is not independent of other
conditions such as surface roughness and atmospheric stability. This means
that further experimental and theoretical work is necessary to find the cor-
relation between C_D and the variables upon which it depends. Much work has
been done on this subject. Some of it has been discussed in this report in
the framework of simple dimensional arguments and supporting observations.
The particular model presented here for C_D over water is not unique, but is
as consistent with laboratory and land-based observations as any other set of
model equations. It is reasonable to assume that it applies in the marine
environment.

146. Verification of hypotheses embedded in the model relies on accu-
rate and complete observations of prototypical conditions. At a minimum, this
means that observations must be made of wind stress and wind speed so that C_D
can be determined from the most primitive model. In addition, certain ancil-
lary parameters must be measured to support or reject hypotheses of dependence
of C_D on these parameters. These hypotheses include such things as air-sea
temperature and humidity differences, water surface mean velocity, and sea
state parameters as outlined above. Verification of these hypotheses also
requires checking to confirm that assumptions concerning the model, for exam-
ple, steadiness and horizontal uniformity, are realized in the prototype. If
not, the model must be allowed to tolerate some error to compensate for these
effects or must be augmented to account for these effects.

60

147. Of the variables mentioned here, some of the most difficult to measure are the turbulent stresses, or, more generally, the turbulent fluxes. It is because of this difficulty that drag coefficient formulae exist; if stresses can be expressed in terms of variables which are simple to measure, then direct stress measurements are not necessary. On the other hand, model verification depends critically on accurate stress measurements. Historically, part of the problem in fixing model constants or interdependency relationships has been related to inaccuracies in stress measurements. In this section, several common methods of direct or indirect stress measurement are described along with some constraints and hazards associated with their use.

148. Attention is focused here on measurements made within the atmospheric surface layer (i.e., the lowest 50 m or so of the atmosphere). This is because of the relative ease of use, generally lower cost, and higher availability of such data. Platforms from which these measurements can be made include surface ships, buoys, and towers. Other platforms, such as balloons, aircraft, and satellites, are further removed from the surface layer problem, have higher costs, and generally provide less data. These are not considered here.

149. Major problems associated with instrumentation are twofold. First is the adequacy of an instrument used to resolve the necessary space and time scales of the phenomenon being observed. Second is proper mounting or placement of an instrument such that the sensing volume primarily detects the desired variable and not one that has been distorted by the mounting platform or instrument frame. Both problems are important in measurements associated with wind-stress estimation and are considered here.

150. There are four common methods of inferring wind stress from measured variables. They are called the bulk method, the profile method, the direct method, and the turbulence inertial subrange (or, sometimes, dissipation) method. All are based on arguments given within this report.

Bulk Method

151. The bulk method is the primary topic of this report. It assumes a relation between wind stress and the square of the air-sea surface speed difference through a drag coefficient which is a function of other mean variables affecting the physics of air-sea interaction. In the model presented here the

61

drag coefficient is given by Equation 42. For a given reference elevation, it depends on the surface roughness scale z_o and the stratification-related length scale L under the assumptions that the flow is steady and uniform. The roughness length can be estimated from the models of Charnock (1955), Kitaigorodskii (1973), or Hsu (1974) but may depend on a more detailed description of sea state, as discussed above. The stratification length can be determined through Equations 37 to 41, given the air-sea temperature and humidity differences.

152. This set of model equations, which is considered here to be subject to refinement, is but one of a suite of bulk coefficient equation sets proposed by various investigators who based their formulae either on physical considerations similar to those used here or on pure correlations of stress observations with wind speed and density measurements. Stress estimates from various schemes vary widely. For example, Blanc (1985) conducted a simple intercomparison of 10 stress-estimating schemes proposed within the last 15 years, using as input over 2,000 mean wind, temperature, and humidity observations from the open North Atlantic Ocean. Typical mean scheme-to-scheme variation was in the range of 15 to 25 percent, which is reasonable. However, maximum scheme-to-scheme variation was between 40 and 80 percent which is somewhat excessive. Since no direct stress measurements were made, it could not be discerned which, if any, of the models was correct. Since the same data were used in all comparisons, the differences had to be a result of the model equations. This suggests that reliable stress estimation by this method requires refinements of some or all of the models, combined with rigorous testing to distinguish the best. This is especially true in coastal regions where effects of finite depth and cross-shore nonuniformity are not fully understood.

153. Bulk formulations are somewhat sensitive to the accuracy of data used in them. In the simplest formulae, this relates to measurements of wind speed, air temperature, water temperature, and air humidity at a reference level z_r. Accuracy is degraded by inadequate frequency response, insufficient averaging time, poor instrument calibration, platform motion, and disturbance of the signal by the platform itself.

154. Rough estimates of length and time scales for the resolution of various attributes of a turbulent flow can be deduced from reported measurements. Errors due to a known range of calibration uncertainty can be deduced

from the model equations. Platform motion can bias results due to spurious apparent signals and due to motion of sensors through a field with curvature in the measured entity. These problems must be resolved by analysis of individual platforms. Of course, ideal platforms for Eulerian observations do not move relative to a fixed coordinate system. Signal distortion due to the presence of a platform in a flow field must also be considered by analysis of individual platforms, if corrections are to be made. However, rough scaling arguments can be employed to locate instruments so as to reduce substantially this effect.

155. In regard to sampling length and time scales, the hypothesis generally employed is that dominant turbulent eddies in the surface layer scale with distance from the boundary. If a wave number spectrum of any turbulent property is measured, it is expected that the wave number axis can be normalized by the reference elevation z_r to obtain similarity. Given the wave number $k = 2\pi/\lambda$, where λ is the wavelength, then spectra should be similar when plotted as a funtion of z_r/λ . Most measurements are made in the frequency domain, however. The relation between frequency and wave number is generally assumed to follow Taylor's hypothesis (Tennekes and Lumley 1972). This asserts that turbulence properties do not change significantly when advected past a fixed point at reference wind speed U_r . The cyclic frequency f corresponding to λ is then $f = U_r/\lambda$. Using this, the quantity z_r/λ becomes fz_r/U_r , which is sometimes called the natural frequency.

156. Spectra of turbulence properties have been measured by several groups of investigators. Among recent papers on this subject are those by Schmitt, Friehe, and Gibson (1979), Large and Pond (1981), and Smith and Anderson (1984). These measurements indicate that the bulk of turbulent fluctuations occur for $fz_r/U_r \gtrsim 0.01$. The time scale corresponding to this frequency is $1/f \simeq 100\ z_r/U_r$. For bulk measurements using mean properties, it is only necessary to have an instrument that responds to frequencies on the order of $0.01\ U_r/z_r$. A reasonably stable estimate of the mean is obtained by averaging over about 10 time periods corresponding to this frequency, i.e., the averaging time T_a is $T_a \simeq 1,000\ z_r/U_r$.

157. For typical values of wind speed and reference elevation this gives characteristic averaging times necessary to resolve mean values. For example, if $z_r = 10$ m and $U_r = 10$ m/sec, then $T_a = 1,000$ sec $= 16.7$ min. For smaller U_r , a longer time is required. For example, with $U_r = 1$ m/sec,

T_a needs to be 10,000 sec = 2.8 hr. Since common averaging times seldom exceed 1 hr, this suggests that a 1-m/sec wind is typically undersampled and so may have substantial variability. In much of the older data used by Kitaigorodskii (1973) and Garratt (1977), averaging times were around 10 to 15 min. By the scaling given here, this suggests that wind speeds less than 11 to 16 m/sec were undersampled (for z_r = 10 m) and so may account for some of the reported data scatter. For wind speeds on the order of 5 m/sec, at which increased wave generation occurs, the averaging time is about 30 min. Note that as z_r increases, so does the averaging time. For z_r = 20 m, all averaging times double over those required at z_r = 10 m.

158. Uncertainties of stress estimates due to instrument error and platform-blockage effects were considered by Blanc (1986a). In this study he compared four bulk schemes using weather-ship data from the open North Atlantic Ocean and allowed the data to vary randomly about its reported values by amounts described in the literature as being characteristic of calibration errors and ship-influence errors. Error estimates used were fixed values and not percentages, so relative errors tended to increase at smaller values of the primary variables. For sensor calibration error, Blanc (1986a) assumed wind-speed errors of ±0.5 m/sec for U_r < 20 m/sec and ±1.0 m/sec for U_r > 20 m/sec, errors in air temperature and wet/dry bulk temperatures (for humidity determination) of ±0.3° C and errors in sea-surface temperature of ±0.5° C. Based on random variations within these limits, Blanc found that all four of his test models agreed very well with each other and were all within 10 to 15 percent of the error-free estimates of wind stress for u_* > 0.25 m/sec. This is a tolerable error for modeling purposes.

159. For ship-induced errors, Blanc (1986a) estimated variations in wind speed due to flow distortion around the ship, temperature errors due to variable solar heating near and on the ship, variation in humidity due to ship-induced spray, and variation in sea-surface temperature due to ship engine cooling water discharge. These variations were of the same order or slightly larger than the calibration errors discussed above. Ship-induced errors resulted in 25- to 35-percent variations in stress estimates relative to those from uncontaminated data. Again, this result is marginally acceptable for modeling purposes.

160. In the study by Blanc (1986a), the wind blockage effect was estimated to be on the order of 10 percent of mean wind speed. This alone would

give variations on the order of 20 percent in wind stress. This estimate of error in wind speed may be conservative for some ship-mounted anemometers, however. In a subsequent publication, Blanc (1986b) reported results of wind-tunnel tests to determine wind speed and direction deviations at standard anemometer locations on a US Navy vessel. He found wind-speed errors ranging from 40 percent low to 50 percent high, depending on direction of wind approach to the ship. If used in a quadratic drag law, these results would give errors in stress ranging from 60 percent low to over 100 percent high. This is not acceptable for use in an otherwise accurate oceanic model.

161. The studies by Blanc (1986a,b) are mentioned because they emphasize that poorly sampled mean data will yield poor results even if the drag- and mass-transfer coefficients are perfectly known. In application of the bulk method, careful consideration of sampling scheme, calibration method, and platform effects are required to ensure results of reasonable quality. The same considerations are even more critical in experiments designed to help refine drag coefficient models. The purpose of this report is to justify and describe such an experiment. Measurement requirements are discussed in the remainder of Part IV, which deals with alternate methods of wind-stress measurement, and in Part V which describes an experiment scheme.

Profile Method

162. In the profile method, measurements of mean horizontal wind speed, mean temperature, and mean humidity are made within the atmospheric surface layer (but above the sublayer) at a minimum of three elevations. The data are then fitted to the set of Equations 34 through 41 to find the three basic flow parameters u_* , z_o , and L . Wind stress is then determined from
$$\tau = \rho(\bar{T},\bar{q})u_*^2 .$$

163. This method is a slightly more objective application of the bulk method. In the bulk method, the flow profile relationships given by Equations 29 to 33 are integrated from the surface ($z = z_o$) to some reference elevation ($z = z_r$). In the profile method, the same equations are integrated between levels in the surface layer only. This has the advantages that a model for z_o is not necessary, sea-surface temperature does not have to be measured, and sea-surface humidity does not have to be assumed to exist at 100-percent saturation. Requirements for sensor accuracy and frequency

response are the same as for instruments used in the bulk method.

164. The disadvantages of the profile method are that it requires the same assumptions of steadiness and horizontal uniformity as are required for the bulk method, more sensors are required, and the platform used must be un-obstructive at all measurement levels. Furthermore, for optimum accuracy, the measurement levels should be spaced logarithmically in z due to the dominant logarithmic nature of the profiles given by Equations 34, 35, and 36. Wide vertical separation of sensors at upper levels is necessary. This places added structural constraints on the platform and runs the risk that upper sen-sors are outside the surface layer during times of low wind speeds or high stable stratification.

165. In the bulk method only four sensors are required (sea-surface temperature along with mean wind speed, air temperature, and humidity at the single reference elevation). In the profile method, at least nine sensors are required (mean wind speed, air temperature, and humidity at a minimum of three elevations) so there are added logistical burdens of obtaining and maintaining a greater number of sensors.

166. Blanc (1983), in an analysis of the mechanical, logistical, and climatological constraints of atmospheric measurements in the marine environ-ment, suggested that the profile method is best suited for flux estimation over long durations and recommended numbers and spacings of instruments to accomplish this. The profile method has been employed over water by Hsu (1972), SethuRaman and Raynor (1975), and Frenzen and Hart (1975).

167. However, no experiment over water has been conducted wherein the flux-profile relationships used in any formulation are tested for validity. This is extremely difficult in the open ocean due to mechanical constraints of sea-going platforms. Near land, such an experiment is more feasible but the higher probability (in general) of horizontal nonuniformity would make the profile method as suspect as the bulk method. Since the bulk method is the easiest to employ in large-scale climatological studies, this suggests that experiments testing flux-bulk formulations may be preferable. The correctness of the profile relationships would then be implicit in the results of such experiments.

Direct Method

168. In the direct method, the total (three component) velocity field is measured at a point at frequencies high enough to resolve the fluctuating horizontal and vertical velocities in the bandwidth wherein the correlation $\overline{u'w'}$, and, by Equation 3, the stress can be computed directly. This method requires the fewest assumptions about the flow field because it is a direct estimator of the vertical Reynolds momentum flux at the level of measurement. The only assumption is that a direct measurement of $\overline{u'w'}$ at some elevation above the sea surface represents the shearing stress at the sea surface. If this assumption is violated due to, say, strong horizontal nonuniformity, then a more complete treatment of the problem is necessary. In such a treatment it is still necessary to know the turbulent flux of momentum through a control surface parallel to the mean sea surface. A direct measurement of this flux is the only reliable estimator in this case, so the need remains for accurate sensing.

169. Devices to measure all three components of velocity at frequencies necessary to resolve the Reynolds stresses are inherently more sensitive than the typically robust instruments used in the bulk and profile methods. This means they are more susceptible to calibration error, platform problems, and environmental degradation. Futhermore, a greater volume of data needs to be accumulated to compute the cross correlations. These conditions increase significantly the expense of obtaining, deploying, and maintaining such instruments. As a result, experiments using such instrumentation tend to be of short duration (usually less than 1 month) and total historic data are somewhat sparse. Blanc (1985) estimated that less than 400 hr of direct measurements over water had been reported in the literature at the time of his search. Any additions to this data base are of great value.

170. In making direct measurements, the averaging time is the same as for the bulk and profile methods. The necessary frequency response of the sensors is higher. Measurements of cospectra of the product $\overline{u'w'}$ by Schmitt, Friehe, and Gibson (1979), Large and Pond (1981), and Smith and Anderson (1984) indicate that the bulk of the stress fluctuations exist for natural frequency $fz_r/U_r \lesssim 10$ or $f \lesssim 10\, U_r/z_r$. If this represents the Nyquist frequency of spectral resolution, then the sampling frequency must be twice this or $f \simeq 20\, U_r/z_r$. Sampling requirements are higher for high

67

reference wind speeds and low measurement elevations. For example, $f \simeq 20$ Hz for $U_r \simeq 10$ m/sec with $z_r \simeq 10$ m and $f \simeq 10$ Hz for $U_r \simeq 10$ m/sec with $z_r \simeq 20$ m but $f \simeq 40$ Hz for $U_r \simeq 20$ m/sec and $z_r \simeq 10$ m.

171. Devices which can resolve these frequencies are typically heat transfer (hot films and hot wires) or acoustic devices. They tend to be fragile, expensive, and short lived in the field. More robust and less expensive mechanical devices (wind vanes and cup or impellor anemometers) tend to have a lower frequency response than that required above. They can be used for direct stress measurements if their signals are corrected through a measured transfer function for decreased high frequency response. Finkelstein et al. (1986) made intercomparison measurements between a sonic anemometer (with good high-frequency response) and six commonly employed configurations of lower frequency response mechanical devices. Their results suggest that transfer functions can be found to improve frequency response up to $fz_r/U_r \simeq 1$. This is still a decade lower than desired. However, a further correction can be employed based on the observed $\overline{u'w'}$ cospectra mentioned above. For a given stability, those spectra appear to be similar in shape so that the missing fractional variance (on the order of 10 to 30 percent) can be estimated from the part of the signal that is resolved with the low-frequency devices. This procedure allows longer term measurements of reasonable accuracy to be performed with less delicate instrumentation.

172. A second consideration in the direct method is leveling of the sensors used to measure the three components of velocity. The reason for this is that $\overline{u'w'}$ is but one element of a nine-element correlation tensor. Small misalignments effectively rotate the tensor so the desired quantity is contaminated by contributions from other terms. The essential argument is that if fluctuating u' and w' are measured in a coordinate system that is out of level by an angle χ , then the measured velocities u'_m and w'_m are related to the true velocities u' and w' by $u' = u'_m \cos \chi - w'_m \sin \chi$ and $w' = u'_m \sin \chi + w'_m \cos \chi$, where χ is the angle in the vertical plane from the true x-axis to the x-axis of the measuring system. Note that here the coordinate system is aligned with the x-axis in the mean wind direction so the cross-wind fluctuating velocity does not enter this argument. It should be included in the general case. The correlation of u' and w' is simply the average of the product of the two expressions. With some manipulation this yields $\overline{u'w'} = (\overline{u'_m u'_m} - \overline{w'_m w'_m}) \cos \chi \sin \chi + \overline{u'_m w'_m} (\cos^2 \chi - \sin^2 \chi)$. This

68

expression can be approximated in terms of the true friction velocity $u_*^2 = -\overline{u'w'}$ and the measured friction velocity $u_{*m}^2 = -\overline{u'_m w'_m}$. Observations of variances of fluctuating velocities (Hinze 1959) in the surface layer indicate that $\overline{w'_m w'_m} \approx u_{*m}^2$ and $\overline{u'_m u'_m} \approx 5 u_{*m}^2$, to within 50 percent or so. Using these approximations in the expression for $\overline{u'w'}$ shows the true friction velocity squared to be $u_*^2 \approx u_{*m}^2 (\cos^2 \chi - \sin^2 \chi - 5 \sin \chi \cos \chi)$. If measured values are assumed to be relative to a level coordinate system, the error is the term in parentheses. Table 4 shows this term as a function of χ .

Table 4

Estimated Error in Wind Stress Due

to Measurement System Being

Out of Level by Angle χ

χ , deg	u_*^2/u_{*m}^2
-3	1.26
-2	1.17
-1	1.09
0	1.00
1	0.91
2	0.82
3	0.73

173. According to Table 4, the measurement system must be level to within about ±2 deg for accuracy to within ±20 percent. This is extremely difficult on a floating platform such as a ship or buoy. It requires that direction estimates be very accurate and that some type of inertial displacement measuring system be employed to correct for all platform motion. This effect and flow distortion by large platforms (such as ships and offshore oil platforms) give cause why little direct wind-stress data have been obtained in the open ocean. These problems are more readily controlled on a fixed tower of small cross section. Such towers are used in shallow and nearshore waters where stays and bracing can be fixed to the seafloor. Geernaert, Katsaros and Richter (1986) used such a tower in 16 m of water to deploy a three-axis impellor anemometer. Smith and Anderson (1984) obtained very good results using a tower placed near the waterline on a beach and upon which was mounted an acoustic anemometer.

174. When the direct method is used in stratified flow, measurements must also be made of the correlations $\overline{w'T'}$ and $\overline{w'q'}$, which are the turbulent fluxes of sensible heat and water vapor, respectively. Fluctuating temperatures are usually made with temperature-sensitive resistance elements of low thermal inertia in a bridge circuit. Humidity fluctuations are often quantified through the absorption of light at a fixed wavelength by water vapor in air. Variations in light intensity are related in a known way to water vapor concentration. The required frequency bandwidth for measurement of these variables is the same as for velocity fluctuations.

175. To obtain the necessary frequency response for temperature and humidity sensors, the sampling volumes are on the order of centimetres in size. This makes such instruments somewhat fragile. In addition, problems have been noted in field use of these instruments due to the relatively high concentrations of salt in the marine atmospheric surface layer. Phelps and Pond (1971) noted curious differences between temperature spectra and humidity spectra in measurements in the Pacific Ocean off San Diego, California. Such differences were not expected in Monin-Obukhov similarity theory. The differences were explained by Schmitt, Friehe, and Gibson (1978) as being due to saltwater accumulation on temperature sensors. Condensation and evaporation of water on the salt droplets in conditions of high humidity yielded a spurious temperature signal because of latent heat released or absorbed. As noted by Blanc (1983), salt accumulation can also alter the optical transmissivity or cause corrosion of windows in light-intensity sensitive devices such as those used to detect humidity.

176. These problems indicate that collecting information from these devices is labor-intensive, requiring virtually constant attention and frequent cleaning and exchange of sensing elements. On the other hand, knowledge of these problems aids in proper experiment design. Furthermore, the added expense is compensated for by the acquisition of direct Reynolds flux measurements, which is the only proper way to calibrate or test model equations.

177. Another constraint on experiment design is in the spacing of sensors. The natural frequency fz_r/U_r is the Taylor transform of wave number dependency z_r/λ . For $fz_r/U_r = 10$, the corresponding high-frequency wavelength is found from $z_r/\lambda = 10$ or $\lambda = z_r/10$. For $z_r = 10$ m, this means that correlations are needed for spacings on the order of $\lambda \approx 1$ m. To correlate temperature or humidity with vertical velocity, the respective sensors

should reside in a volume of length scale 1 m or less. For z_r = 20 m, the spacing should be less than 2 m.

Inertial Subrange Method

178. A fourth method of estimating turbulent fluxes is related to the functional shape of turbulence spectra in a particular band of wave numbers. As with the bulk and profile method, it is indirect and relies on the assumptions of steadiness and horizontal uniformity.

179. The method is derived from Kolmogorov's hypothesis (Tennekes and Lumley 1972) which argues that, for large Reynolds number flows, there exists a band in the wave number spectrum of turbulent kinetic energy the structure of which depends only on wave number and turbulent energy dissipation rate. That is, if $S(k)$ is velocity variance per wave number increment at wave number k and ε is the rate of dissipation from Equation 20, with units of velocity variance per time, then a closed set of variables is $S(k)$, k, and ε. Dimensional analysis dictates the relationship as

$$S(k) = A\varepsilon^{2/3}k^{-5/2} \tag{45}$$

where A is the universal constant, often called Kolmogorov's constant.

180. If the flow is unstratified, then ε in Equation 45 can be replaced by Equation 28 which yields

$$S(k) = A\left(\frac{u_*^3}{\kappa z}\right)^{2/3} k^{-5/3} \tag{46}$$

The next step is to convert Equation 46 from wave number dependence to frequency dependence through Taylor's hypothesis. The relation between cyclic frequency f (in Hertz) and radian wave number k in a Taylor transformation is $k = 2\pi f/U$ where U is local mean wind speed. Since $S(k)$ is velocity variance per wave number increment, it is converted to frequency dependence by $S(f) = U \, S(k)/2\pi$. Using these transformations in Equation 46 and combining terms gives

71

$$S(f) = Au_*^2 \left(\frac{U}{2\pi\kappa z}\right)^{2/3} f^{-5/3} \qquad (47)$$

181. The range of frequencies for which Equation 47 is valid is called
the inertial subrange. Since there is no direct dependence on production of
turbulence in this high-frequency range, it is generally assumed that the
motions follow the theory of isotropic turbulence. In this case, the spectrum
of u' follows Equation 47 and the spectra of v' and w' (the cross-wind
components) are each four-thirds times this. Thus, if A is the Kolmogorov
constant for the downwind spectrum, then the coefficient of Equation 47 for
the spectrum of horizontal winds should be 7/3A and the coefficient for the
spectrum of winds in all directions should be 11/3A . Frenzen (1983) lists
some experimentally determined values of A , which cover the range 0.50 < A
< 0.59 , and recommends A = 0.52 from his own work. Schmitt, Friehe, and
Gibson (1979) use A = 0.50 in their work. Large and Pond (1981, 1982) and
Smith and Anderson (1984) use A = 0.55 . This last value is a reasonable
estimator and can be assigned an uncertainty of ±10 percent.

182. The way in which Equation 47 is used to estimate u_*^2 is to mea-
sure and compute the one-, two-, or three-dimensional spectrum of fluctuating
velocities and then fit Equation 47 to these measurements by varying u_*^2 .
This is subject to two constraints. The mean flow Reynolds number (Uz/ν) must
be large enough for an inertial subrange to exist and the curve-fitting pro-
cess must only be done in that subrange of frequencies. Tennekes and Lumley
(1972) estimate that an inertial subrange should exist for $Uz/\nu > 10^5$.
Since $\nu = 1.5 \times 10^{-5}$ m^2/sec for air, this constraint is satisfied for mean
wind speeds as low as 1 m/sec at elevations as low as 1 m. Higher wind speeds
and higher observation elevations serve to increase the Reynolds number so
this constraint is not a problem in most flows of interest.

183. Spectral measurements over water by Schmitt, Friehe, and Gibson
(1979), Large and Pond (1981) and Smith and Anderson (1984) indicate that the
inertial subrange has a low frequency bound at a natural frequency of about
$fz/U = 1$. Since the upper frequency bound in the direct method of stress
estimation was found to be $fz/U = 10$, this means that sensors of the same
type can be used in the inertial subrange method. That is, if the spectrum
is resolved for the range $1 < fz/U < 10$, then Equation 47 can be used to
find u_*^2 .

72

184. The advantages of this method are several. First, only a one-dimensional spectrum is necessary to estimate stress so it is not necessary to measure all three velocity components. Second, stress can be estimated from spectra of just horizontal velocities, as could be obtained from a cup anemometer with a high enough frequency response. Frenzen (1983) describes results from measurements using such a device. Third, because the range of frequencies in the inertial subrange is relatively high, measurements are less sensitive to platform motion than are measurements using the direct method. This suggests that such devices can be used on shipboard if adequate care is taken to avoid flow distortion by the ship's structure. Since sensors which work at the frequencies cited tend to be fragile, long term, unattended deployment on buoys or remote stations is not recommended.

185. If the flow is stratified, then the inertial subrange method must be adapted to account for the fluxes of temperature and humidity. The conventional derivation is given here for temperature, following Tennekes and Lumley (1972). The arguments for humidity are identical. When Kolmogorov's hypothesis is applied to a state variable (temperature or humidity) it is assumed that the variable acts as a passive contaminant at wave numbers in the inertial subrange. That is, density variations have a primary effect at large (production) length scales but not directly at shorter length scales. It is then assumed that the temperature variance spectral density $S_T(k)$ is a function of wave number k and the molecular loss rate of temperature variance ε_T . One more variable is needed because ε_T has dimensions of squared temperature per time and time is not a dimension of k or $S_T(k)$. The added variable is assumed to be ε , the energy dissipation rate.

186. The set of variables $S_T(k)$, k , ε_T , and ε forms a dimensionally unique grouping which can be written as

$$S_T(k) = A_T \varepsilon^{-1/3} \varepsilon_T k^{-5/3} \tag{48}$$

where A_T is a universal constant. The same argument applied to humidity yields

$$S_q(k) = A_q \varepsilon^{-1/3} \varepsilon_q k^{-5/3} \tag{49}$$

73

where A_q is a universal constant. Equations 45, 48, and 49 are used to find the fluxes once ε, ε_T, and ε_q are modeled.

187. In the case of stratified flow, an estimate of ε is obtained from Equation 27 under the assumption that $D = 0$ by using the Monin-Obukhov length L as notation in the second term on the right side and then replacing the term on the left side with Equation 29. The expression for ε is then

$$\varepsilon = \frac{u_*^3}{\kappa z}\left[\phi_m\left(\frac{z}{L}\right) - \frac{z}{L}\right] \tag{50}$$

This expression is subject to argument because it has not been shown that D is negligible in stratified flow. Frenzen (1983) indicates that D may be on the order of 20 to 40 percent of the dissipation rate. Long (1981) argues that D is on the order of 4 times the buoyant sink term in Equation 27 for stratified flow which is stable. This is a matter for future research. Equation 50 has been used in several recent investigations (Schmitt, Friehe, and Gibson 1979; Large and Pond 1981; Smith and Anderson 1984; Boyle, Davidson, and Spiel 1987) and so is worth consideration as an interim model.

188. The dissipation rate for temperature variance is estimated from the temperature-variance equation (Tennekes and Lumley 1972). For steady, uniform flow and by assuming negligible gradient diffusion of temperature variance (like assuming $D = 0$ in the energy equation), this is

$$- \overline{w'T'}\, \frac{\partial \overline{T}}{\partial z} = \varepsilon_T \tag{51}$$

When combined with Equation 30, which was deduced from Monin-Obukhov similarity, the temperature gradient $\partial \overline{T}/\partial z$ can be eliminated. This yields

$$\varepsilon_T = \frac{(\overline{w'T'})^2}{u_* z}\, \phi_T\left(\frac{z}{L}\right) \tag{52}$$

The equivalent expression for humidity is

$$\varepsilon_q = \frac{(\overline{w'q'})^2}{u_* z}\, \phi_q\!\left(\frac{z}{L}\right) \tag{53}$$

Using Equations 50 and 52 in Equation 48, converting $S_T(k)$ and k to $(U/2\pi)S_T(f)$ and $(2\pi/U)f$, respectively, by the Taylor transformation and rearranging terms gives

$$S_T(f) = A_T\, \frac{(\overline{w'T'})^2}{u_*^2}\, \frac{\phi_T\!\left(\frac{z}{L}\right)}{\left[\phi_m\!\left(\frac{z}{L}\right) - \frac{z}{L}\right]^{1/3}}\left(\frac{U}{2\pi\kappa z}\right)^{2/3} f^{-5/3} \tag{54}$$

The expression for the spectrum of humidity is

$$S_q(f) = A_q\, \frac{(\overline{w'q'})^2}{u_*^2}\, \frac{\phi_q\!\left(\frac{z}{L}\right)}{\left[\phi_m\!\left(\frac{z}{L}\right) - \frac{z}{L}\right]^{1/3}}\left(\frac{U}{2\pi\kappa z}\right)^{2/3} f^{-5/3} \tag{55}$$

The one-dimensional velocity variance spectrum is obtained by using Equation 50 in Equation 45, transforming Taylor's hypothesis, and rearranging terms. This yields

$$S(f) = A u_*^2\, \left[\phi_m\!\left(\frac{z}{L}\right) - \frac{z}{L}\right]^{2/3}\left(\frac{U}{2\pi\kappa z}\right)^{2/3} f^{-5/3} \tag{56}$$

189. Flux estimates are obtained through spectral measurement of fluctuating velocity, temperature, and humidity and then fitting Equations 54, 55, and 56 to these measurements using Equations 32 and 33 for ϕ_m, ϕ_q, and ϕ_T along with the definition of L following Equation 28. Values for mean wind velocity U and measurement elevation z are also needed. Large and Pond (1982) and Smith and Anderson (1984) use $A_T = A_q = 0.80$ for the Kolmogorov constants, citing an uncertainty on the order of 10 percent based on previous work. Where wind stress is the primary variable sought, uncertainty in these constants is not too harmful since the mass fluxes are determined only for corrections to stress estimates. The equation set is transcendental in z/L

and so the curve-fitting process must be done in an iterative fashion. This can be done readily on any common computer.

190. Tests of the hypotheses made in the derivation of this method have been carried out by Schmitt, Friehe, and Gibson (1979), Large and Pond (1981, 1982), Smith and Anderson (1984), and others in measurements over water. Results were very good where reasonable assurance of negligible platform blockage, platform motion, nonuniformity, and instrument error effects could be obtained. All spectra had an $f^{-5/3}$ dependence to within measurement uncertainity. Spectral amplitudes in the inertial subrange agreed well with measurements made over land. A direct comparison of u_* determined from the inertial subrange method with u_* determined from the direct method was made by Large and Pond (1981). In the mean, the two methods agreed to within about 3 percent. The scatter was generally within ±20 percent, which is reasonable since the uncertainty from each method is about ±10 percent for u_*.

191. An application of the method was reported by Boyle, Davidson, and Spiel (1987) in measurements over the open Pacific Ocean. In steady, uniform conditions the inertial subrange method gave results that compared very favorably with the bulk method, based on results given by Large and Pond (1982). As mentioned previously, this experiment showed that the bulk method severely underestimated wind stress when wind and wind-driven waves were not in equilibrium. Since wind-driven waves tend to be long lived, relative to time scales of Reynolds stresses and inertial subrange variances, this suggests that the inertial subrange method is a better indicator of instantaneous wind stress than the bulk method. That is, corrections to or further modeling of the bulk method to account for time dependence, variations in sea state, finite water depth, etc., can be achieved using the inertial subrange method to estimate wind stress.
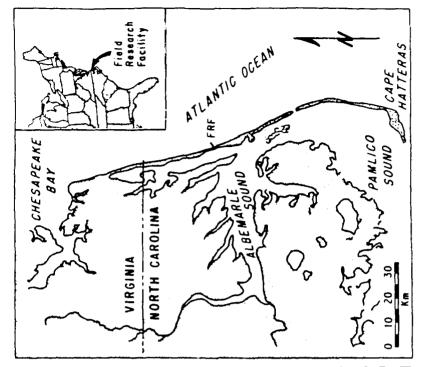
Summary

192. Four methods are described here for direct or indirect methods of wind-stress measurement. General instrumentation requirements, averaging times, and frequency responses are given. To effect an improved parametric dependence of the bulk method, alternate stress estimates need to be made simultaneously. In order of preference, the best method is the direct method, followed by the inertial subrange and profile methods. In order of expense of

instrument acquisition and maintenance, the list is reversed. In all of the methods, the theory, instrument capability, and deployment constraints are being developed and improved concurrently. For this reason, any experiment design should include as many of these methods as is possible to intercompare results and ensure reliability. This is especially true in shallow water and nearshore environments where the physics of air-sea-land interaction is more complex than in steady, uniform conditions over land or over the open ocean.

PART V: AN EXPERIMENT PROGRAM

193. An experiment program has been designed to test and evaluate some of the hypotheses expressed above concerning modification of drag coefficients in shallow and nearshore waters. The intent is to measure over-water mean wind speed and wind stress, so as to compute a drag coefficient, and a number of auxiliary parameters to determine drag coefficient dependence on them. These parameters include wind direction, air-sea-land temperatures, fluxes of heat and humidity, water depth, distance to shore, and detailed sea state parameters derived from currents and directional wave spectra.

194. For logistical and physical reasons, the site chosen for the experiment program was the Field Research Facility (FRF) of the US Army Engineer Waterways Experiment Station, Coastal Engineering Research Center. This site is on the Atlantic coastal barrier islands of North Carolina just north of the village of Duck (Figure 1). A pier extending about 500 m seaward of the waterline provides dry access to an over-water location, ideal for nearshore wind stress measurements. The site is also very uniform for several kilometres in the alongshore direction. This allows reasonable correlation of drag coefficient with the parameters listed, without added complication due to a convoluted coastline.

195. Because of the wide variety of parameters needed, this program was conducted as part of a large-scale joint experiment known as SUPERDUCK. It was coordinated by the Corps of Engineers and had added participation by university scientists and other government research groups. Overview papers describing SUPERDUCK are expected to appear soon in the literature. This report describes the wind-related measurements of this experiment.

196. The atmospheric measurement program took place in two parts. The first part took place in the fall of 1985 in a pre-SUPERDUCK experiment known as DUCK85. This work was intended to provide a preliminary survey of horizontal variability of winds at the FRF and a measure of the adequacy of various existing platforms for accurate wind-stress measurements. Based in part on the results of DUCK85, the main experiment was designed to make optimum use of existing platforms yet minimize data contamination due to platform effects. This report describes the DUCK85 experiment and results in detail and gives a cursory description of the SUPERDUCK experiment. A detailed description of the latter experiment and its results will be given in a subsequent report.
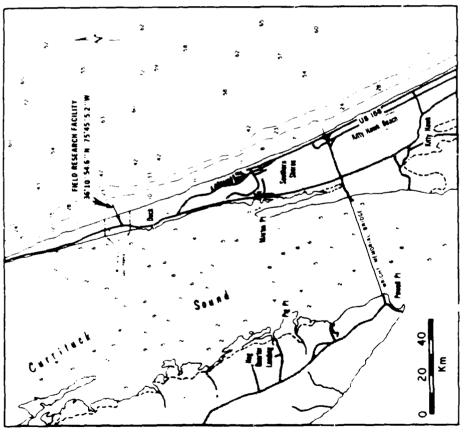
78

Figure 1. Site locations of the CERC Field Research Facility (from Miller 1982)

197. The preliminary wind experiment had four main objectives. The first was to provide over-water environmental wind conditions for other participants in the DUCK85 experiment (Hubertz 1987). The second was to determine the magnitude of cross-shore horizontal nonuniformity of winds from various directions at the FRF site. The third was to compare measurements by the permanently installed anemometer, used by FRF personnel for routine weather observations, to measurements over water to see how well it represented over-water winds. The fourth objective was to test the adequacy of a tower at the seaward end of the pier for making wind-stress measurements using the profile method described in Part IV.

Instrumentation

198. Wind measurements were made from three platforms, two on land near the landward end of the pier and one at the seaward end of the pier. Figure 2 is a schematic plan view of the FRF site, showing locations of some of the instrumentation from the DUCK85 experiment. Figure 3 is a schematic diagram showing, in three pieces, shore-normal sections of the three wind measurement platforms.

199. The pier-end tower (Figure 2, Item 12; and Figure 3) is an open-frame, three-legged tower with legs 0.61 m apart, and with a maximum elevation of 22.1 m above mean sea level (msl). Its base is on the southern end of the terminal bent of the pier at 6.8 m above msl. The pier deck is at 7.7 m above msl. One of the land-based platforms is a 6.2-m tower atop the FRF laboratory building (Figure 2, Item 13; Figure 3). The top of this tower is at 18.7 m above msl. It is called the Skyvane platform in this report because of the manufacturer's name for the instrument mounted there. The Skyvane tower is about 600 m from the pier-end tower. The other land-based platform is an antenna tower located about 50 m north of the Skyvane tower and equidistant from the beach. Called here the north tower, it is even in the alongshore direction with Item 18 in Figure 2 and its section view is the center sketch in Figure 3. It is an open-frame, three-legged telescoping tower with legs varying between 0.61 m and 0.33 m apart. It reaches a maximum elevation of about 22 m above msl.

200. Basic wind instrumentation consisted of four cup anemometers, four wind-vane direction sensors and one impellor vane, and a combination speed and
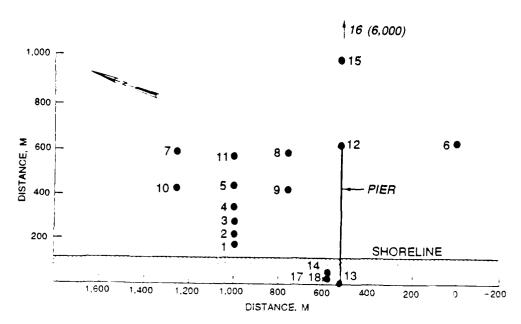
Figure 2. Nearshore waves and currents experiment station
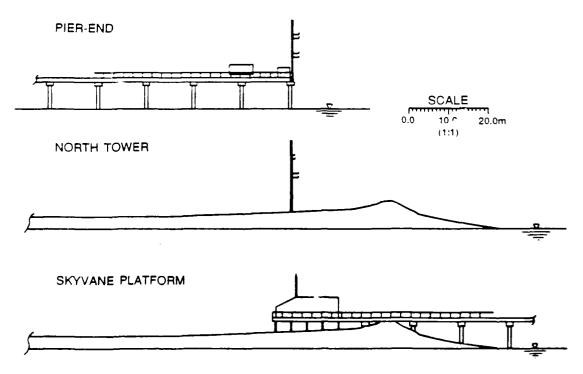locations during DUCK85

Figure 3. Schematic diagram of sections of the three primary wind-measuring
platforms: pier-end tower (top), north tower (middle), and Skyvane platform
(bottom)

81

horizontal direction sensor (the Skyvane). Table 5 lists some of the attributes of these devices. The cup-and-vane sensor sets were installed at two elevations on the pier-end tower and at two elevations on the north tower. The Skyvane was at an elevation of 18.7 m above msl, so cup anemometers were also placed at this elevation on the pier-end and north towers. Wind vanes were installed 1 m below this level, at 17.7 m above msl. Cup anemometers were also placed at 14.0 m above msl on the pier-end and north towers to investigate vertical variations in mean horizontal wind speed. Wind vanes were also mounted 1 m below these at 13.0 m above msl. Lines protruding normal to the pier-end and north towers in Figure 3 represent the mounting booms and show these sensor locations. Mounting booms were at least three characteristic tower diameters long to minimize flow distortion due to the towers proper. The Skyvane was at the top of the Skyvane tower shown in Figure 3.

201. For gross climatology, the air temperature over land was measured at site 18 in Figure 2, which represents the permanently installed FRF weather station. Sea temperature measurements were made in conjunction with deployment of a Sea Data PUV wave gage at site 11 in Figure 2. The temperature sensor of this gage was located near the seabed and so does not necessarily represent sea-surface temperature. Air temperature over water was not measured. Temperature differences ΔT (air temperature minus water temperature) give a crude signature of possible nearshore thermal forcing. Some of the thermometer characteristics are given in Table 5. Characteristic wave heights were obtained through standard spectral analysis of data from a pressure gage located at site 5 in Figure 2 and described in Table 5.

Data collection and editing

202. With the exception of the Sea Data temperature gage, all sensors were sampled at 2 Hz for 40 min, beginning on the hour. Data collection and processing was executed using a Data General Nova Model 1200 computer. Mean values and standard deviations were printed soon after each 40-min sampling interval. Raw time series were stored on magnetic tape. For this study, only mean values were used for analysis. Variances were used for error checking. The Sea Data gage was internally recording. Temperature data from this gage were entered in a master data file after the experiment.

203. Prior to deployment, all wind-speed sensors were calibrated at the National Bureau of Standards test facility in Washington, DC. All gages were found to perform to within manufacturer's specifications. Direction sensors

Table 5

Instrumentation Used in the Wind Measurement Study During the DUCK85 Experiment

Sensor	Manufacturer/ Model	Station in Figure 2	Elevation m above msl	Sampling	Manufacturer's Stated Accuracy	Notes
Cup anemometer	Met One Model 010B	12	18.7	Hourly, 2 Hz for 40 min	Largest of ±1% or 0.07 m/sec	0.2-m/sec threshold 1.5-m distance constant
Cup anemometer	Met One Model 010B	12	14.0	Hourly, 2 Hz for 40 min	Largest ot ±1% or 0.07 m/sec	0.2-m/sec threshold 1.5-m distance constant
Cup anemometer	Met One Model 010B	18	18.7	Hourly, 2 Hz for 40 min	Largest of ±1% or 0.07 m/sec	0.2-m/se: threshold 1.5-m distance constant
Cup anemometer	Met One Model 010B	18	14.0	Hourly, 2 Hz for 40 min	Largest of ±1% or 0.07 m/sec	0.2-m/sec threshold 1.5-m distance constant
Wind vane	Met One Model 020B	12	17.7	Hourly, 2 Hz for 40 min	±3°	0.2-m/sec threshold 0.4-0.6 damping ratio 1.0-m delay distance
Wind vane	Met One Model 020B	12	13.0	Hourly, 2 Hz for 40 min	±3°	0.2-m/sec threshold 0.4-0.6 damping ratio 1.0-m delay distance
Wind vane	Met One Model 020B	18	17.7	Hourly, 2 Hz for 40 min	±3°	0.2-m/sec threshold 0.4-0.6 damping ratio 1.0-m delay distance
Wind vane	Met One Model 020B	18	13.0	Hourly, 2 Hz for 40 min	±3°	0.2-m/sec threshold 0.4-0.6 damping ratio 1.0-m delay distance
Impellor vane	Weathermeasure Skyvane	13	18.7	Hourly, 2 Hz for 40 min	Largest of ±3% or 0.45 m/sec and ±2°	0.9-m/sec threshold
Water pressure	Sensa-Metric Model CP973C	5	-4.0	Hourly, 2 Hz for 40 min	±0.02 m	Used to estimate characteristic wave height
Air temperature (over land)	Yellow Springs Instruments Model 705	18	5.0	Hourly, 2 Hz for 40 min	±0.01° C	
Water temperature	Sea Data Model 635-12	11	-5.4	Hourly, 1 Hz for 3.75 min	±0.002° C	

83

were assumed accurate to manufacturer's specifications. They were aligned after mounting by locking the vanes parallel to the mounting booms and averaging the measurements for 40 min in this configuration. The boom azimuths were found through triangulation to fixed points about the FRF site, the locations of which were determined with a Zeiss Elta-2 three-axis theodolite. In this way, absolute directions were determined to within ±1 deg which is better than instrument accuracy.

204. Data were collected round the clock with the exception of one hour daily for computer maintenance. With the further exception of infrequent problems due to poor connections and cross-talk, data return was excellent. Problems were detected through observed radical changes in mean values or variance. To ensure that all data were above instrument threshold, no data were retained for a speed and direction sensor pair where the speed was less than 1 m/sec.

205. For the general climatology, data determined to be satisfactory in the sense of instrument response were used in toto. However, for the other objectives of the experiment, an intercomparison among sensors was conducted. To minimize some of the problems of platform blockage on these comparisons, data were edited further by eliminating from analysis all speeds and directions for which the sensors were directly downwind of a tower or large building.

206. Table 6 shows the ranges of azimuths excluded from intercomparison analyses. The coordinate system used in this report is a compass system (direction increasing clockwise) with the effective North azimuth directed northward parallel to the beach. True North is at 20 deg in this coordinate

Table 6

Wind Azimuths for Which Data Have Been Eliminated from Analysis

Sensor Location	Range of Azimuths, deg
Pier end (18.7 m)	101 to 118
Pier end (14.0 m)	95 to 126
North tower (18.7 m)	114 to 178, 0 to 8, and 343 to 360
North tower (14.0 m)	114 to 178, 0 to 8, and 343 to 360
Skyvane	No blockage assumed

system. True East is at 110 deg, and the direction seaward along the pier is 90 deg. Winds are considered in their vector sense so directions given are those toward which the wind blows. Thus, a wind blowing southward along the beach has an azimuth of 180 deg. A wind blowing directly onshore (toward land) has an azimuth of 270 deg.

Experiment duration and climatology

207. Figure 4 gives a summary of some of the general climatology of the DUCK85 experiment. Data from the wind and other sensors have been tabulated by Hubertz et al. (1987). Data were collected more or less continuously from 2100 (all times here are Eastern Standard Time) on 5 September 1985 to 0700 on 21 September 1985 when the experiment was scheduled to terminate. However, during the cleanup and equipment disassembly period following the experiment, it became obvious that the path of Hurricane Gloria would pass near, if not over, the FRF. To sample this unique event, some of the sensors were re-mounted and reconnected. Additional data were then collected from 1100 on 26 September 1985 to 0700 on 28 September 1985.

208. Wind data are shown as five sets of stick diagrams in Figure 4. From the beginning of the experiment until 11 September the winds were rela-tively light, generally less than 7 m/sec. About midday on 11 September, a front passed the FRF and became stationary just offshore. Wind speeds were typically in the range of 10 to 15 m/sec until the evening of 14 September. The influence of the front continued until 18 September. During this time the winds continued to blow from the northeast at 5 to 9 m/sec. The winds became more variable from 18 to 21 September.

209. During Hurricane Gloria, the wind followed the classic pattern for a low-pressure center approaching from the south. The winds were generally from the east and intensified as the storm center neared the FRF. Gloria passed the FRF at about midnight on 26 September. The winds shifted by almost 180 deg in 5 hr and reached a peak speed of about 23 m/sec. It is noted that the stick vectors representing the Skyvane appear different from those repre-senting the pier-end tower and north tower. This is examined in detail shortly.

210. The axis in Figure 4 marked ΔT shows the temperature difference between the air over land (near the FRF laboratory building) and the water at about 5-m depth and roughly 700 m away. The record is incomplete because the Sea Data device had a limited duty cycle. The measurements are somewhat crude
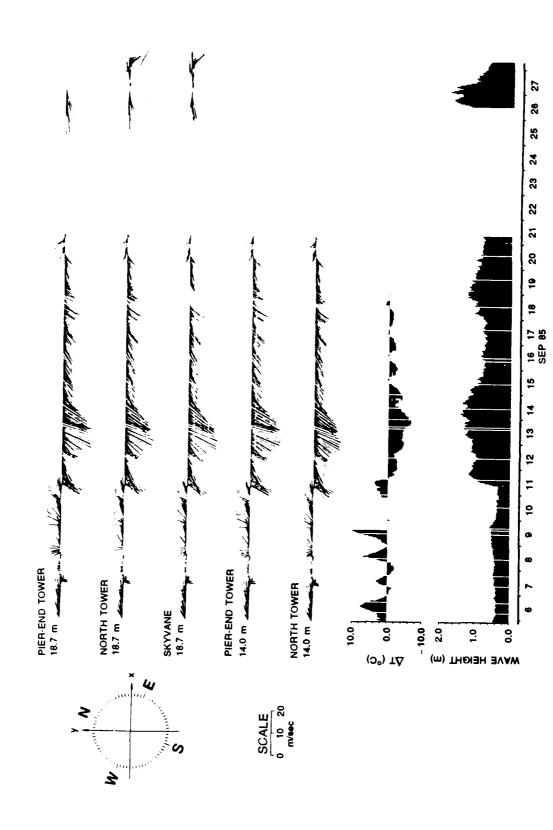
Figure 4. Summary of data from the DUCK85 wind measurement experiment

for quantitative interpretation but, nonetheless, show a clear diurnal cycle. This daily variation in temperature difference can be visually correlated with daily variations in the wind patterns from all five gages and under all wind conditions. The most noticeable effect is the ordered rotation of the wind vectors as the temperature difference intensifies or weakens. This suggests that the sea-breeze forcing, brought about by land-sea temperature differences, acts to modulate larger scale forcing mechanisms. The effect seems to dominate at lower wind speeds. During the northeast storm of 11-15 September, a diurnal variation is present but does not appear to be a major modulating force.

211. Observed wave heights are shown on the bottom axis of Figure 4. They are characterized as four times the standard deviation of sea-surface elevation where the latter estimate was obtained from the Sensa-Metric pressure gage described above. The sea was relatively calm for the first few days of the experiment but wave heights grew rapidly at the onset of higher winds from the northeast storm. Characteristic wave heights reached about 1.5 m (at the location of this sensor) at the height of the storm as compared with 0.4 m prior to the storm. Wave heights stayed high after the main part of the storm passed on 15 September, due partly to forcing by 6- to 8-m/sec winds and probably due to added storm waves propagating landward from the somewhat distant front. Wave heights increased again during the passage of Hurricane Gloria, approaching saturation for the water depth in which the gage was located. However, Gloria passed the FRF site relatively quickly and the wind blew seaward (opposite the propagation direction of landward-traveling storm waves) with reasonably high intensity after the storm passage so wave heights dropped off rapidly.

212. These observations indicate two important features of nearshore wind coupling to the sea. First, the wave field tends to grow rapidly at the onset of high winds. This suggests that instantaneous sea state conditions are in equilibrium with the wind when seas are building. A wave-growth model could thus be designed using this concept. Second, in decaying winds the seas can remain high due to the relatively long-lived nature of waves and their ability to radiate from the region of generation. In this case, winds and waves are not in equilibrium so that coupling (drag) coefficients can be expected to vary greatly, i.e., not be coupled uniquely to instantaneous sea state. Accurate modeling of a drag coefficient must rely on observations
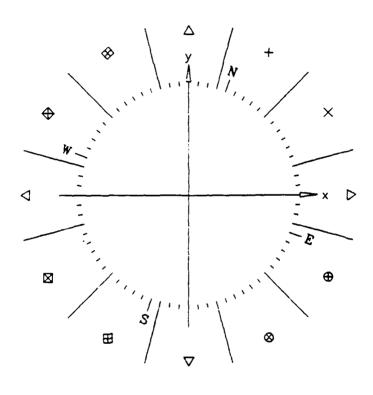
87

under a wide variety of conditions like these because the physics of these interactions is quite complex and is not understood fully.

213. The sequence of wind vectors denoted by the stick diagrams in Figure 4 indicates that, for this set of observations, the wind field generally satisfies the conditions of quasi-steadiness given by scaling arguments in the last section. Two minor exceptions to this are noted. At low wind speeds, less than 5 m/sec and for which little wave generation occurs, the speeds often change by more than 10 percent per hour and directions change by more than 20 deg per hour. For low-energy conditions this is not critical. Also, at the onset of the northeast storm on 11 September the wind increased and changed directions somewhat rapidly. However, since it was a transition from low- to high-wave generation conditions, it is only the onset of high winds that is important. The nature of the transient, low-wind conditions preceding this is not too critical.

214. On the other hand, a major exception to the quasi-steady scaling occurs during the passage of Hurricane Gloria on 26 to 28 September. During the storm passage, the winds shifted at rates approaching 90 deg per hour. In 3 hr the winds shifted by almost 180 deg. Thus, while wind speeds were high enough (>20 m/sec) for efficient wave generation, the rapid change in wind direction resulted in either the wind blowing nearly perpendicular to the direction of propagation of waves generated the previous hour or the wind blowing opposite the direction of propagation of waves generated several hours previously. In the latter case, momentum transfer is likely to be from waves to wind (or negative momentum transfer from wind to waves) with a consequent loss of wave energy. A quantification of the rate of momentum transfer (i.e., a drag coefficient) is likely to be quite different from that for growing waves, but its magnitude is not known. Clearly, this is an important topic for further research.

Correlations between sensors

215. The primary analysis of this data set is done through correlation plots comparing various pairs of sensors. Relative sensor behavior and wind-field differences are seen readily in this way. Of major importance are comparisons of wind speeds. Since wind-speed differences are likely to be strong functions of wind direction, it is useful to classify the data by wind direction.

216. This was done by dividing the azimuth circle into 12 equal parts

as shown in Figure 5. Each sector is 30 deg wide. Four of the sectors are
centered on cardinal points in the pier-aligned coordinate system. Symbols
are shown in Figure 5 to define uniquely each sector. Triangles designate
cardinal points (in the pier system) and can be thought of as arrowheads
pointing in the direction toward which the wind blows. Intervening symbols
also represent directions toward which the wind blows, e.g., the plus symbol
represents winds blowing toward 15 to 45 deg clockwise from the y-axis. The
y-axis is shore-parallel and positive northward. The x-axis is pier-parallel
and positive seaward.

LEGEND

Figure 5. Symbol legend showing wind-direction
bands and representative symbols

217. Correlations between the three wind-speed and wind-direction
sensor sets at the 18.7-m level are shown in Figures 6-8. Symbols denote wind
direction, and axes denote wind speeds. Figure 6 shows pier-end winds com-
pared with north tower winds. There is some scatter in the data, and some
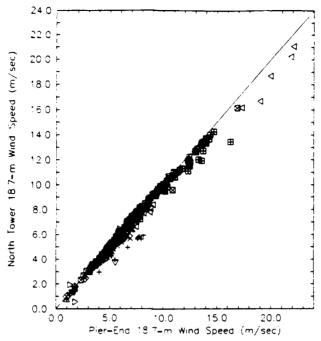trends can be seen within symbol groupings. This will be discussed in detail

Figure 6. Correlation plot of north tower 18.7-m
wind speed compared with pier-end 18.7-m wind speed
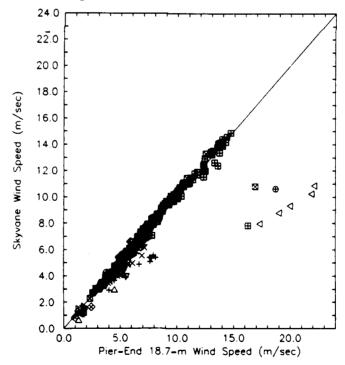using data from all direction bands

Figure 7. Correlation plot of Skyvane wind
speed compared with pier-end 18.7-m wind
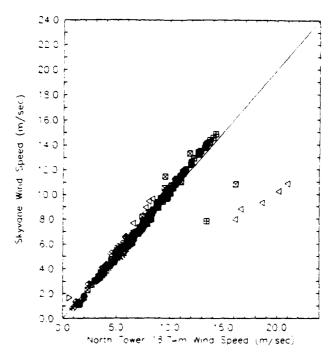speed using data from all direction bands

90

Figure 8. Correlation plot of Skyvane wind
speed compared with north tower 18.7-m wind
speed using data from all direction bands

below. The general observation in Figure 6 is that the bulk of the data agree
to within about 10 percent. If these sensors were over the open ocean, one
would expect a perfect correlation. The scatter indicates that the two
sensors are not detecting the same wind pattern. The difference, of course,
is that one sensor is over land and the other is over water; the boundary
layer structure in and between the two regimes is different.

218. The general difference shown in Figure 6 is less than about
10 percent over a horizontal separation of about 600 m. Based on the scaling
arguments given in the section on horizontal nonuniformity, this suggests that
the flow is uniform to a roughly acceptable degree between the two stations
for most of the data at the 18.7-m level. That is, wind measurements from the
north tower are roughly representative of winds over water 600 m away. The
more detailed analysis below indicates that improved representations are
possible.

219. Figure 7 shows a correlation of pier-end winds with those detected
by the Skyvane. At wind speeds less than about 10 m/sec the general data

91

pattern in Figure 7 is about the same as in Figure 6. However, for speeds between 10 and 15 m/sec the Skyvane tends to register slightly higher wind speeds than sensors at the pier end. This should be compared with the north tower which tends to register sligntly low relative to pier-end sensors. Alarmingly, the Skyvane does not register speeds in excess of 15 m/sec even though the pier-end anemometer senses speeds exceeding 22 m/sec. In fact, for the higher pier-end speeds the Skyvane does not read above 11 m/sec; this behavior is not seen in data from the north tower.

220. Figure 8 shows the correlation between the north tower 18.7-m wind speed and the Skyvane. Since both towers are equidistant from the beach their readings should be identical. The correlation is quite good for speeds up to about 9 m/sec. From this to speeds of about 15 m/sec the Skyvane appears to overspeed slightly and, as with the pier-end comparison, drop considerably for north tower winds in excess of 15 m/sec.

221. There are two possible explanations for this behavior. One is that the sensor malfunctioned. Though it calibrated to within manufacturer's specifications prior to the experiment and behaved properly both before and after Hurricane Gloria (compare the stick vectors in Figure 4 for 27 and 28 September), it is possible that the sensor signal was degraded during the high winds of the hurricane. A more likely explanation is that the wind was strongly affected by the bluff upwind faces of the FRF building such that the Skyvane sensor was in a low-velocity wake region of flow at high wind speeds. The symbols for the highest wind speeds indicate air flow directly onshore. The Skyvane platform section shown in Figure 3 indicates that, for onshore winds, the air passed up the seaward dune face and immediately had to pass over or around the FRF building.

222. There is no simple theory for flow separation around angular obstructions (like the FRF building). However, Batchelor (1970) notes that fluids tend to have a stagnation zone downstream of sharp edges, and that this zone increases with increasing Reynolds number (governed by wind speed in this case). He also notes that fluid flow tends to follow a tangent to the upwind surface of an obstruction. In the case of the FRF building, the upwind surface is vertical so the effect would be expected to be dramatic. The apparent slight overspeeding of the Skyvane at speeds of 9 to 15 m/sec is also indicative of flow-acceleration effects around an obstacle.

223. While more detailed mapping of the wind field over and around the

92

FRF building at high wind speeds is necessary to resolve this problem, it is evident that the Skyvane sensor did not detect the same wind field as the north tower sensor. Since instrument malfunction or platform distortion are suspected to be the cause of this, the Skyvane data are not considered further in this report. It is recommended that the Skyvane platform and platforms like it be studied in detail to ensure that they do not induce grievous errors in field observations.

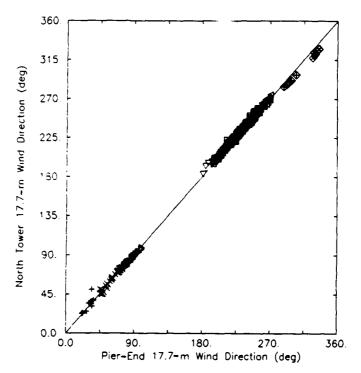224. Figure 9 is a correlation plot of wind direction at the pier-end

Figure 9. Correlation plot of north tower
17.7-m wind direction compared with pier-
end 17.7-m wind direction

tower with that at the north tower. Most of the data is within one symbol width (about 6 deg) of the perfect correlation line. The only clear deviate trend occurs for winds with an azimuth between 270 and 360 deg, i.e., winds heading northwest or coming from the southeast. Winds in this direction pass over the pier structure itself (see Figure 2) prior to reaching the north tower. It is possible that the flow in the wake of the pier may have had some effect on wind direction at the north tower. Another possibility is that the vane on the north tower was deflected by flow around the tower. The vane

93

would be nearest the tower at the instrument boom azimuth of 336 deg. Flow
deflection around the tower would tend to result in a reduced reading for the
north tower. This is consistent with deviations seen in Figure 9. Aside from
this possible platform effect, no major direction deviation trends are evident
in this data set.

225. The scatter of points shown in Figure 6 is due, at least in part,
to the combining of wind data from all directions on a single graph. The wind
system at the FRF site is more orderly than is suggested by Figure 6. This is
shown in Figures 10 to 17 where pier-end and north tower 18.7-m wind speeds
are correlated for each of eight azimuthal bands. The four azimuthal bands
not shown had too little data to be instructive. Figures 10 to 17 are ordered
by increasing wind azimuth such that Figures 10 to 12 contain winds with an
offshore-directed component and Figures 13 to 17 contain winds with an
onshore-directed component (see Figure 5 for symbol legend).

226. The greatest fractional wind deviation occurs in Figure 10. Here
the wind is headed northeasterly. Examination of Figure 1 shows that these
winds have traveled the greatest distance over land before reaching either
tower and, further, wind at the pier-end tower has passed the greatest dis-
tance over water (for winds with an offshore component) prior to reaching the
pier-end tower. Thus, one would expect the highest contrast between the
sensors in this direction (and its symmetric counterpart about the x-axis,
i.e., the circle-x symbols, not shown because sensors were in the wakes of
towers). The over-land boundary layer would be most fully developed and
register maximum land-roughness effects in the retardation of wind flow. Wind
at the pier end would have passed generally over the most quiescent, and
therefore smoothest, water surface since fetch limitations would inhibit any
significant local wave growth. This sensor would then show the least retarda-
tion. The contrast, about 25 percent for an 8-m/sec pier-end wind speed, is
significantly large. A wind stress based on the land-derived (north tower)
wind would be about 50 percent low using a quadratic stress law.

227. In the next azimuthal band (x symbols, Figure 11) the north tower
wind also tends to read systematically low relative to the pier end. Here the
maximum deviation is only about 15 percent. This is because the north tower
air has passed less distance over land than for the azimuthal band discussed
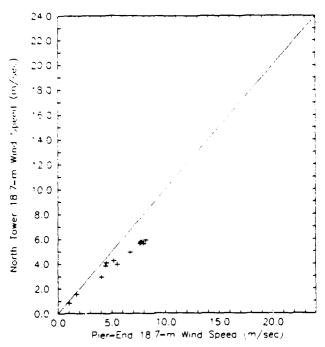in the last paragraph. Also, the pier-end wind has passed less distance over

Figure 10. Correlation plot of north tower 18.7-m wind speed compared with pier-end 18.7-m wind speed for winds blowing toward 15 to 45 deg in the pier coordinate system
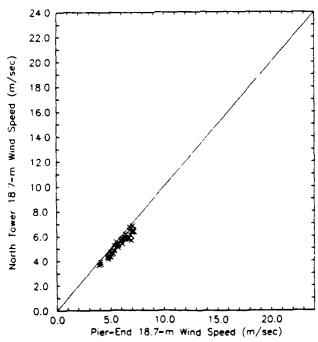

Figure 11. Correlation plot of north tower 18.7-m wind speed compared with pier-end 18.7-m wind speed for winds blowing toward 45 to 75 deg in the pier coordinate system
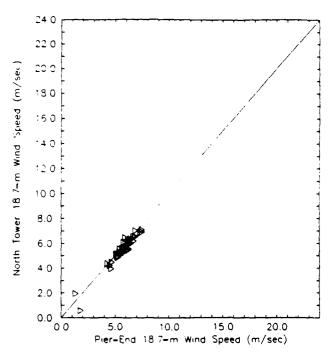
Figure 12. Correlation plot of north tower 18.7-m wind speed compared with pier-end 18.7-m wind speed for winds blowing toward 75 to 105 deg (generally offshore) in the pier coordinate system

Figure 13. Correlation plot of north tower 18.7-m wind speed compared with pier-end 18.7-m wind speed for winds blowing toward 195 to 225 deg in the pier coordinate system
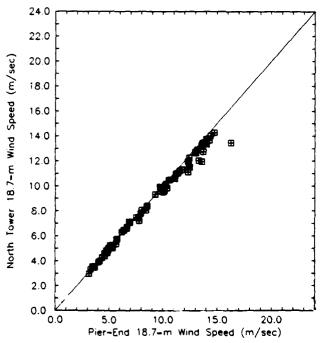
96

Figure 14. Correlation plot of north tower 18.7-m wind
speed compared with pier-end 18.7-m wind speed for winds
blowing toward 225 to 255 deg in the pier coordinate system

Figure 15. Correlation plot of north tower 18.7-m wind
speed compared with pier-end 18.7-m wind speed for winds
blowing toward 225 to 285 deg (generally onshore) in the
pier coordinate system

97

Figure 16. Correlation plot of north tower 18.7-m wind speed compared with pier-end 18.7-m wind speed for winds blowing toward 285 to 315 deg in the pier coordinate system

Figure 17. Correlation plot of north tower 18.7-m wind speed compared with pier-end 18.7-m wind speed for winds blowing toward 315 to 345 deg in the pier coordinate system
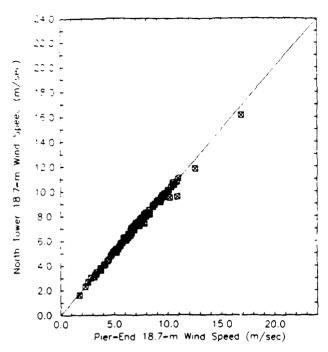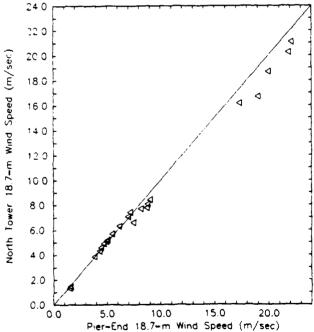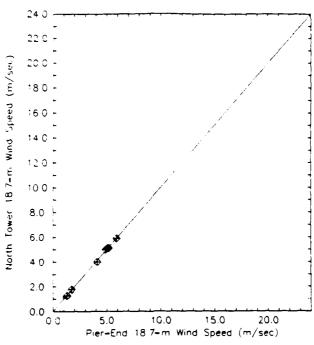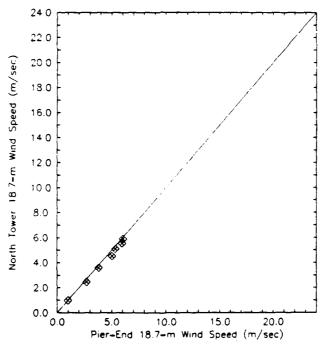
water and so still retains some land-derived turbulence (see the section on horizontal nonuniformity in Part III).

228. Figure 12 shows the correlations for the azimuthal band centered on the offshore-directed axis. There is some scatter, but the systematic pattern is closer to the perfect correlation line than in either of the two previous cases. Here the wind has passed a minimum distance over land at the north tower and a minimum distance over water at the pier end. Evidently the land-influenced flow has not adjusted to over-water conditions in this short (600 m) distance so that for speeds in excess of about 4 m/sec the two wind measurements are about the same. The two deviate readings at speeds less than 2 m/sec were obtained at times of light and variable winds. Threshold problems and high variances in instantaneous speeds and directions used to constitute mean values may have caused the deviations seen.

229. Figures 13 to 17 show correlations for winds with an offshore component. Symmetry about the x-axis in Figure 5 suggests that Figures 13 and 17 should be identical and that Figures 14 and 16 should also be identical. To within the data scatter at wind speeds less than about 6 m/sec (the maximum speeds attained in Figures 16 and 17), this is seen to be the case. For this reason, references to Figures 13 and 14 will imply references to Figures 16 and 17, respectively, in the following discussion.

230. Figure 13 shows that for winds with a slight onshore component the correlation is very good to speeds of about 10 m/sec. For higher speeds, the north tower winds are retarded somewhat, in general. The point of maximum deviation (about 16 m/sec at the pier end) occurred during Hurricane Gloria at a time of rapid temporal change and so could be due, in an unknown way, to flow acceleration effects. The lesser but systematic deviations for the higher wind speeds are likely due to the influence of air flow over the dune shown in Figure 3. A line tangent to the maximum slope of the seaward dune face passes above the 1 .7-m level of the north tower. The argument given for the Skyvane platform also applies here. At some wind speed, it is expected that air flow due to the wake of the dune will reach the 18.7-m elevation. In Figure 3 this appears to occur for wind speeds between 10 and 13 m/sec. The increased scatter at a speed of about 13 m/sec may also be due to this.

231. The dune effect is expected to become evident at lower wind speeds as winds become more shore-normal since such winds have a stronger onshore component. This is evident in Figure 14 where a slight overspeeding of the

99

north tower signal at speeds around 7 m/sec suggests flow acceleration over the dune crest. The increase in scatter occurs at speeds around 10 m/sec compared with 13 m/sec in the last case discussed. In Figure 15 the overspeeding of the north tower winds occurs at speeds around 5 m/sec and the increase in scatter at about 7 m/sec. Winds in Figure 15 are blowing within ±15 deg of directly onshore, and so would show dune wake effects at the lowest wind speeds. Note in Figure 15 that the higher wind speeds encountered during Hurricane Gloria resulted in about 10-percent retardation of the north tower winds relative to those at the pier end.

232. If the conjecture is true in the foregoing discussion about variations in the wind pattern at the 18.7-m level, then deviations would be even more pronounced at lower levels. Figure 18 shows the general comparison of
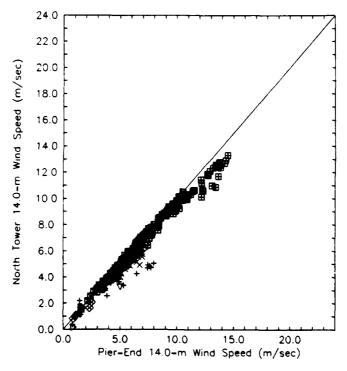
Figure 18. Correlation plot of north tower
14.0-m wind speed compared with pier-end
14.0-m wind speed

pier-end and north tower wind speeds at the 14.0-m level, analogous to Figure 6. Comparison of Figures 6 and 18 shows that the deviation is, in fact, stronger at the 14.0-m level. Though Figure 18 is not disassembled by wind azimuth classes as was done for Figure 6, the trends of some of the classes are clear. For instance, wind blowing toward 15 to 45 deg (plus symbol)

deviates at the north tower by almost 40 percent from pier-end winds of about 8 m/sec. This is somewhat larger than the 25-percent difference found at the 18.7-m level. Also, winds blowing toward 195 to 225 deg (boxed plus symbol) show about 10-percent attenuation at the north tower in Figure 18 as compared with roughly 5 percent in Figure 6.

233. One result of this analysis is that, though there are differences between sensors separated by 600 m across the nearshore zone, the differences are highly systematic in wind speed and direction. If other potentionally important parameters, such as air-sea and sea-land temperature differences or sea-state variables, were included, wind differences may be even more highly systematized. Such additional analysis was not done here because of the paucity of data. Nonetheless, this means that very good corrections to land-based observations are possible (for this site and between the two observation platforms considered) by way of direct correlations. Moreover, wind differences are explainable qualitatively in terms of recognized boundary layer behavior. This suggests that further research can enable good numerical modeling of nearshore winds. Such modeling would have broader application than at this single experiment site and therefore be more generally useful.

234. The last objective in this experiment is to evaluate the pier-end tower for adequacy in making wind-profile measurements. The test performed was a comparison of wind speeds at two elevations (18.7 m and 14.0 m) on the pier-end tower to examine variations in wind shear. Figure 19 is a correlation plot of the speeds recorded at the two elevations. This result is very remarkable. The plot shows that the 14.0-m wind speeds are less than the 18.7-m wind speeds by about 0.2 m/sec for all wind speeds and directions; this is not an expected behavior. If the flow was neutrally stratified, such that the logarithmic profile (Equation 5) is valid, then the velocity difference $U_2 - U_1$ between two elevations z_2 and z_1 , would be $U_2 - U_1$ = $(u_*/\kappa)\ln(z_2/z_1)$. Since κ , z_2 , and z_1 are fixed in this case at 0.41 m, 18.7 m, and 14.0 m, respectively, then the result $U_2 - U_1$ = 0.72 u_* should hold. If $U_2 - U_1$ is constant, then u_* must be constant, by this derivation, and the wind stress must also be constant.

235. For $U_2 - U_1 \approx 0.2$ m/sec, the above expression gives u_* ≈ 0.3 m/sec. This is a reasonable value for a general estimate of u_* . However, according to Garratt (1977), u_* should be 0.16 and 0.64 m/sec for wind speeds of 5 and 15 m/sec, respectively. By the expression given above,
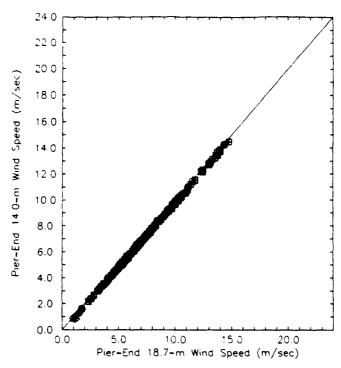
101

Figure 19. Correlation plot of pier-end wind
speeds at 14.0-m compared with those at 18.7-m

$U_2 - U_1$ should then be 0.12 and 0.46 m/sec, respectively. Figure 19 shows
that this is not the case, so something is amiss. It is possible that the
instruments malfunctioned or were recorded incorrectly. It is also possible
that the sensor at the 14.0-m elevation was detecting a wind field distorted
by structures and appendages at the pier deck level. Figure 3 shows a small
building of about 2 m in height near the base of the pier-end tower. The rule
of thumb for flow around isolated obstacles is that the flow is distorted
within three characteristic length scales of the center of obstacle. For the
size and location of the small building at the end of the pier, this indicates
that measurements up to the 15-m elevation on the pier-end tower would be
affected. Note that, except in the wake of the small building, the flow would
tend to be accelerated in the vicinity of the obstruction. This would reduce
the velocity difference between the two measuring heights on the pier-end
tower. Measurements in the wake of the tower were edited out before analysis.
This excluded measurements in the wake of the small building, so only accel-
erated measurements are seen in Figure 19.

236. This explanation of observations leads to the conclusion that,

102

unless some particularly imaginative mechanical engineering is done to mount instruments well away from pier blockage effects at lower elevations, it would be a grave mistake to attempt profile measurements from the pier-end structure.

Summary of results

237. Results of the preliminary wind experiment in the fall of 1985 provided valuable insight into the mechanics of the nearshore wind field at the experiment site and guidance for the design of the main experiment. Near-shore winds appear to vary in the horizontal in a highly systematic way, depending strongly on wind speed and direction. This means that long-term correlations between wind speeds and directions at two points at a given site can be used to deduce an empirical transfer function for land-based winds to over-water winds. It also suggests that, with further study, a reasonably simple model could be constructed to predict the transformation for a more arbitrary site. Caution is advised in arbitrary placement of a land-based anemometer. Results from this experiment indicate that the rule of thumb of three characteristic length scales of upwind and lateral separation of instruments from possible flow-distorting obstructions is a strict rule. The data analysis suggests that measurements from the building top anemometer and the lower pier-end anemometer were both affected by nearby structures. The analysis also suggests that the pier-end tower should not be used for wind-stress estimation by the profile technique.

SUPERDUCK

238. In view of the results of the DUCK85 experiment, it was decided to use the direct method for measuring wind stress over water during the fall of 1986 experiment known as SUPERDUCK. This endeavor was a joint venture with CERC and (with CERC funding) the Department of Marine, Earth and Planetary Sciences of North Carolina State University (NCSU) in Raleigh, North Carolina. Instrumentation type, method of deployment, data collection, and data editing were mostly selected, designed, or performed by NCSU personnel. Instruments were provided by NCSU. Data analysis is currently in progress and will be described in a future report. The intent of this section of this report is to describe the experiment design, instrumentation, and data collection logistics associated with the wind measurements.

Measurement requirements

239. In direct flux measurements where stratification is important, it is necessary to measure fluctuating temperature, humidity, and three components of velocity. Cross correlations of these quantities provide a measure of the Reynolds fluxes of heat, humidity, and momentum. Relating these observations to the bulk method requires that mean horizontal wind speed, wind direction, air-sea temperature difference, and air-sea humidity difference be measured (or estimated) as well. These fluxes and mean parameters are the primary variables sought in this experiment.

240. In analysis of data from this experiment it is necessary to have measurements of air temperature over land, sea state variables (at least characteristic wave height, wave period, and dominant travel direction) and sea-surface current. These variables are necessary to test, calibrate, or modify the hypotheses and models given in Part II of this report. Measurements of all these variables were made during SUPERDUCK by other groups of investigators. They have agreed to share their data for use in wind-stress analysis.

Platform

241. The primary measurements in the wind measurements part of SUPERDUCK were all made at or very near the seaward end of the FRF pier (station 12 in Figure 2). Three instrument mounting booms were attached to the pier-end tower. A 2.4-m retractable main boom was located at 18.7 m above msl, corresponding in location to the upper boom shown for the pier-end tower in Figure 3. A 2.0-m fixed boom, called the top boom, was located at 22 m above msl, corresponding to the top of the pier tower in Figure 3. A second 2.0-m fixed boom, called the lower boom, was located at 13.7 m above msl, corresponding (about) to the lower of the lower pair of booms on the pier-end tower in Figure 3.

242. A sea-temperature gage was mounted on the second pier piling from the pier end at depths varying between 0.6 and 2.0 m below msl. Depths varied because several mounting schemes were tried before a satisfactory arrangement was found. Measurements from this gage were recorded automatically and were checked three times a day with a bucket thermometer lowered from the pier deck at a location generally midway between the last two pier pilings.

243. Hand-held air temperature and relative humidity instruments were also operated three times daily at about 9 m above msl (roughly waist high above the pier deck in the lee of the instrument trailer). This trailer is

schematized in Figure 3 as a rectangle centered over the second piling from the pier end.

Instrumentation

244. Thirteen sensors were deployed to provide primary and redundant measurements of mean and fluctuating variables of the wind field. Sensors were divided into groups depending on the frequencies at which their outputs were sampled. Data from each group of sensors were recorded on separate data logging devices. The two sampling frequencies were 5 and 10 Hz.

245. The low-frequency (5 Hz) sensors were intended primarily to measure mean quantities for use both in bulk parameterization and in checking for mean drift in the high-frequency sensors. Table 7 lists the variables measured, the devices used, the number of data channels, and the locations of the low-frequency sensors. These measurements include three orthogonal

Table 7

Devices Sampled at Low Frequency (5 Hz) During Wind

Measurements Component of SUPERDUCK

Variable	Number of Channels	Manufacturer/ Model/Sensor Type	Location Elevation above msl
Horizontal wind speed and direction	2	R. M. Young Model 05103 Impellor vane anemometer	22.0 m (top boom)
Vertical wind speed	1	R. M. Young Model 27106 Gill impellor anemometer	22.0 m (top boom)
Air temperature over water	1	Yellow Springs Model 205 Thermistor	18.7 m (main boom)
Humidity over water	1	Campbell Scientific Model 207 Phys-Chemical Research Relative humidity sensor	18.7 m (main boom)
Horizontal wind speed	1	Met-One Model 010B Cup anemometer	13.7 m (lower boom)
Sea temperature	1	Yellow Springs Model 205 Thermistor	-0.6 m to -2.0 m

components of wind speed at the top (22-m elevation) of the pier-end tower, mean air temperature and humidity at the level of the main boom, horizontal wind speed at the lower boom (13.7-m elevation), and sea temperature.

246. The high-frequency (10 Hz) devices were intended to resolve the fluctuating (turbulent) components of temperature, humidity, and all three speed components of the wind. These sensors were all mounted on the main boom within a volume of characteristic dimension 1 m. Cross correlations between sensors could then be used to estimate Reynolds fluxes of mass and momentum. Variables measured, devices used, and numbers of data channels are given in Table 8. Three axes of wind speed were measured with an orthogonal impellor anemometer. A redundant vertical velocity was obtained with a sonic anemometer, and a redundant horizontal wind speed was measured with a hot film

Table 8

Devices Sampled at 10 Hz on Main Instrument Boom During

Wind Measurement Component of SUPERDUCK

Variable	Number of Channels	Manufacturer/Model/Sensor Type
Three axis wind speed	3	R. M. Young Model 27005 Gill UVW impellor anemometer
Vertical wind speed	1	Campbell Scientific Model CA27T Sonic anemometer
Horizontal wind speed	1	TSI Model 1610 Hot film anemometer
Air temperature over water	1	Campbell Scientific Model CA27T Chromel constantan thermocouple
Air temperature over water	1	Atmospheric Instrumentation Research Model FT-1A Platinum wire resistance
Humidity over water	1	Weathermeasure Model 5120-B Thin film capacitor
Humidity over water	1	Krypton Model KH-20 Optical absorption hygrometer

106

anemometer. Redundant air temperatures were measured with a fine wire resis-
tance thermometer and a fine wire thermocouple thermometer. Redundant humid-
ity measurements were obtained with a thin film capacitor, a relative humidity
sensor, and an optical absorption hygrometer.

Data collection

247. Data were collected using two programmable, internally storing
data loggers (Campbell Scientific Model 21X). These made mean and covariance
calculations in real time to save raw data storage media. The data loggers
were internally clocked and had battery back-up power sources to avoid data
loss when conventional 60-Hz power was interrupted.

248. All mean and cross-correlated variables were sampled for 1 hr to
ensure adequate low-frequency resolution. About every 2 days, data in the
data logger memory buffers were transferred in binary format to standard audio
cassette tape. Data on these tapes were read by a microcomputer and trans-
ferred via phone to a large computer on the NCSU campus for archiving and
analysis.

249. Since high accuracy is required for turbulent flux measurements,
raw data from the high-frequency data logger were collected once daily for
30 min. This allowed for detailed error checking and for computation of spec-
tra of various turbulence quantities. The data loggers had digital displays
to monitor input on individual data channels. Several of the sensors had
analog displays. These were checked frequently to ensure that all sensors
were functioning properly.

250. The primary variable to be measured is the Reynolds stress. In
general, this is a tensor with nine elements. In terms of velocity compo-
nents, it has six unique terms of which the two representing vertical fluxes
of horizontal momentum, i.e., $\overline{u'w'}$ and $\overline{v'w'}$, are most important. In terms
of horizontal wind speed, this is $\overline{s'w'}$ where $s' = (u'^2 + v'^2)^{1/2}$. In this
case, the horizontal stress vector is assumed to align with the mean horizon-
tal wind vector. With the instrumentation described here, the Reynolds stress
can be estimated in five ways. With the three-axis impellor anemometer (see
Table 8) $\overline{u'w'}$ and $\overline{v'w'}$ can be computed directly. Using the sonic anemom-
eter for w' and the hot film anemometer for s' , $\overline{s'w'}$ can be computed
directly. With w' from the impellor anemometer and s' from the hot film
anemometer, $\overline{s'w'}$ can be computed directly. With u' and v' from the

107

impellor anemometer and w' from the sonic anemometer, $\overline{u'w'}$ and $\overline{v'w'}$ can be computed directly. From the raw data tapes, spectra of horizontal wind speed can be computed from the hot film anemometer data and, from this, the inertial subrange method (see Part IV) can be used to estimate u_* .

251. Three additional, but less reliable, estimates of stress can also be made. Correlation of horizontal wind speed from the top-boom impellor vane anemometer with w' from the top-boom vertical impellor anemometer (both sampled at 5 Hz, Table 7) provides an estimate of $\overline{s'w'}$ but at somewhat re-duced high-frequency resolution. Spectra of u' and v' from raw measure-ments by the three-axis impellor anemometer can be used to estimate u_* by the inertial subrange method if corrections are applied to compensate for reduced high-frequency response. If allowance is made for platform blockage effects at the 13.7-m level on the pier-end tower (as deduced in the DUCK85 experiment), then the profile method can be used to estimate u_* from mean wind speeds measured with the cup anemometer on the lower boom, any of the speed sensors on the main boom, and the impellor vane anemometer on the top boom.

252. In a like manner, various combinations of temperature and vertical velocity or humidity and vertical velocity sensors can be used to make esti-mates of Reynolds fluxes of heat and humidity. These can be used in combi-nation with stress measurements to deduce stratification effects in drag coefficient formulae based on Monin-Obukhov similarity theory (Part III).

Data analysis

253. When the data from the experiment have been compiled and edited for completeness and accuracy and when data from the phases of SUPERDUCK re-lating to auxiliary parameters, such as ocean-surface current, sea state, and over-land air temperature, have been compiled, then the model equations given in this report can be tested for similarity with results obtained in open-ocean conditions. A report describing tests, results, and recommended changes to the model, if any, will follow.

PART VI: CONCLUSIONS

254. Drag coefficients, relating wind stress to a set of mean environmental parameters, are highly useful and practical forms of closure for characterizing wind forcing of waves and currents in large-scale numerical models. A survey of recent literature on the subject indicates that drag coefficients are neither constant nor simply dependent on wind speed, but are dependent on a broader range of parameters intimately related to the subjects of air-sea interaction and physics of the atmospheric boundary layer.

255. Research has shown that bulk formulations depending on gravity, wind speed, air-sea temperature differences, and air-sea humidity difference provide reasonable estimates of wind stress over the open ocean under steady, horizontally uniform conditions. However, errors in excess of 100 percent occur under unsteady conditions when wind and sea state are not in dynamic equilibrium. This suggests that in shallow and nearshore waters, where waves are influenced by the sea bottom as well as the wind and where wave-induced currents are different than in deep water, bulk formulae based on deep-ocean work may be substantially in error. Evidence to this effect has been given in recent literature.

256. Since the bulk of Corps interests are in waters of intermediate to shallow depths, it is imperative that improved models be developed so that proper modeling of nearshore processes can be done. Based on physical reasoning and research reported in the literature, it is hypothesized that nearshore drag coefficients depend on water depth, distance from shore, instantaneous sea state (at least significant height, peak period, and primary propagation direction), wind direction, local water-surface speed and direction, and land-sea air temperature differences in addition to parameters used in deep water.

257. To test this hypothesis, an experiment has been conducted wherein these parameters and wind stress are measured. Wind stress is not a simple variable to measure. Besides bulk coefficient estimates, there are three commonly used methods to determine wind stress. They are the profile, direct, and inertial subrange methods. Of these, the direct method is to be preferred since it requires the fewest assumptions.

258. There are constraints on the applicability of any model or the reliability of any experiment in cases of extreme unsteadiness or horizontal inhomogeneity. The latter condition may be of considerable importance in

109

waters near land with high relief or strong temperature contrast. In such cases, considerable additional research is necessary to resolve an accurate drag-coefficient closure. Near land of low relief, and during high wind conditions, where gradients of air density have less importance, the parametric dependence proposed here should be adequate.

259. An experiment was conducted in two phases to provide insight into the parametric dependency proposed above. The site chosen was the CERC's FRF, an area of low relief, frequent high winds, and extensive logistical support. This includes a pier which extends 500 m seaward of the beach and which can be used for over-water stress measurements. The first phase of the experiment took place during what is known as the DUCK85 experiment. It was a preliminary exploration of nearshore uniformity of wind, wind steadiness, and adequacy of various platforms for mean wind and wind-stress measurements. Results indicated that, most of the time, unsteadiness and nonuniformity are not major problems at this site and that nonuniformity is principally due to land topographic effects for strong onshore winds. On occasion when these effects are important, they can be recognized and compensated for since variations in the nearshore wind field appear to be highly systematic. Results indicated that the permanently installed FRF anemometer may be suspect in very high winds. Also, air-flow blockage effects may be substantial at lower elevations on the seaward end of the FRF pier.

260. The second phase of the experiment took place in the fall of 1986 during what is known as the SUPERDUCK experiment. In this experiment, bulk meteorological parameters were measured along with wind stress. This is being determined by the direct and inertial subrange methods from instruments mounted on the pier-end tower at elevations high enough to avoid effects of flow distortion by the pier. Sufficient redundancy in instrumentation was employed to assure reasonable continuity and accuracy of results. Simultaneous observations of sea state, water currents, and other relevant parameters were obtained by other investigators. These parameters, in combination with variables measured in the wind experiment, will provide a basis for testing various model hypotheses.

261. Data from the SUPERDUCK experiment is believed to be unique in its intent and completeness, and so will provide valuable insight and guidance in the evaluation and design of wind-stress closures for nearshore hydrodynamic models.

110

REFERENCES

Abramowitz, M., and Stegun, I. A. 1970. Handbook of Mathematical Functions, Dover, New York.

Amorocho, J., and DeVries, J. J. 1980. "A New Evaluation of the Wind Stress Coefficient over Water Surfaces," Journal of Geophysical Research, Vol 85, pp 433-442.

Batchelor, G. K. 1970. An Introduction to Fluid Mechanics, Cambridge University Press, London.

Blanc, Theodore V. 1983. "A Practical Approach to Flux Measurements of Long Duration in the Marine Atmospheric Surface Layer," Journal of Climate and Applied Meteorology, Vol 22, No. 6, pp 1093-1110.

_____. 1985. "Variation of Bulk-Derived Surface Flux, Stability, and Roughness Results Due to the Use of Different Transfer Coefficient Schemes," Journal of Physical Oceanography, Vol 15, No. 6, pp 650-669.

_____. 1986a. "The Effect of Inaccuracies in Weather-Ship Data on Bulk Derived Estimates of Flux, Stability and Sea-Surface Roughness," Journal of Atmospheric and Oceanic Technology, Vol 3, No. 1, pp 12-26.

_____. 1986b. "Superstructure Flow Distortion Corrections for Wind Speed and Direction Measurements Made from TARAWA Class (LHA1-LHA5) Ships," Report 9005, Naval Research Laboratory, Washington, DC.

Boyle, P. J., Davidson, K. L., and Spiel, D. E. 1987. "Characteristics of Over-Water Surface Stress During STREX," Dynamics of Atmospheres and Oceans, Vol 10, pp 343-358.

Businger, J. A., and Arya, S. P. S. 1974. "Height of the Mixed Layer in the Stably Stratified Planetary Boundary Layer," Advance in Geophysics, Vol 18A, Academic Press, New York, pp 73-92.

Businger, J. A., Wyngaard, J. C., Izumi, Y., and Bradley, E. F. 1971. "Flux-Profile Relationships in the Atmospheric Surface Layer," Journal of the Atmospheric Sciences, Vol 28, pp 181-189.

Chalikov, D. V. 1986. "Numerical Simulation of the Boundary Layer Above Waves," Boundary-Layer Meteorology, Vol 34, pp 63-98.

Charnock, H. 1955. "Wind Stress on a Water Surface," Quarterly Journal of the Royal Meteorological Society, Vol 81, pp 639-640.

Dyer, A. J. 1974. "A Review of Flux-Profile Relationships," Boundary-Layer Meteorology, Vol 7, pp 363-372.

Dyer, A. J., and Bradley, E. F. 1982. "An Alternate Analysis of Flux-Gradient Relationships at the 1976 ITCE," Boundary-Layer Meteorology, Vol 22, No. 1, pp 3-19.

Dyer, A. J., and Hicks, B. B. 1970. "Flux-Gradient Relationships in the Constant Flux Layer," Quarterly Journal of the Royal Meteorological Society, Vol 96, pp 715-721.

Finkelstein, P. L., Kaimal, J. C., Gaynor, J. E., Graves, M. E., and Lockhart, T. J. 1986. "Comparison of Wind Monitoring Systems, Part I:

In Situ Sensors," Journal of Atmospheric and Oceanic Technology, Vol 3, No. 4, pp 583-593.

Frenzen, P. 1983. "On the Role of the Flux Divergence Terms in the Turbulent Energy Equation," Proceedings, Sixth Symposium on Turbulence and Diffusion, Boston, American Meteorological Society, pp 305-308.

Frenzen, P., and Hart, R. L. 1975. "Wind Stress and Turbulent Energy Budget Measurements in the Undisturbed Surface Boundary Layer over the Sea; The Tern Buoy Experiment," Bomex Bulletin No. 12, National Oceanic and Atomospheric Administration, Washington, DC., pp 79-86.

_____. 1983. "A Further Note on the Kolmogorov - von Karman Product and the Values of the Constants," Proceedings, Sixth Symposium on Turbulence and Diffusion, Boston, American Meteorological Society, pp 24-27.

Garratt, J. R. 1977. "Review of Drag Coefficients over Oceans and Continents," Monthly Weather Review, Vol 105, pp 915-929.

Geernaert, G., and Katsaros, K. B. 1986. "Incorporation of Stratification Effects on the Oceanic Roughness Length in the Derivation of the Neutral Drag Coefficient," Journal of Physical Oceanography, Vol 16, No. 9, pp 1580-1584.

Geernaert, G. L., Katsaros, K. B., and Richter, K. 1986. "Variation of the Drag Coefficient and Its Dependence on Sea State," Journal of Geophysical Research, Vol 91, No. C6, pp 7667-7679.

Haugen, D. A., Kaimal, J. C., and Bradley, E. F. 1971. "An Experimental Study of the Reynolds Stress and Heat Flux in the Atmospheric Surface Layer," Quarterly Journal of the Royal Meteorological Society, Vol 97, pp 168-180.

Hinze, J. O. 1959. Turbulence, McGraw-Hill, New York.

Högström, U. 1985. "Von Karman's Constant in Atmospheric Boundary Layer Flow: Reevaluated," Journal of the Atmospheric Sciences, Vol 42, No. 3, pp 263-270.

Hsu, S. A. 1970. "Coastal Air-Circulation System: Observations and Empirical Model," Monthly Weather Review, Vol 98, No. 7, pp 487-509.

_____. 1972. "Wind Stress on a Coastal Water Surface," Proceedings, 13th Conference on Coastal Engineering, Vancouver, Canada, American Society of Civil Engineers, pp 2531-2541.

_____. 1974. "A Dynamic Roughness Equation and Its Application to Wind Stress Determination at the Air-Sea Interface," Journal of Physical Oceanography, Vol 4, pp 116-120.

_____. 1976. "Determination of the Momentum Flux at the Air-Sea Interface under Variable Meteorological and Oceanographic Conditions: Further Application of the Wind-Wave Interaction Method," Boundary-Layer Meteorology, Vol 10, pp 221-226.

_____. 1979. "Mesoscale Nocturnal Jetlike Winds within the Planetary Bondary Layer over a Flat, Open Coast," Boundary-Layer Meteorology, Vol 17, pp 485-494.

_____. 1981. "Models for Estimating Offshore Winds from Onshore Meteorological Measurements," Bondary-Layer Meteorology, Vol 20, pp 341-351.

Hsu, S. A. 1986. "Correction of Land-Based Wind Data for Offshore Applications: A Further Evaluation," _Journal of Physical Oceanography,_ Vol 16, pp 390-394.

Huang, N. E., Bliven, L. F., Long, S. R., and DeLeonibus, P. S. 1986. "A Study of the Relationship among Wind Speed, Sea State, and the Drag Coefficient for a Developing Wave Field," _Journal of Geophysical Research,_ Vol 91, No. C6, pp 7733-7742.

Huang, N. E., Long, S. R., Tung, C. C., Yuen, Y., and Bliven, L. F. 1981. "A Unified Two-Parameter Wave Spectral Model for a General Sea State," _Journal of Fluid Mechanics,_ Vol 112, pp 203-224.

Hubertz, J. M. 1986. "Observations of Local Wind Effects on Longshore Currents," _Coastal Engineering,_ Vol 10, pp 275-288.

_____. 1987. "A Wind- and Wave-Driven Nearshore Current Model; The One Dimensional Model," Miscellaneous Paper CERC-87-4, US Army Engineer Waterways Experiment Station, Vicksburg, MS.

Hubertz, J. M., Long, C. E., Rivers, P., and Brown, W. A. 1987. "DUCK '85 Nearshore Waves and Currents Data Summary Report," Miscellaneous Paper CERC-87-3, US Army Engineer Waterways Experiment Station, Vicksburg, MS.

Jacobs, S. J. 1987. "An Asymptotic Theory for the Turbulent Flow Over a Progressive Water Wave," _Journal of Fluid Mechanics,_ Vol 174, pp 69-80.

Jonsson, I. G., and Carlsen, N. A. 1976. "Experimental and Theoretical Investigations in an Oscillatory Turbulent Boundary Layer," _Journal of Hydraulic Research,_ Vol 14, No. 1, pp 45-60.

Kinsman, B. 1984. _Wind Waves,_ Dover, New York.

Kitaigorodskii, S. A. 1973. _The Physics of Air-Sea Interaction,_ English translation from Russian by Israel Program for Scientific Translations, Jerusalem, for US Department of Commerce and the National Science Foundation, Washington, DC.

Kraus, E. B. 1972. _Atmosphere-Ocean Interaction,_ Oxford University Press, London.

Large, W. G., and Pond, S. 1981. "Open Ocean Momentum Flux Measurements in Moderate to Strong Winds," _Journal of Physical Oceanography,_ Vol 11, pp 324-336.

_____. 1982. "Sensible and Latent Heat Flux Measurements over the Ocean," _Journal of Physical Oceanography,_ Vol 12, No. 5, pp 464-482.

Lo, A. K., and McBean, G. A. 1978. "On the Relative Errors in Methods of Flux Calculations," _Journal of Applied Meteorology,_ Vol 17, No. 11, pp 1704-1711.

Long, C. E. 1981. "A Simple Model for Time-Dependent, Stably Stratified Boundary Layers," Ph.D. dissertation, University of Washington, Seattle, WA.

Miller, H. C. 1982. "CERC Field Research Facility Environmental Data Summary, 1977-79," Miscellaneous Report CERC-82-16, US Army Engineer Waterways Experiment Station, Vicksburg, MS.

Munk, W. H. 1955. "Wind Stress on Water: an Hypothesis," _Quarterly Journal of the Royal Meteorological Society,_ Vol 81, pp 320-332.

Nowell, A. R. M., and Long, C. E. 1983. "An Evaluation of von Karman's Constant," Pollutant Transfer and Sediment Dispersal in the Washington-Oregon Coastal Zone, B. Hickey, ed., Report of Progress, 1 August 1982 - 31 July 1983, to the US Department of Energy, University of Washington Report RLO 2225 TA25-64, Seattle, WA.

Papadimitrakis, Y. A., Hsu, E. Y., and Street, R. L. 1984. "On the Structure of the Velocity Field Over Progressive Mechanically-Generated Water Waves," Journal of Physical Oceanography, Vol 14, pp 1937-1948.

Papadimitrakis, Y. A., Hsu, Y. -H. L., and Wu, J. 1986. "Turbulent Heat and Mass Transfers Across a Thermally Stratified Air-Water Interface," Journal of Geophysical Research, Vol 91, No. C9, pp 10607-10619.

Paulson, C. A. 1970. "The Mathematical Representation of Wind Speed and Temperature Profiles in the Unstable Atmospheric Surface Layer," Journal of Applied Meteorology, Vol 9, No. 6, pp 857-861.

Phelps, G. T., and Pond, S. 1971. "Spectra of the Temperature and Humidity Fluctuations and of the Fluxes of Moisture and Sensible Heat in the Marine Boundary Layer," Journal of the Atmospheric Sciences, Vol 28, pp 918-928.

Phillips, O. M. 1969. Dynamics of the Upper Ocean, Cambridge University Press, London.

Resio, D. T., and Vincent, C. L. 1977. "Estimation of Winds over the Great Lakes, Journal of Waterway, Port, Coastal, and Ocean Engineering, Vol 103, WW2, pp 265-283.

Resio, D. T., Vincent, C. L., and Corson, W. D. 1982. "Objective Specification of Atlantic Ocean Wind Fields from Historical Data," CERC, WIS Report 4, US Army Engineer Waterways Experiment Station, Vicksburg, MS.

Schlichting, H. 1979. Boundary-Layer Theory, McGraw-Hill, New York.

Schmitt, K. F., Friehe, C. A., and Gibson, C. H. 1978. "Humidity Sensitivity of Atmospheric Temperature Sensors by Salt Contamination," Journal of Physical Oceanography, Vol 8, No. 1, pp 151-161.

_____. 1979. "Structure of Marine Layer Turbulence," Journal of the Atmospheric Sciences, Vol 36, pp 602-618.

Schwab, D. J., Meadows, G. A., Bennett, J. R., Schultz, H., Liu, P. C., Campbell, J. E., and Dannelongue, H. H. 1984. "The Response of the Coastal Boundary Layer to Wind and Waves; Analysis of an Experiment in Lake Erie," Journal of Geophysical Research, Vol 89, No. C5, pp 8043-8053.

SethuRaman, S. 1978. "Influence of Mean Wind Direction on Sea Surface Wave Development," Journal of Physical Oceanography, Vol 8, No. 5, pp 926-929.

_____. 1979. "Momentum Flux and Wave Spectra Measurements from an Air-Sea Interaction Buoy," Boundary-Layer Meteorology, Vol 16, pp 279-291.

SethuRaman, S., and Raynor, G. S. 1975. "Surface Drag Coefficient Dependence on the Aerodynamic Roughness of the Sea," Journal of Geophysical Research, Vol 80, No. 36, pp 4983-4988.

Sheng, Y. P., and Butler, H. L. 1982. "A Three-Dimensional Numerical Model of Coastal, Estuarine and Lake Currents, ARO Report 82-3," Proceedings of the 1982 Army Numerical Analysis and Computers Conference, pp 531-574.

Shore Protection Manual. 1984. 4th Edition, 2 Vols, US Army Engineer Waterways Experiment Station, Coastal Engineering Research Center, US Government Printing Office, Washington, DC.

Smith, S. D., and Anderson, R. J. 1984. "Spectra of Humidity, Temperature, and Wind over the Sea at Sable Island, Nova Scotia," *Journal of Geophysical Research,* Vol 89, No. C2, pp 2029-2040.

Stunder, M., and SethuRaman, S. 1985. "A Comparative Evaluation of the Coastal Internal Boundary-Layer Height Equations," *Boundary-Layer Meteorology,* Vol 32, pp 177-204.

Taylor, G. I. 1916. "Skin Friction of the Wind on the Earth's Surface," *Proceedings of the Royal Society of London, Series A,* No. 92, pp 196-199.

Telford, J. W., and Businger, J. A. 1986. "Comments on 'Von Karman's Constant in Atmospheric Boundary Layer Flow; Reevaluated'," *Journal of the Atmospheric Sciences,* Vol 43, No. 19, pp 2127-2134.

Tennekes, H., and Lumley, J. L. 1972. *A First Course in Turbulence,* MIT Press, Cambridge, MA.

Wierenga, J. 1980. "A Reevaluation of the Kansas Mast Influence on Measurements of Stress and Cup Anemometer Overspeeding," *Boundary-Layer Meteorology,* Vol 18, pp 411-430.

Wu, J. 1980. "Wind Stress Coefficients over the Sea Surface during Near Neutral Conditions - A Revisit," *Journal of Physical Oceanography,* Vol 10, pp 727-740.

_____. 1986. "Stability Parameters and Wind-Stress Coefficients under Various Atmospheric Conditions," *Journal of Atmospheric and Oceanic Technology,* Vol 3, pp 333-339.

APPENDIX A: NOTATION

$\overline{(\ )}$	Time average of ( )
a_1, a_2, a_3	Dimensionless similiarity model constants
A	Kolmogorov constant for momentum
A_q	Kolmogorov constant for humidity
A_T	Kolmogorov constant for temperature
b_1, b_2, b_3	Dimensionless similarity model constants
C	Water-wave phase speed
C_D	Drag coefficient
C_o	Water-wave phase speed associated with peak spectral density
C_{max}	Phase speed at which maximum air-sea interaction occurs
d	Water depth
D	Turbulent kinetic energy gradient diffusion term
e'^2	Instantaneous turbulent kinetic energy per unit mass
f	Cyclic frequency
f_c	Coriolis parameter
g	Gravitational acceleration
G	A function in the simplified Wallops spectrum
H_s	Characteristic wave height
i	Direction index
j	Direction index
k	Radian wave number
k_R	Characteristic size of physical roughness elements
L	Monin-Obukhov length scale
m	A function in the simplified Wallops spectrum
p	Total atmospheric pressure
$\overline{p}$	Mean atmospheric pressure

A1

p'	Fluctuating atmospheric pressure
q	Total specific humidity
$\bar{q}$	Mean specific humidity
q'	Fluctuating specific humidity
$\bar{q}_o$	Mean surface specific humidity
R_a	Ideal gas constant for air
s'	Resultant of fluctuating horizontal wind speed components
S	Variance spectral density
S_q	Humidity variance spectral density
S_T	Temperature variance spectral density
t	Time
T_a	Averaging time
T_r	Readjustment time
T	Temperature
$\bar{T}$	Mean temperature
T'	Fluctuating temperature
T_o	Mean wave period
$\bar{T}_o$	Mean surface temperature
T_p	Spectral peak period
T_v	Virtual temperature
$\bar{T}_v$	Mean virtual temperature
T'_v	Fluctuating virtual temperature
u	Wind speed in x-direction
u'	Fluctuating wind speed in x-direction
u'_m	Measured fluctuating wind speed in x-direction
u_*	$(\tau/\rho)^{1/2}$ friction velocity
u_{*m}	Friction velocity estimated from measurements

U	Mean velocity in x-direction
U_1, U_2	Particular measured mean wind speeds
U_r	Reference mean wind speed
U_o	Surface mean wind speed
v'	Fluctuating wind speed in y-direction
w	Vertical velocity
w'	Fluctuating vertical velocity
w'_m	Measured fluctuating vertical velocity
x	Primary horizontal coordinate
y	Secondary horizontal coordinate
z	Vertical coordinate
z_1, z_2	Particular vertical coordinates
z_a	Vertical elevation at which $U(z_a) = C$
z_o	Surface roughness length scale
z_r	Reference elevation
α	Coefficient in Charnock's model
β	Phillips constant
γ	Incomplete gamma function
δ	Boundary layer thickness
Δ	Finite increment operator
ε	Viscous dissipation rate of turbulent kinetic energy
ε_q	Molecular dissipation rate of humidity variance
ε_T	Molecular dissipation rate of temperature variance
θ	Azimuth direction in horizontal plane
θ_o	Azimuth of mean flow at air-boundary interface
θ_r	Reference horizontal wind direction
κ	von Karman constant

A3

λ	Wavelength
λ_p	Water wavelength associated with peak spectral density
ϕ	Latitude
μ	Dynamic viscosity
ν	Kinematic viscosity
ρ	Total air density
$\bar{\rho}$	Mean air density
ρ'	Fluctuating air density
σ_η	Standard deviation of sea-surface elevation
τ	Wind stress
ϕ_m	Dimensionless mean shear
ϕ_q	Dimensionless mean humidity gradient
ϕ_T	Dimensionless mean temperature gradient
χ	Angular deviation from level of measuring system
ψ_m	Dimensionless integral of ϕ_m
ψ_q	Dimensionless integral of ϕ_q
ψ_T	Dimensionless integral of ϕ_T
ω	Radian frequency
ω_{max}	Frequency at which maximum air-sea interaction occurs
ω_p	Sea-surface elevation peak frequency
Ω	Planetary rotation rate

A4